Anti-Neurotoxic and Pro-Survival Strategies in Degenerative Disease: The Relevance, Utility, and Challenges of Small Molecule Development

Sean Jmaeff

Doctor of Philosophy

Department of Pharmacology & Therapeutics

McGill University

Montreal, Quebec, Canada

A thesis submitted to the Faculty of Graduate and Postdoctoral Studies in partial fulfillment of the requirements of the degree of Doctor of Philosophy

December 2019

Dedication

This thesis is dedicated to my family, particularly my parents, wife Elise, and son Victor who never ceased in encouraging me, and to all those who are bold and/or crazy enough to commit themselves to scientific pursuit.

Abstract

Neurodegenerative diseases are a vast grouping of conditions which invariably result in the loss of neurons. This loss is irreversible, and is one of many reasons why these diseases are notoriously difficult to treat. However, a glimmer of hope rests with the neurotrophins and their receptors, a family of proteins highly involved in survival, differentiation, and migratory processes. Employing trophic factors therapeutically has been a grand failure, despite a deeper understanding of their biology as well as methods for their delivery. By and large, bulky proteins possess poor pharmacological properties, many of which are inescapable. Slow and unpredictable diffusion, instability, and the fact that they are promiscuous in the targets they interact with are but a few examples. Small molecules offer a tantalizing solution to these issues. The seemingly infinite molecular landscape has barely been navigated, and as we explore further, we begin to uncover novel ways to intervene therapeutically, beyond the capabilities of the endogenous ligands. For simplicity and continuity's sake, the work will be divided into 2 overarching categories pertaining to small molecule therapeutic strategies for degenerative diseases: Anti-Neurotoxic and Pro-Survival.

A truncated form of TrkC, known as TrkC.T1, and p75 have emerged recently as interesting targets in a number of diseases. Their full biological roles are not yet understood, however it is clear that they are involved in mediating cytotoxic cascades, through messengers such as TNFa. A generalized hallmark of neurodegeneration is a trophic imbalance, a shift towards pro-death signaling. Blocking these effects with the use of antagonists is thus a relatively simple approach to mitigating the pathological toxicity associated with TrkC.T1 and p75. This is true within the retina, as the first body of work suggests

We determined that the deleterious TrkC.T1 isoform was upregulated in the RHOP347S mouse model of retinitis pigmentosa, a blinding condition resulting from photoreceptor loss. Using retinal explants, we demonstrated that small molecule blockade of this receptor by KB1368 decreased photoreceptor loss significantly. Furthermore, the anti-neurotoxic mechanism was elucidated using these cultures, from the finding that compound-treated retinas possessed consistently lower levels of pErk and consequently TNFa. These data were corroborated *in vivo*, whereby intravitreal injection of KB1368 was performed. In additional

experiments, KB1368 also resulted in long-term retinal preservation in live mice as measured by optical coherence tomography (OCT). The data lend strong support for the need to develop more selective TrkC.T1 antagonists, as KB1368 is a broad-spectrum blocker and also targets the full-length form of TrkC.

P75 was also found to be consistently upregulated in RHOP347S mice, as well as in the rd10 model of RP. Following these findings, we performed the first tests with a small molecule antagonist of p75, THX-B, in retinal cultures. We found that exposure to THX-B resulted in a significant preservation of the photoreceptor layer, measured both by the TUNEL assay, as well as histologically after administering the drug by intravitreal and subconjunctival routes.

Taken together, these data underscore the value in reducing toxicity through mediators like TrkC.T1 and p75, and that small molecule antagonists provide a solid basis for therapy. In addition, they may be used as tools to deepen our understanding of the pathological processes that are at work as a disease progresses.

The next body of work constitutes the bulk of the thesis, and is a meandering tale of drug discovery that has not yet seen its proper end. Being someone who takes much pride in following through completely in any endeavor, I often write these words with a bit of reservation. The future is uncertain, of course, however at the current time of this writing I firmly intend to move this project forward and imbue it with the value it truly deserves.

The REarranged-during-Transfection (RET) receptor is a relative of the neurotrophin family, and is broadly expressed by neuronal populations. Like its relatives, RET has been a worthy target for development efforts, though in fact, surprisingly little progress has been made. Another way to restore the imbalance observed in degenerative disease is to drive trophic signaling with an agonist, and this is the basic rationale for RET-based therapy in this instance.

An interesting characteristic of RET is the fact that it does not seem to have any direct endogenous ligands known. Membrane-bound or soluble co-receptors are required to initiate signaling. This is the case for Glial cell line-derived neurotrophic factor (GDNF) and the GDNF Family Receptor Alpha-1 (GFRa1), the most studied of the RET ligands. Cellular screening assays identified a panel of parent compounds from the NCI database which activated RET and

its major downstream effectors, pAkt and pErk. Surprisingly, many compounds in this library were able to signal in the complete absence of the GFRa1 co-receptor, unlike GDNF, and this marked a significant discovery in RET-targeting approaches.

Rational design was then undertaken, sectioning the parent structure into discrete units and screening the resulting analogues. From these efforts, lead Compound 8 emerged as being modestly potent, highly selective for RET and maintaining GFRa1-independence. Employing these molecules as biological tools allowed us to probe the functional interactions between RET and GFRa1. GFRa1 was shown to be a negative regulator of compound signaling, and this interaction is likely through an allosteric mechanism that can be surmounted with increasing Compound 8 concentrations. Pre-treatment with a positive GFRa1-modulator also inhibited Compound 8, further supporting the negative regulatory role of the co-receptor.

Therapeutic assessment of Compound 8 was performed in mouse retinal explants of RP mice. Robust preservation of the photoreceptor layer was observed, contrary to even high doses of GDNF. Subsequent histological studies identified the major glial-cell type in the retina, the Muller cells, as likely being the primary cell-type targeted. Thus, a paracrine mechanism of photoreceptor support is suggested.

As a whole, these data highlight the strengths of small molecules over their protein counterparts, as they can expand upon the pharmacological scope of a receptor's native ligands. They can be used as tools to address new biological questions, and ultimately lend validation to targets like RET in the search for effective therapies.

In summing up this portion of the work, one glaring detail remains unanswered. Following an in-house synthesis directive, it was discovered that the major component of compound 8 was biologically inert in its purest form. From there extensive purification efforts commenced to identify the active fractions. Trace amounts of a highly potent substance (easily less than 5% of the total composition) were eventually isolated, albeit not in sufficient amounts to permit structural elucidation. Furthermore, the NMR spectrum of compound 8 itself was inconsistent with that reported by the NCI database. We determined the correct structural assignment of Compound 8 as being a positional isomer, and these findings are to serve as a

warning to those undertaking database screening, and in perhaps a more idealistic sense, to raise the issue of better interaction between researchers and chemical database curators.

During the structural elucidation work, we had hypothesized that the true active material was likely an oxidative by-product of the major, inactive, fraction. This led into the screening of a select panel of naphthoquinone derivatives, some of which were indeed found to be RET-activating. Knowing the precise structures now enabled an exploration into structure-activity relationships. Side-chain modifications produced molecules with GFRa1-independence, while N-substitution in the ring system impacted RET selectivity primarily. Combining these new leads with a GFRa1-modulator resulted in differential signaling biases through pAkt and pErk.

Lead Q525 was tested in the RP model, where it was effective in rescuing photoreceptors from death. The mechanism appeared to be similar to that of compound 8 reported previously, in that the Muller glial cells were activated following treatment.

The data here support the importance and implications of SAR, in that minor structural changes may have major impacts on factors such as potency, selectivity, and toxicity. We also report the rarely documented occurrence of ligand bias driven by co-receptor interaction, which adds new considerations for developing drugs with improved properties. Finally, they lend more support for RET as a valid therapeutic target in degenerative diseases like RP.

Résumé

Les maladies neurodégénératives sont un vaste ensemble de conditions qui entraînent invariablement la perte de neurones. Cette perte irréversible est l'une des nombreuses raisons pour lesquelles il est si difficile de traiter ces maladies. On trouve cependant une lueur d'espoir auprès des neurotrophines et de leurs récepteurs, une famille de protéines fortement impliquées dans les processus de survie, de différenciation et de migration. L'usage thérapeutique des facteurs trophiques s'est avéré un grand échec, malgré une meilleure compréhension de leur biologie et des méthodes de leur délivrance. En gros, les protéines volumineuses possèdent de pauvres propriétés pharmacologiques, dont beaucoup sont impossibles à ignorer : leur diffusion lente et imprévisible, leur instabilité et leur réaction de promiscuité avec les cibles n'en sont que quelques exemples.

Les petites molécules proposent une solution alléchante à ces problèmes. Nous avons à peine parcouru le paysage moléculaire qui semble infini, et, lorsque nous poussons l'exploration plus loin, nous pouvons découvrir de nouveaux modes d'interventions thérapeutiques qui dépassent le potentiel des ligands endogènes. Pour des raisons de simplicité et de continuité, le travail suivant sera divisé en deux grandes catégories de stratégies thérapeutiques des petites molécules pour les maladies dégénératives : anti-neurotoxique et neuroprotectrice.

P75 et TrkC.T1 (une forme tronquée de TrkC) se sont récemment présentés comme des cibles intéressantes pour un certain nombre de maladies. Leur rôle biologique complet n'est pas encore compris, mais il est clair qu'ils sont impliqués dans la médiation des cascades cytotoxiques par le biais de messagers tels que le TNFa. Une caractéristique généralisée de la neurodégénérescence est un déséquilibre trophique, un glissement vers la signalisation promort. Le blocage de cette conséquence par l'utilisation d'antagonistes est donc une approche relativement simple pour atténuer la toxicité pathologique associée à TrkC.T1 et p75. C'est le cas avec la rétine, comme le suggère la première partie de ce travail.

Nous avons déterminé que l'isoforme délétère TrkC.T1 était régulée à la hausse dans le modèle murin RHOP347S de rétinite pigmentaire, une condition où la perte de photorécepteurs mène à la cécité, puis démontré à l'aide d'implants rétiniens que le blocage de petites molécules par KB1368 diminuait considérablement cette perte de photorécepteurs. La découverte de

niveaux de pERK et de TNFa constamment inférieurs chez les rétines traitées avec ces composés a révélé le mécanisme anti-neurotoxique. Ces données ont été corroborées in vivo, ce qui a permis une injection intravitréenne de KB1368. Lors d'expériences supplémentaires, KB1368 a également entraîné une conservation rétinienne à long terme chez des souris vivantes, mesurée par tomographie par cohérence optique (OCT.). Les données confirment fortement la nécessité de développer des antagonistes TrkC.T1 plus sélectifs, car KB1368 est un bloqueur à large spectre qui cible la forme complète de TrkC.

P75 a également démontré une régulation à la hausse chez les souris RHOP347S, ainsi que dans le modèle rd10 de RP. Suite à ces résultats, nous avons effectué les premiers tests dans des cultures rétiniennes avec un antagoniste de petites molécules de p75, THX-B. Nous avons constaté que l'exposition au THX-B entraînait une conservation significative de la couche de photorécepteurs, mesurée une première fois fois avec la méthode TUNEL, puis histologiquement après l'administration du médicament par voie intravitréenne et sous-conjonctivale.
Ensemble, ces données soulignent l'intérêt de réduire la toxicité avec des médiateurs comme TrkC.T1 et p75, de même que la validité des antagonistes de petites molécules comme base solide pour la thérapie. Ces médiateurs peuvent aussi être utilisés comme outils pour approfondir notre compréhension des processus pathologiques à l'œuvre lors de la progression de la maladie.

La seconde partie du travail, qui compose l'essentiel de cette thèse, raconte le parcours sinueux d'une découverte de médicament qui n'a pas abouti comme souhaité. Comme ma capacité à aller au fond des choses m'inspire beaucoup de fierté, j'écris ces mots avec réserve. Évidemment, on ne peut prévoir le futur, mais, au moment de coucher ces lignes, j'ai la ferme intention de poursuivre ce projet en lui accordant toute la valeur qu'il mérite.

Largement exprimé par les neurones, le récepteur RET (Rearranged-during-Transfection) appartient à la famille neurotrophine. Comme ses parents, le RET a été l'objet de nombreux efforts de développement au succès toutefois curieusement mitigé. Une autre manière de restaurer le déséquilibre observé dans les maladies dégénératives est de conduire la signalisation trophique comme agoniste, et c'est le phénomène derrière notre thérapie basée sur le RET.

Une caractéristique unique qui distingue le RET est le fait qu'il ne semble pas avoir de ligands endogènes directs. Des corécepteurs solubles ou liés à la membrane sont nécessaires pour initier la signalisation. C'est le cas du facteur neurotrophique dérivé des lignées cellulaires

gliales (GDNF) et du GDNF Family Receptor Alpha-1 (GFRa1), le ligand RET le plus étudié. Les tests de criblage cellulaire ont identifié un panel de composés parents de la base de données NCI ayant activé RET et ses principaux effecteurs en aval, pAkt et pERK. Étonnamment, plusieurs composés de cette banque de données ont réussi à émettre des signaux en l'absence totale de co-récepteur GFRal, contrairement au GDNF, ce qui a marqué une découverte importante dans les approches de ciblage RET.

Nous avons ensuite entrepris une conception rationnelle en divisant la structure mère pour cibler les analogues résultants. Ces efforts ont démontré que le composé principal 8 était modérément puissant, hautement sélectif pour le RET et indépendant du GFRa1. Nous avons pu sonder les interactions fonctionnelles entre RET et GFRa1 en utilisant ces molécules comme outils biologiques. GFRa1 s'est avéré être un régulateur négatif de la signalisation des composes, une interaction sans doute causée par un mécanisme allostérique pouvant être surmonté en augmentation la concentration du compose 8.Un prétraitement avec un modulateur GFRa1 positif a également inhibé le composé 8, soutenant le rôle régulateur négatif du co-récepteur.

L'évaluation thérapeutique du composé 8 a été réalisée sur des souris avec des explants rétiniens RP. Une conservation robuste de la couche photoréceptrice a été observée, un résultat contraire à celui de doses de GDNF aussi élevées. Des études histologiques ultérieures ont identifié les cellules Muller, soit le principal type de cellules gliales dans la rétine, comme espèce probable de cellule ciblée. Un mécanisme paracrine de support des photorécepteurs est donc suggéré.

L'ensemble de ces données démontrent la supériorité des petites molécules sur leurs homologues protéiques puisqu'elles peuvent étendre la portée pharmacologique des ligands natifs des récepteurs. Elles peuvent être utilisés pour soulever de nouvelles questions biologiques et ultimement valider des cibles comme RET dans la recherchée de thérapies efficaces.

Il manque toutefois un détail d'une importance capitale à cette portion du travail. Une directive de synthèse interne a révélé que le composant majeur du compose 8 était biologiquement inerte dans sa forme la plus pure. Nous avons alors accumulé les efforts de purification pour identifier les fractions actives pour finalement réussir à isoler une solution hautement active (aisément moins de 5 % de la composition totale), mais malheureusement en quantités trop infimes pour en élucider les structures. Plus encore, le spectre RMN du composé 8

lui-même n'était pas cohérent avec celui rapporté par la base de données NCI. Nous avons déterminé l'affectation structurelle correcte du composé 8 comme étant un isomère positionnel, mais ces résultats devraient serveur d'avertissement à ceux qui entreprennent de tels filtrages, dans l'intention peut-être idéaliste de souligner l'importance d'une meilleure interaction entre les chercheurs et les fournisseurs de bases de données chimiques.

Lors de la phase d'élucidation de la structure, nous avions pour hypothèse que le composant actif est en réalité un sous-produit de l'oxydation d'une fraction en réalité largement inactive. Cette possibilité nous a conduits au criblage d'un panel restreint de dérivés de naphtoquinone, dont certains se sont en effet révélés activateurs du RET. Connaître les structures précises permettrait de comprendre en profondeur les relations structures-activités (SAR). La modification des chaînes latérales a produit des molécules indépendantes de GRFa1, tandis que la substitution N dans le système cyclique a principalement affecté la sélectivité RET. La combinaison de ces nouvelles pistes avec un modulateur GFRa1 a entraîné pour sa part des biais de signalisation différentiels via pAKT et pERK.

Le plomb Q525 a été testé dans le modèle RP, où il a prouvé son efficacité pour sauver les photorécepteurs de la mort. Le mécanisme semble similaire au compose 8 rapporté précédemment puisque les cellules gliales Muller ont été actives après le traitement.

Les informations contenues ici appuient l'importance et les implications de SAR, prouvant que des changements structurels mineurs peuvent avoir des conséquences majeures sur des facteurs comme la puissance, la sélectivité et la toxicité. Nous avons aussi rapporté l'occurrence rarement documentée d'un biais de ligand entraîné par l'interaction de co-récepteurs, ce qui ajoute de nouvelles considérations pour le développement de médicaments aux propriétés améliorées. Enfin, ce travail soutient la validité du RET comme cible thérapeutique dans le traitement de maladies dégénératives comme les rétinites pigmentaires (RP).

Table of Contents

Preface/Acknowledgements

The path to objective truth is an arduous one. The work contained within these pages hopefully offers a glimpse as to what my journey entailed; from fledgling undergrad to hardened researcher. Drug development, as this thesis hinges on, presents many unique challenges, and requires a heavy reliance on multidisciplinary approaches. Molecules themselves may take on a sort of personality as one works with them. Personalities change, as I am certain we can all attest. Under such circumstances, as cliché as it sounds, one *must* expect the unexpected, and pluck away at the veil of truth with thorough and proper experimental design. Despite our best efforts we may still be misled, and so the would-be drug-developer must tread lightly until grounded enough to move forward in leaps. Scientific work is geared toward the community, which is not to say that the personal element should be overshadowed. I have grown immeasurably as a scientist and as a human being throughout this journey, and I feel my work is as much a testament to that as it is anything else.

That being said, I have not walked this path in solitude, and there are many who deserve recognition. First and foremost I would like to mention Dr. Horacio Uri Saragovi as an instrumental figure in my successes as a researcher (he was my boss, after all). His hard-line approach to science was difficult to grasp in my early years, but has now given me the tools to face life's obstacles with a clarity and confidence I never had before.

A shout out is also due for my advisory committee, comprising Drs. Paul Clarke, Przemyslaw (we call him Mike) Sapieha, and Sylvain Chemtob, whose diverse knowledge lent some useful perspectives on the work. In particular I would like to thank Dr. Clarke for his support and discussions, and for his clever quips which never ceased to be refreshing and destabilizing at the same time.

My collaborators with the Saarma lab at the University of Helsinki are worthy of mention owing to the lengthy e-mails and conference calls that were critical in getting my main project off the ground, as well as never failing to provide me with helpful supplies. On the rare occasions we met, their drinking abilities always struck me as commendable. The Lumb lab and

its members belong here as well, grounding me in the realm of Chemistry and graciously providing the lab space to help arrive at some critical conclusions.

I will extend my deepest gratitude to members of the Saragovi lab (in no particular order), Drs. Alba Galan-Garcia, Fouad Brahimi, Hinyu Nedev, Sylvia Josephy, Pablo “Diablo” Barcelona, and Mario Maira. Hayley Lippiatt also worked closely alongside me, and together we shared in the ups and downs of research life. Collectively these people gave the lab its character, and provided an environment for continuous learning and personal growth.

Lastly I would like to thank my family and friends, who have been a pillar of support and have held me up throughout. My wife, Elise Henripin, has stood tirelessly by my side, and even though the most dreaded words known to any PhD. Candidate (*When* are you going to graduate?) have escaped her lips numerous times, she has never failed to make me smile and endow me with the drive to keep pushing forward.

“Ride the spiral to the end, it may just go where no one’s been.” – Tool, Lateralus

List of Figures

List of Tables

Contributions of Authors

This thesis is written in a manuscript-based format in accordance with the regulations of the Faculty of Graduate studies and Research from McGill University. The thesis is composed of:

Chapter 2 which includes 2 published articles, one of which in its entirety, and the other as an excerpt.

Chapter 3 follows **Chapter 2** and includes a published article. Its supplemental information is presented in **Appendix I.**

Chapter 4 follows **Chapter 3** and includes a published article. Its supplemental information is presented in **Appendix II.**

In **Chapter 2**, the first manuscript was prepared by Dr. A. Galan, S. Jmaeff, and Dr. H. Uri Saragovi, and edited by co-auhors. I am the second author. In the second manuscript, preparation was done by M. Platón-Corchado and Dr. E. de la Rosa with data contribution by S. Jmaeff. An excerpt is included to support the conclusions of **Chapter 2**. I am the third author.

In **Chapter 3** and **Chapter 4**, the manuscripts were prepared by S. Jmaeff and Dr. H. Uri Saragovi, and edited by co-authors. I am the first author on both articles.

Chapter 2 entitled "In retinitis pigmentosa TrkC.T1-dependent vectorial Erk activity upregulates glial TNF-α, causing selective neuronal death" is an article published in the journal *Cell Death and Disease* in 2017.

Figure 2.1 Dr. A. Galan and I acquired the samples and data for experiments shown in 1A and 1B. Dr. A. Galan performed the experiments relating to 1C and 1D, and she prepared the figure.

Figure 2.2 Dr. A. Galan and I acquired the samples for analysis. She performed the experiments and prepared the figure.

Figure 2.3 Dr. A. Galan and I acquired the samples for analysis. She performed the experiments and prepared the figure.

Figure 2.4 Dr. P. Barcelona performed the experiments in 4A-C. Dr. A. Galan and I acquired the samples in experiments 4D-G. She performed the experiments and prepared the figure.

Figure 2.5 Dr. A. Galan and I acquired the samples for analysis. She performed the experiments and prepared the figure.

Figure 2.6 I performed the experiments and figures in 6A, 6B and 6D. Dr. A. Galan and I together performed experiments in 6C and 6E.

Figure 2.7 Dr. A Galan and and I together performed the experiments, and she prepared the figure.

Figure 2.8 I performed the experiment and prepared the figure in 8A. Dr. P Barcelona and I prepared the samples used in experiments and analysis for 8B-E.

Figure 2.8 is an excerpt from the article entitled “p75NTR antagonists attenuate photoreceptor cell loss in murine models of retinitis pigmentosa”, published in the journal *Cell Death and Disease* in 2017.

Chapter 3 entitled “Small molecule ligands that bind the RET receptor activate neuroprotective signals independent of but modulated by co-receptor GFRa1” is an article submitted to the journal *Molecular Pharmacology* in 2019, and published officailly in May 2020.

Figure 3.1 I performed all the experiments and prepared the figure.

Figure 3.2 I performed all the experiments and prepared the figure.

Figure 3.3 Dr. M. Hancock performed the SPR experiments and I prepared the figure. Dr. Yulia Sidorova performed experiments in panels 3E-G.

Figure 3.4 I performed all the experiments and prepared the figure.

Figure 3.5 I performed all the experiments and prepared the figure.

Chapter 4 entitled “Small-molecule agonists of the RET receptor tyrosine kinase activate biased trophic signals that are influenced by the presence of GFRa1 co-receptors” is an article submitted to the *Journal of Biological Chemistry* in 2019, and published officially in April 2020.

Figure 4.1 I performed all the experiments and prepared the figure, with the exception of 1B and 1E which were performed by Dr. Y. Sidorova.

Figure 4.2 I performed all the experiments and prepared the figure.

Figure 4.3 I performed all the experiments and prepared the figure.

Figure 4.4 I performed all the experiments and prepared the figure.

Figure 4.5 I performed all the experiments and prepared the figure.

Contributions to Original Knowledge

1. Support for the 'trophic imbalance' hypothesis of neurodegenerative disease with a two-pronged approach.
2. Anti-neurotoxic: Target validation of TrkC.T1 and p75 in RP with the use of small molecules.
3. TrkC.T1 activation causes an Erk-dependent rise in TNFa in RP.
4. Blockade of TrkC.T1 in RP abrogates pErk signals, decreases TNFa, and preserves photoreceptors in retinal explants and *in vivo*.
5. Selective antagonism of p75 in RP preserves photoreceptors in retinal explants.
6. Pro-survival: Validation of RET in RP through the discovery of two novel classes of agonists.
7. Identification of some of the first potent and selective GFRa1-independent RET activators, allowing for direct receptor targeting.
8. Demonstration of the GFRa1 co-receptor as a negative regulator of RET signaling.
9. A lead Compound 8 is robustly neuroprotective in RP retinal explants, while GDNF is not.
10. Compound 8 activates pAkt and pErk specifically in glial cells, supporting a paracrine model of photoreceptor protection.
11. Discovery of naphthoquinone/quinoline RET activators.
12. Modification of these molecules by side-chain, chlorine substitution, and N-substitution in the ring system can control GFRa1-independence, RET selectivity, and toxicity.
13. Combination of quinone/quinoline agonists with a GFRa1-modulator results in ligand-dependent signaling biases through pAkt and pErk.
14. A selective quinoline RET activator, Q525, protects photoreceptors in RP retinal explants.

15. Q525 activates pAkt and pErk in retinal glial cells, mirroring the findings from Compound 8 studies.
16. Chemical databases are a valuable, though unreliable resource for drug development.

List of Abbreviations

BSA: Bovine Serum Albumin

CHO: Chinese Hamster Ovary

CRALBP: Cellular Retinaldehyde Binding-Protein

DAPI: 4',6-diamidino-2-phenylindole

DMEM: Dulbecco's Modified Eagle's Medium

DMSO: Dimethyl sulfoxide

FBS: Fetal Bovine Serum

FGF2: Fibroblast Growth Factor 2

GDNF: Glial cell line-derived neurotrophic factor

GFRα1: GDNF Family Receptor alpha 1

GPI: Glycosylphosphatidylinositol

INL: Inner Nuclear Layer

NCAM: Neuronal Cell Adhesion Molecule

NGF: Nerve Growth Factor

ONL: Outer Nuclear Layer

PBS: Phosphate Buffered Saline

PD: Parkinson's Disease

PFA: Paraformaldehyde

PTP: Protein Tyrosine Phosphatase

pTyr: phospho-tyrosine

RGC: Retinal Ganglion Cell Layer

RP: Retinitis Pigmentosa

RTK: Receptor Tyrosine Kinase

RU: Resonance Units

SAR: Structure-Activity Relationship

SFM: Serum-free Media

SPR: Surface Plasmon Resonance

SSC: Saline Sodium Citrate

TdT: Terminal Deoxynucleotidyl Transferase

TGF: Transforming Growth Factor

TrkA: Tropomyosin Receptor Kinase A

TUNEL: Terminal deoxynucleotidyl transferase dUTP nick end labeling

Chapter 1

General Introduction

The Neurotrophins and Disease

The neurotrophins and their receptors make up a diverse family of proteins that are intimately tied to the development and maintenance of the nervous system. Many neuronal populations depend on trophic support for their survival, and as such their interest as drug targets has remained strong for the past 3 decades. Broadly, the neurotrophin receptor family is comprised of the Trk tyrosine kinases A-C, and the catalytically inactive p75 receptor. The GDNF receptor, better known as the RET tyrosine kinase, while not classically defined within the neurotrophin axis, is a distant relative of sorts and is involved in many of the same biological processes (**Fig 1.1)**. Generally, the neurotrophin ligands are synthesized as precursors, known as pro-neurotrophins (proNTFs) , that possess their own distinct biological roles namely through p75. While mature neurotrophins carry out their functions through a high-affinity receptor interaction, NT3 through TrkC for example, they may also signal through low-affinity binding to p75 [1]. Ligand binding to Trks and RET induces their dimerization, and consequently conformational changes in the receptor ectodomain. These propagate through the cell membrane and activate the receptor's intracellular kinase domain. Key tyrosine residues along the C-terminal tail become phosphorylated, and serve as docking sites for various adaptor proteins bearing SH2 or PTB domains. Major signaling pathways such as PI3K/Akt, Ras/Erk, and PLC-

gamma carry out the biological functions. These functions are generally seen as being "positive" in the nervous system; cell survival, differentiation, migration, and synaptogenesis and maintenance of these connections. P75, while not possessing a kinase domain, is still able to recruit adaptor proteins to transmit signals, and is considered to play "negative" roles, pro-death [2]. It tends to be highly promiscuous and can interact with numerous other receptors or membrane proteins to modulate its signaling outcome. While p75 is considered to work in opposition to the Trks, p75/sortilin complexes for example can either enhance or hinder Trk signaling depending on the context [3]. Additionally, receptors like TrkC exist in various isoforms due to alternative splicing, giving rise to truncated forms such as TrkC.T1 [4]. The complex regulatory scheme of the neurotrophin axis makes therapeutic strategies particularly challenging.

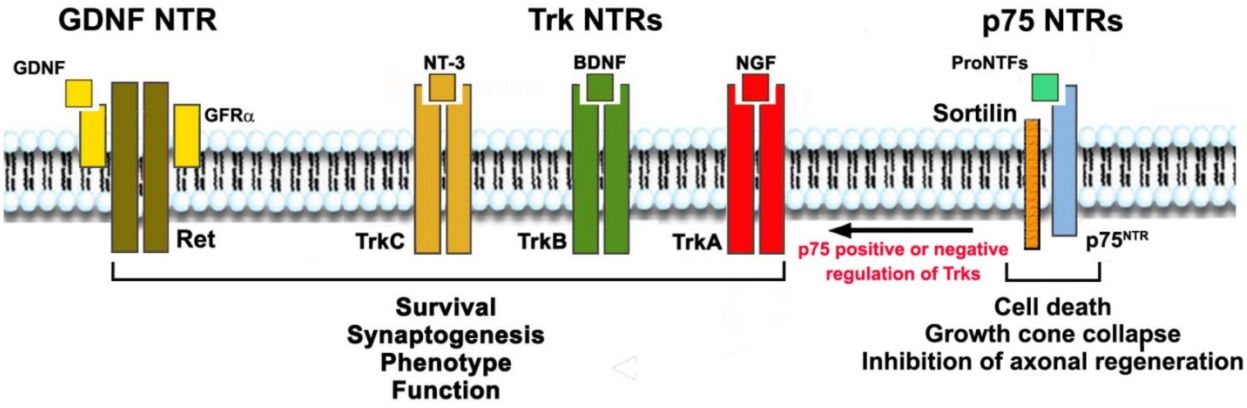

Figure 1.1: Overview of the neurotrophin family and their characteristics

There are 3 Trk receptor subtypes, each with their own respective ligands. The GDNF receptor, RET, is distinct from the Trk family but is functionally related as it mediates similar biological processes. The p75 receptor binds neurotrophin precursors, proNTFs, preferentially, though all mature NTs also act as low-affinity ligands. P75 activation generally works in opposition to those of the Trks and RET, but can actually positively or negatively modulate Trks depending on the signaling partners it interacts with. Figure is adapted from Neuroprotection: Pro-survival and Anti-neurotoxic Mechanisms as Therapeutic Strategies in Neurodegeneration, Saragovi et al, *Frontiers in Cellular Neuroscience* 13, 231 (June 2019)

Surprisingly, in the context of neurodegenerative diseases, a general and elegant paradigm has taken shape. This has allowed for the spearheading of drug development efforts. Homeostasis, a basic tenet of nature, applies to pro-survival and pro-death signals in the nervous system. Under normal circumstances in the adult nervous system, these signals are harmonious with each other. In diseased states however, this balance is disrupted, favoring cytotoxic and/or pro-apoptotic processes and thus a number of disease phenotypes depending on the neuronal population affected (**Fig 1.2**). Negative signal cascades through p75 and TrkC.T1 tend to be over-activated, while positive signals through Trks or RET are diminished. These trends outline two approaches that can be employed to restore trophic balance, both of which are explored in this thesis.

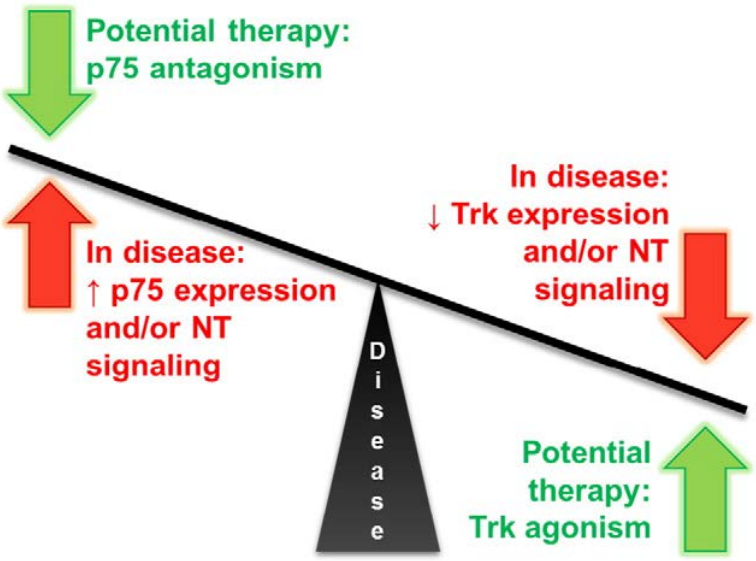

Figure 1.2: Dysregulation of neurotrophic signaling as a therapeutic strategy

Neurodegenerative diseases are highly variable in their etiology as a whole, however trophic imbalances are a feature which is common to many of them. In some pathological states, pro-death signaling is enhanced through p75 upregulation. Antagonism of these pathways is one method to counteract this influence. In other cases, trophic receptor expression may be decreased or their signaling capacity hindered in some way. Activation of pro-survival pathways therefore represents an alternative method for therapy. Figure is adapted from Neurotrophin

receptor agonists and antagonists as therapeutic agents: An evolving paradigm, Sylvia Josephy-Hernandez, Sean Jmaeff, et al, *Neurobiology of Disease* 97, 139-155 (January 2017)

Overview of TrkC.T1

A common phenomenon in biology is to repurpose existing systems rather than to evolve new ones. An elegant example of this occurs within the Trk receptor family. Alternative splicing can give rise to truncated forms of the receptor, which differ from the fully intact version in that they lack the intracellular kinase domain. While catalytically dead, the TrkC.T1 isoform binds its native ligand NT3 with a roughly equal affinity to the full length TrkC (TrkC.FL) [5]. Both forms signal via NT3 in a completely different manner however, and this is an effective means to generate an array of biological outcomes from the same ligand. Truncated and full-length TrkC differ in their expression patterns during nervous system development, likely for this reason [6]. Overexpression of truncated TrkC *in vivo* results in a lethal phenotype, and supports its role as a negative regulator [7]. In the mature nervous system, TrkC.T1 is present but in low levels. Mounting evidence has revealed that TrkC.T1 is upregulated in diseased states, and becomes neurotoxic owing to the production of tumor-necrosis factor alpha (TNFa) [8, 9]. The mechanistic route of this upregulation appears to be governed at least in some capacity at the micro-RNA level. TrkC.T1 expression is enhanced in both mouse and human ALS for example, and this coincides with a marked decrease in miR-128, a micro-RNA which controls TrkC.T1 mRNA stability [10]. Additionally, TrkC.T1 increases are implicated in the pathology of glaucoma [8], and interestingly, studies examining miR-128 levels in human aqueous humor found detectable levels of this micro-RNA in normal controls, but were unable to observe it in glaucomatous patients [11]. Increased TrkC.T1 effectively leads to a disturbance in the TrkC.T1/TrkC.FL ratio, and would therefore negate the use of a non-selective ligand like NT3 as a rational strategy. Indeed, the development of selective TrkC.FL agonists which avoid TrkC.T1 activation are therapeutically promising [10].

Alternatively, antagonism of TrkC.T1 is relevant as well, and outlines the first anti-neurotoxic approach described herein. Silencing TrkC.T1 expression prevents the secretion of TNFa by NT3 and enhances its efficacy [10, 12], and therefore paves the way for development and testing of TrkC.T1 antagonists.

P75: A Neurotoxic TrkC.T1 relative?

The p75 receptor has been of major interest over the past two decades, and continues to remain in the limelight as an attractive therapeutic target. It bears striking similarity to TrkC.T1. Like its truncated counterpart, p75 does not possess any enzymatic activity, and transmits signals into the cell by a variety of conformational changes. To further complicate the situation, p75 is remarkably promiscuous and is known to associate with a number of signaling partners. These include all members of the Trk family, where its presence has been shown to modulate ligand docking, and even expose new or "cryptic" binding sites [3]. As a result, and in a similar fashion to TrkC.T1, the functional outcomes directed by p75 are vast and depend on the cellular context.

Despite all these intricacies, the same rationale for targeting p75 as for TrkC.T1 in disease has generally been accepted. P75 expression tends to be much higher during development of the nervous system, whereby it plays a 'negative' role in pruning synaptic connections and the killing off of extraneous cells. In the normal, adult nervous system, p75 remains at very low levels. Interestingly, in many disease cases, p75 levels rise and trigger the pathological loss of neurons. The overexpression of p75 may be the result of transcriptional activation via numerous factors, as the nervous system undergoes a pathological transition back into a developmental state [13]. P75 mediated signals through messengers such as TNFa contribute to neurotoxicity. As such, the receptor can be typified as being primarily pro-death in nature, so its blockade is of therapeutic value. A noteworthy point following these observations is that since neurotrophins bind p75, their positive effects may be undermined when p75 is upregulated.

Although over-generalizing can be detrimental, it is done so here to highlight the power of simplicity. In the context of therapy the relations between TrkC.T1 and p75 are abundantly clear. Both receptors are important for proper nervous system development, with p75 generally involved in many of the neurodegenerative diseases under study and exhibiting a broad expression pattern among neuronal and glial cell types. TrkC.T1 expression tends to be more limited, and as such may have more relevance for particular pathologies. Nonetheless, both TrkC.T1 and p75 are enzymatically inactive although engage in diverse signaling mechanisms,

are upregulated in disease, and promote toxicity through TNFa. They also both pose as barriers to neurotrophin-based therapies by counteracting their effects.

Overview of RET

The RET receptor is one that continues to maintain an element of mystery. Its initial discovery was accidental, and at the time revealed a new and unusual tenet of cell biology. Transfection assays in mouse fibroblasts using human lymphoma DNA identified a highly oncogenic gene which was not present in the same manner is in the primary lymphoma. It was concluded that a DNA rearrangement had occurred following transfection, activating the oncogene [14], and thus the name REarranged-during-Transfection was born. Further work revealed the protein possessed a transmembrane sequence and a C-terminal domain highly homologous to the tyrosine kinase family [15], securing its place as a receptor tyrosine kinase (RTK). Some years later, Lin and colleagues isolated a growth factor secreted by glial cultures, with impressive trophic capabilities in dopaminergic neurons [16].

Eventually the link between RET and GDNF had been established [17], but in another twist it was found that GDNF could not functionally activate RET on its own, despite evidence for direct interaction. The GFRa1 co-receptor had been cloned, and proved to be necessary for GDNF signaling through RET [18]. Since GFRa1 was membrane bound, but could also function with GDNF when tested in soluble form, the first models of the signaling cascade were proposed. The GDNF/GFRa1 heterodimer formed the initial complex, acting as a bridge connecting two RET monomers together. This was thought to cause activation of the intracellular kinase domain, and therefore recruit adaptor proteins involved in transmitting the trophic signals observed. The notion was further solidified by the discovery of oncogenic RET mutations which resulted in RET-dimerization and a constitutively active kinase [19].

Other ligand complexes were discovered; neuturin, artemin, and persephin along with their corresponding GFRa2, 3, and 4 partners, painted an unusual picture for any resident RTK expert. Each ligand displayed a preferential binding affinity for its associated GFRa, however lower affinity interactions, between GDNF and GFRa2 for example, were found to be possible and perhaps biologically relevant [20]. The expression patterns of RET and the GFRas became increasingly diverse, and it was clear that this receptor played instrumental roles during

development and in maintenance of the nervous system, as well as in peripheral tissues such as the kidney and testis. RET was becoming an attractive target for neurodegenerative therapy, although its bizarre signaling characteristics made any drug development a daunting task.

Mechanisms of RET Signaling

As the story of RET unfolded, further insights were made which shaped the understanding of RTK biology as a whole. Key experiments creating GDNF mutants which were deficient in GFRa1 binding , yet were still RET-activating, demonstrated the likelihood that pre-formed complexes at the membrane were present [21]. This led to a refining of the RTK signaling scheme, perhaps best referred to as the 'dynamic equilibrium model' [22]. Here, fluid associations between RET and the GFRas exist, ultimately causing the formation of an inactive RET/GFRa complex, with a small fraction being active. The presence of a ligand such as GDNF therefore shifts the equilibrium to favor an active conformation, and a biologically relevant signaling event. This has also been suggested for the related TrkA receptor, albeit on a simpler scale compared to RET [23]. The paradigm shift in receptor biology was monumental for drug development. It validated early claims that small molecules could be made to engage these massive proteins and induce conformational changes [24], a concept that defied logic under the older models.

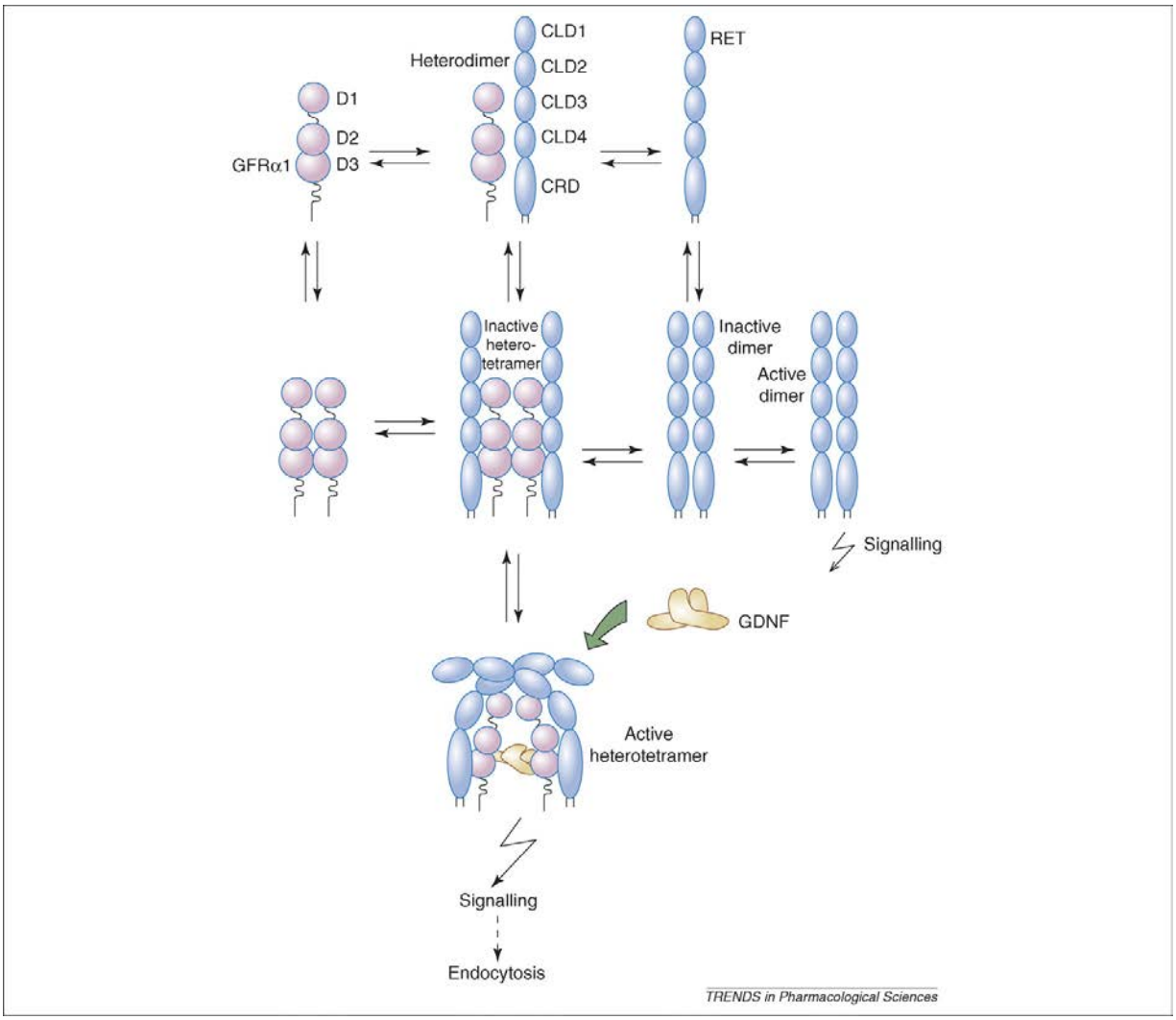

Figure 1.3: RET tyrosine kinase signaling as a dynamic equilibrium

RET signaling is unlikely to be an "all or nothing" event. A plausible scenario involves the continuous formation/deformation of multimers on the membrane surface. For example, a complex of two molecules of RET and its co-receptor GFRa1 could exist in a preformed, inactive state. Ligand binding, such as that of GDNF, stabilizes the conformation necessary to activate the kinase domain inside the target cell. This view of a more dynamic signaling scheme strongly supports the fact that small molecules can induce similar signaling outcomes, despite their limited size and surface area. Figure is adapted from GDNF family receptor complexes are emerging drug targets, Maxim Bespalov, Mart Saarma, *Trends in Pharmacological Sciences* 28, 68-74 (February 2007)

An activated RET complex transmits a conformational change through its transmembrane domain and into its intracellular kinase region. The kinase is then able to autophosphorylate several critical tyrosine residues along the RET C-terminal tail. These serve as specific interaction sites for adaptor proteins bearing src-homology 2 or phosphotyrosine-binding domains. In particular, the Tyr1062 residue is noteworthy since its phosphorylation status is linked to the PI3K/Akt and ERK pathways, both regulators of cellular survival and differentiation.

RET-based therapies in degenerative disease, and relevance of GFRas

As GDNF was discovered through its trophic effects on dopaminergic neurons, the connection to diseases like Parkinson's is clear. Indeed, GDNF in particular has shown efficacy in animal models of Parkinson's, and created high expectations for RET and its family members as valid targets. Hence, the subsequent failure of GDNF in these trials was disappointing.

Retinal degenerative conditions like RP, Glaucoma, and Diabetic Retinopathy are currently incurable though may benefit from a RET-based approach. Retinal neurons and glial cells are known to express RET, and there is a solid rationale stemming from numerous animal studies. The major issue with much of this work is that GDNF must be repeatedly administered in some fashion in order to be efficacious, which increases the occurrence of side effects. Viral vectors and infusion pumps serve as a handy proof-of-concept, but they offer little in the way of therapeutic relevance at the present moment.

The bottom line is that complex and invasive administration methods are necessary because large proteins are unsuitable drug candidates. Poor diffusion from the delivery site is a major weakness that has likely contributed to clinical failures [25]. This is not only due to sheer size but also in part to interactions with heparan sulfates, components of the extracellular matrix [26]. Recent work with mutant proteins lacking the heparan sulfate binding domain have improved their kinetic properties to an extent [27, 28], although they still cannot be given systemically since they are unable to cross the blood-brain-barrier. Moreover, protein preparations are unstable and so special consideration must be given to proper storage. They are

inherently very costly to produce, and quality-control is more difficult; these traits that make the proteins hard to apply as pharmaceutical agents.

Aside from the obstacles in delivering endogenous RET ligands, it is important to consider the influence that GFRas may have. GFRa1 has been shown to act as a negative regulator of RET signaling, and this may impact the efficacy of a given treatment within diseases states. To build upon this notion, there are instances whereby RET expression appears to be stable throughout disease progression, however there are dynamic changes in GFRa expression [29, 30]. Moreover, soluble forms of GFRas may also be liberated and have biological consequences. The roles of the GFRas can be troublesome to study and/or model in the context of therapeutic interventions. Clearly, this presents additional challenges that must not be left unaddressed when validating a target like RET. Overall though, RET can be viewed as a positive modifier of the trophic imbalances that commonly occur in diseased states. Progress has stagnated simply because the tools at our disposal are limited.

Conclusion: The Advantages of Small Molecules

As mentioned previously, the world of small molecule development is a burgeoning one, and much advancement has been made in recent years [31]. It is important and also encouraging to recognize that this approach offers us not only new ways to intervene in disease, but also to examine pathological mechanisms.

This body of work contributes to these concepts, and is meant to showcase the value in correcting disease phenotypes from both sides of the balance; mitigating toxicity through antagonism, or driving trophic signals through agonism. The deleterious roles of p75 and TrkC.T1 are being uncovered, and targeting them will undoubtedly be a focus for therapy in the years to come. Our discovery that RET can be targeted directly is a major leap forward because it navigates around the complexity of the GFRas. It also allows for the study of how GFRas may influence the signaling and functional outcomes of a ligand. The success of any drug development initiative depends on being aware and accounting for as many variables as possible.

These unknown variables extend into the very identity of the material one is working with. The work is also meant to be a cautionary tale of the pitfalls in screening from large

chemical databases. While being a wealthy resource for advancement of research, it can potentially cause setbacks since many of these 'compounds' are in fact complex mixtures and/or are incorrectly characterized altogether. In a scientific climate where data reproducibility is often called into question, having certainty in what is being tested can be a deciding factor in whether or not a development project continues.

Rationale and Objectives

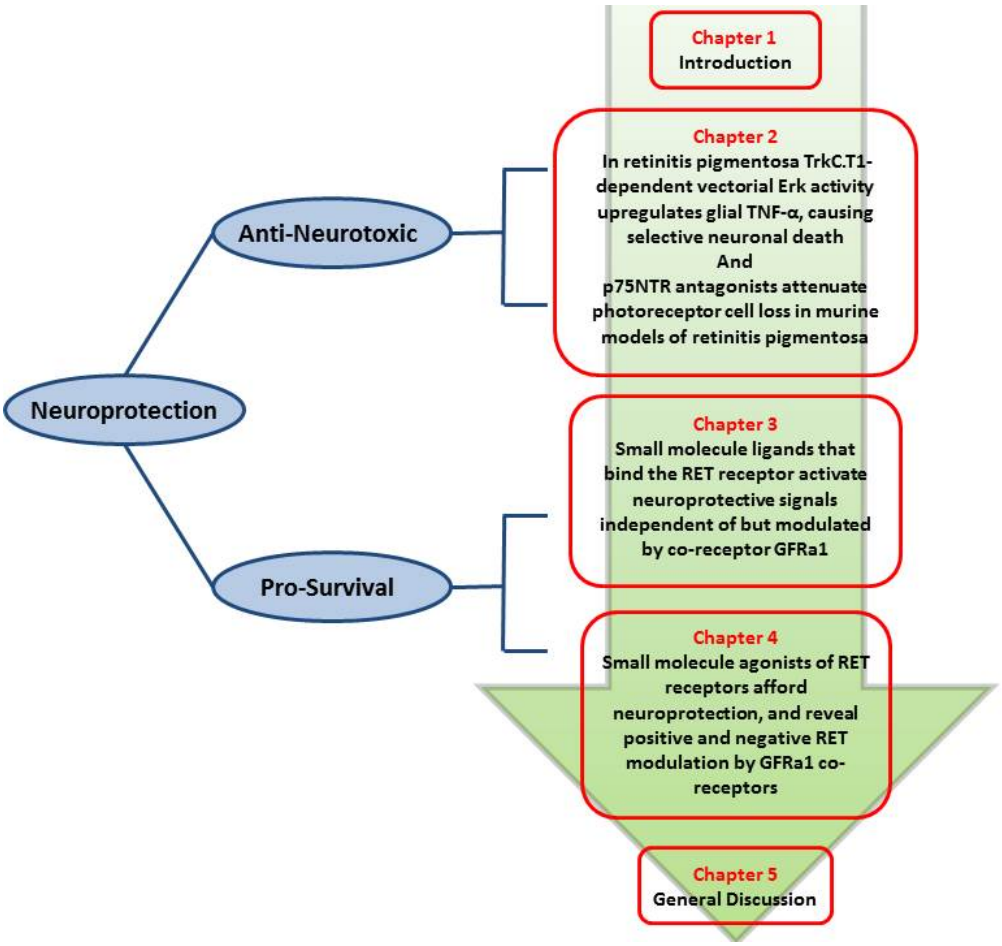

As mentioned in the **Chapter 1**, the neurotrophin signaling axis is worthy of exploration in a therapeutic context. The overarching goal of this work is to use small molecule-based

approaches as a means to examine receptor biology and further validate disease targets. This was achieved using a two-pronged strategy that falls in line with the trophic imbalance hypothesis of neurodegeneration.

Chapter 2 takes a look at the anti-neurotoxic side of the balance, and attempts to rescue neuronal loss through the targeting of TrkC.T1 and p75. We reveal some novel insights into the deleterious roles these receptors play in a retinal degeneration model, and demonstrate the therapeutic potential of small molecule antagonists. **Chapters 3 and 4** look at neuroprotection by driving pro-survival signals, and herein we outline the discovery and characterization of agonists at the RET tyrosine kinase receptor. These molecules were used to study RET/GFRa1 interactions on a level not previously possible, owing to the lack of biological tools at our disposal. Additionally, they showcase the strengths in activating RET directly, and lend more credence to its value as a disease-modifying target. Lastly, **Chapter 5** takes a broad look at all of the findings and serves to tie together several key points relating to the relevance, utility, and challenges of small molecule development in degenerative disease.

Chapter 2

In Retinitis Pigmentosa TrkC.T1–dependent vectorial Erk activity upregulates glial TNF-α, causing selective neuronal death

Alba Galán [1], Sean Jmaeff [1, 2], Pablo F. Barcelona [1], Fouad Brahimi [1], Marinko V. Sarunic [4], and H. Uri Saragovi [1,2,3,*]

[1] Lady Davis Institute-Jewish General Hospital, McGill University, Montréal, QC, Canada H3T 1E2.

[2] Department of Pharmacology and Therapeutics, McGill University, Montréal, QC, Canada

[3] Department of Ophthalmology, McGill University, Montréal, QC, Canada

[4] School of Engineering Science, Simon Fraser University, BC, Canada

[*] corresponding author

Abstract

In some diseases the TrkC.T1 isoform is up-regulated in glia, associated with glial TNF-α production and neuronal death. What remains unknown are the activating signals in glia, and how paracrine signals may be selective for a targeted neuron while sparing other proximate neurons. We studied these questions in the retina, where a Müller glia contacts photoreceptors on one side and Retinal Ganglion Cells on the other. In a mutant Rhodopsin mouse model of Retinitis Pigmentosa (RP) causing progressive photoreceptor death –but sparing Retinal Ganglion Cells– TrkC.T1 and NT-3 ligand are up-regulated in Müller glia. TrkC.T1 activity generates p-Erk, which causes increased TNF-α. These sequential events take place predominantly in Müller fibers contacting stressed photoreceptors; and culminate in selective death. Each event and photoreceptor death can be prevented by reduction of TrkC.T1 expression, by pharmacological antagonism of TrkC, or by pharmacological inhibition Erk. Unmasking the sequence of non-cell autologous events and mechanisms causing selective neuronal death may help rationalize therapies.

Introduction

Retinitis pigmentosa (RP) is an inherited degenerative retinal disease characterized by progressive apoptosis of photoreceptors that ultimately leads to irreversible loss of vision [32]. Photoreceptors death can be triggered by one of more than 250 gene mutations [33-35]. There are no effective treatments that can halt or reverse the disease due to the extremely heterogeneous nature of the mutations, and the poor understanding of molecular mechanisms that cause photoreceptor cell death. Here, we investigate a disease mechanism that could yield a disease-modifying target.

Inflammatory events such as expression of glial TNF-α are clearly involved in photoreceptor degeneration [36, 37]. The mechanisms that activate retinal TNF-α production in disease remain unclear, and may involve the mitogen-activated-kinase (MAPK) ERK1/2[38, 39]. Phosphorylation/activation of ERK1/2 can play multiple and seemingly opposite roles from pro-survival to pro-death / pro-inflammatory pathways [40]. However, very few studies have ascribed a clear function to ERK1/2 in the injured retina [41] and the underlying mechanisms leading to ERK1/2 activation during disease remain unknown.

Neurotrophins are a family of protein growth factors -NGF, BDNF and NT-3- that regulate the nervous system and other tissues. All the neurotrophins bind the p75 receptor whose function is generally associated with pro-death signals in many neurodegenerative diseases, including retinopathies [42-45]' [46]. The neurotrophic activities are mediated by selective ligand binding to the Trk family of receptor tyrosine kinases (TrkA, TrkB, TrkC and p75). NGF binds to TrkA, BDNF binds preferentially to TrkB [47], whereas NT-3 interacts mainly with TrkC but also with TrkA [48]. Survival is mediated by full-length kinase active Trk receptors [49-52], but there are also truncated isoforms that lack kinase activity.

Here, we postulated that a truncated TrkC receptor isoform (TrkC.T1) may be implicated in RP pathology, in analogy to other neurodegenerative diseases [8, 10]. A single *TrkC* locus transcribes mRNA encoding for full length TrkC (TrkC-FL), and the mRNA can be alternatively spliced to a truncated isoform TrkC.T1 mRNA that lacks the kinase domain and gains a short new intracellular domain with new signaling properties. Both TrkC-FL and TrkC.T1 are bound and activated by the growth factor Neurotrophin-3 (NT-3). However, ligand activation of each

receptor yields a different functional outcome. Because TrkC.T1 is upregulated in disease [8, 10], its signals prevail. TrkC.T1 has a dominant negative function upon TrkC-FL [53, 54], and can activate Rac1 signals [5] to cause neuronal death in a paracrine manner [8, 10].

For example, in glaucoma models caused by high intraocular pressure, TrkC.T1–dependent secretion of TNF-α by Müller cells is etiological to the degeneration of Retinal Ganglion Cells (RGCs) [8], the neuronal population specifically affected in this disease. It is intriguing that while RGCs die in a TrkC.T1-dependent manner other neuronal populations remain unaffected in early stages of glaucoma. This is especially curious given that TrkC.T1 expression occurs in Müller glia and not in injured RGCs.

Here, we use the RHOP347S (Rhodopsin mutant, RHOP) mouse model of RP to examine the mechanism of TrkC.T1 in the *selective* death of photoreceptors, the neuronal population specifically affected in this disease; and to elucidate TrkC.T1 intracellular signaling events leading to TNF-α–mediated photoreceptor death. We provide genetic, anatomical, and pharmacological evidence showing that during RP disease Müller glia upregulates TrkC.T1 and its ligand NT-3, to activate p-Erk, causing increased TNF-α, which induces photoreceptor degeneration. The mechanism accounting for the selective impact on photoreceptors may relate to these signals in Müller cell fibers being “vectorial” in the direction of stressed photoreceptors. Our data point to a non-cell autologous or paracrine mechanism of photoreceptor cell death. This is the first evidence that shows the relevance of TrkC.T1 in RP, and disease mechanisms that may help rationalize therapies for retinal degenerative pathologies.

Materials and Methods

Cell lines

HEK293 cells were transfected with human full-length *TrkC* cDNA (293-TrkC-FL) or with rat *TrkC.T1* cDNA (293-TrkC.T1). The cells are stably transfected subclones that express high levels of TrkC-FL or TrkC.T1 receptors and are respectively grown under drug selection (0.5 mg/ml G418 or 1 mg/ml Puromycin). The rat glial cell line, rMC-1, was kindly donated by Dr. Adriana Di Polo. rMC-1 has been previously characterized [55].

RNAi knockdown of TrkC.T1

A short hairpin RNA (shRNA) specifically targeting a unique 3' sequence of the TrkC.T1 mRNA was designed using the DSIR algorithm (http://biodev.cea.fr/DSIR/DSIR.html). The TrkC.T1-targeting shRNA sequence 5'-GGACAATAGAGATCATCTAGT-3', or a scrambled control sequence 5'-CCTAAGGTTAAGTCGCCCTCG-3' were cloned into a pLKO.1 lentiviral shRNA-expression vector. pLKO.1^{scrambled} and pLKO.1$^{TrkC\text{-}T1}$ lentiviral vectors were packaged in HEK-293T cells and active viral particles were purified. rMC-1 cells were then transduced with lentiviral particles, and selected with 1 mg/ml puromycin. TrkC.T1-specific depletion (and no effect upon TrkC-FL expression) was determined by real-time quantitative PCR and by Western blotting. Levels of p-Erk and p-Akt were quantified in rMC-1 cells treated with NT-3, and to assess TrkC.T1–dependence its expression was silenced using PLKO.1TrkC.T1 lentivirus that destabilizes TrkC.T1 mRNA[10].

Animal models

All animal procedures respected the IACUC guidelines for use of animals in research, and to protocols approved by McGill University Animal Welfare Committees. All animals were housed under a 12 hour dark-light cycle with food and water *ad libitum*. Wild-type (WT) healthy C57/BL6 mice were used as experimental controls. Previously we used the truncated TrkC.T1 knockout mouse [8], and the "RHOP347S" transgenic mouse (Rhodopsin mutant) model of retinitis pigmentosa (termed RHOP in the experimental designs) was kindly donated by Dr. T. Li. Rhodopsin mutant is exclusively expressed in photoreceptors and generates stress in these

cells due to protein misfolding. Both mice models were consistently backcrossed onto a pure C57BL/6J (B6) background.

The RHOP347S (RHOP) mice were crossed with homozygous TrkC.T1 knockout mice (TrkC.T1$^{-/-}$) to generate the RHOP:TrkC.T1$^{+/-}$ genotype (retinitis pigmentosa-diseased mice, TrkC.T1 heterozygous; hereafter RHOP:T1). These mice express the RHOP mutant gene, lack the ability to produce TrkC.T1 mRNA from one allele, and have 50% less TrkC.T1 protein. Homozygous TrkC.T1$^{-/-}$ mice do not have any abnormality and are viable [8]. However, the complete deletion of TrkC.T1 (TrkC.T1$^{-/-}$) in RHOP mice yields small size-litters, and low-weight offspring with some mice showing abnormal small eyes, and do not open the eye lids normally. Therefore, only heterozygous RHOP:T1 mice were used experimentally.

Genotypic screening

We used a PCR-based method for subsequent genotyping of the animals. Screening of TrkC.T1 was done using the same conditions as previously described in our laboratory [8]. We used the following primers: RM015 Rho F 5' GGATTCTGTTTGACATGGGG 3' and RM016 Rho R 5' TCCAGTCAGGACTCAAACCC 3' for RHOP mice screening, and forward 5' ACCACAGTCCATGCCATCAC 3' and reverse 5' TCCACCACCCTGTTGCTGTA 3' for GAPDH controls. PCR reactions were done using the "Extracta ^{TM} DNA Prep for PCR-Tissue" kit (Quanta Biosciences, MD, USA). All PCR conditions were performed as follows: 35 cycles at 96°C for 2 minutes, 94°C for 30 minutes, 58°C for 30 minutes; 35 cycles at 72°C for 40 minutes, 72°C for 7 minutes.

Intravitreal injections

Intravitreal injections were performed as previously described [43]. Briefly, mice were anesthetized with 3% isoflurane, delivered through a gas anesthetic mask. The drugs were delivered using a Hamilton syringe. Injections were done using a surgical microscope to visualize the Hamilton entry into the vitreous chamber and confirm delivery of the injected solution. After the injection, the syringe was left in place for 30 sec and slowly withdrawn from the eye to prevent reflux. Experimental right eyes were injected with the test agents and control left eyes serve as internal control.

Drug regimen

Pharmacological inhibition: All intravitreal injections delivered 2 µl of the MAPK/ERK inhibitor PD98059 (10 mM stock) or the selective-TrkC antagonist KB1368 (1mM stock). Control eyes were injected with 50% DMSO vehicle for PD98059 assays or 5% DMSO vehicle for KB1368 assays. Intravitreal injections in wild-type or RHOP-mice were done at post-natal day 17 (PN 17). Experimental time points to measure ONL thinning were set at PN day 18, 22, 24 and 28. The effect of the compounds on the expression of p-Erk and p-Akt was analyzed at PN day 18 (24 hours after intravitreal injection).

NT-3 stimulation: Cells were uninfected (control) or infected with control lentivirus pLKO-$1^{scrambled}$, or with pLKO-$1^{TrkC.T1}$ that specifically reduces TrkC.T1 mRNA. Cells were serum-starved for 1 hour, then treated with vehicle or 4 nM NT-3 for 10 min. Then, cells were collected and processed for Western blot analysis.

Optical Coherence Tomography imaging

We used non-invasive spectrometer-based Fourier-Domain Optical Coherence Tomography FD-OCT techniques in longitudinal studies to quantify the structural changes occurring during the progressive retinal degeneration in the RHOP transgenic model of RP. FD-OCT is a noninvasive method that allows time-kinetic studies in the same animal, with axial resolution in tissue nominally better than 3 µm and repeatability of the measurements from B-scans better than 1 µm. Data acquisition was performed using custom software written in C++ for rapid frame grabbing, processing, and display of two-dimensional images [56, 57]. Manual segmentations were used to measure the thicknesses of the mice retinas. During retinal scanning, three volumes (~5 s/vol) were acquired in different sectors of the retina using the ON head as landmark. After processing, three B-scans were randomly selected from each volume.

The retinal thickness measurements were performed with Image J software using the saved data. In each B-scan, the thickness of the Nerve fiber layer–Ganglion cell layer (GCL)–Inner plexiform layer , hereafter referred to as NGI and outer nuclear layer (ONL), where the cell body of the photoreceptors reside, was measured at three adjacent points, as described [43]. Measurements of the NGI controlled for the photoreceptor specificity of the damage. Data are

shown for wild-type (WT), RHOP and RHOP:T1 as average ONL thickness in μm ± SEM (absolute values), or as average of percent ONL thickness ± SEM (relative values). For relative values, each vehicle-treated eye (left eye) was set as 100% *versus* the drug-treated eye (right eye).

Fluorescence "In situ" hybridization (FISH)

The RNA probes for the "in situ" hybridization were prepared as described. For TrkC.T1, the mouse TrkCT1-specific sequence of exon 13b and 14b and the subsequent 286 bases of the 3′ un-translated region [5]; for NT-3, a 392 base pair region of rat genomic DNA corresponding to bases 481-873 of the rat NT-3 cDNA sequence [58] was cloned into the pBluescript II KS(+) phagemids; for TNF-α**,**. a 235 base pair region of mouse genomic TNF-α corresponding to base 837-1072 was synthesized by PCR using Forward: 5`-gagtccgggcaggtctacttt-3' and Reverse: 5` taatacgactcactatagggagacaggtcactgtcccagcatct-3' primers for the sense probe; and Forward 5`-taatacgactcactatagggagagagtccgggcaggtctacttt -3' and Reverse 5`-caggtcactgtcccagcatct3' primers for the antisense probe. Fluorescence "in situ" hybridization was done as described [43]. Briefly, retinal sections (20 μm thick) were mounted onto gelatin-coated glass slides, re-fixed in 4% PFA, permeabilized with proteinase K and acetylated. Hybridization was carried by incubating the slides with either 200 ng/ml of digoxigenin-labeled TNFα or TrkC.T1 or NT-3 antisense RNAs probes overnight at 72° C in a hybridization oven (Robbins Scientific). As controls, hybridization with either 200 ng/ml of digoxigenin-labeled TNFα or TrkC.T1 or NT-3 sense RNAs probes was performed on sequential slides in parallel using the same experimental conditions. Images were obtained using an IX81 confocal microscope (Olympus) equipped with Fluoview 281 3.1 software (Olympus).

Histology, image acquisition and data analysis

The eyes were enucleated and immersed for 1 hour in fixative composed of 2% glutaraldehyde in PBS at room temperature. After, cornea was removed and the eye cups were placed in fresh 2% glutaraldehyde and incubated on nutator, overnight at room temperature. The eye cups were dehydrated in ascending grades of reagent alcohol and embedded into epon resin. Sections (800 nm thick) were cut on a LKB ultratome (LKB 2088 Ultrotome V, Sweden) and

placed onto Superfrost Plus Slides (Fisher Scientific, ON, Canada). Slides were stained with 1% toluidine blue and mounted with Permount (Fisher Scientific, ON, Canada).

Images were collected using the Leica DM LB 2 microscope equipped with the LAS acquisition software and a Leica DFC480 camera for detection, applying a 40X objective. Images were saved directly in TIF format and adjusted using Adobe Photoshop CS8.0 for unbiased brightness and contrast. For each experimental condition, 6 images were acquired from 3 sections cut from different areas of the retina (n=2 retinas per group) starting at 500 μm from the optic nerve head to avoid thickness variability due to the thinning of the retinal layers close to the boundaries of the optic nerve. The number of photoreceptors nuclei contained inside a rectangle of a fixed area (0.0156 mm^2), drawn in the ONL, was counted using ImageJ software (developed by Wayne Rasband, National Institutes of Health, Bethesda, MD, USA; http://imagej.nih.gov/ij). Data are shown as the average number of cells per mm^2 ± SEM.

Immunohistochemistry, image acquisition and data analysis

After enucleation, the eyes were immersed overnight in fixative composed of 4% PFA in PBS at 4°C, followed by cryoprotection by soaking in 30% sucrose overnight at 4°C. Eyes were frozen in O.C.T tissue TEK and cryostat sections were cut and mounted onto gelatin-coated glass slides. Sections (20 μm thick) were washed with phosphate-buffered saline (pH 7.4, PBS) and then, incubated in PBS containing 5% normal goat serum and/or 5% normal donkey serum, 0.3% Triton X-100 and 0.5% bovine serum albumin (BSA) for 2 hours. After, sections were incubated overnight at 4°C with primary antibody (Table 1). The 2B7 (anti-TrkC-FL) antibody is specific for the full length TrkC receptor [10], whereas TrkC.T1 antibody (Rockland) specifically recognizes the TrkC.T1 isoform, but not full length TrkC. The sections were rinsed and incubated with secondary antibody (**Table 1**) for 1-2 hours at room temperature. Finally, sections were washed and cover-slipped using Permafluor (Thermo Fisher Scientific, Fremont, CA, USA) or Vectashield mounting media with DAPI.

Images were collected using a Leica DMI6000 B microscope equipped with the Quorum technologies WaveFX spinning disk confocal microscopy system, the Volocity software, and a high dynamic ImagEM EM-CCD camera for detection. Pictures were taken as Z-stacks of

confocal optical sections applying a 20X objective. Images were exported directly in TIF format and adjusted using Adobe Photoshop CS 8.0 for unbiased brightness and contrast.

For each experimental condition, a minimum of 6 images were acquired from 3 sections cut from different areas of the retina (n=3-4 retinas per group). The area of the profiles of the cells expressing p-Akt and p-Erk was measured using ImageJ software. For the "in situ" studies, an arbitrary rectangle of 129 x 97 pixels was drawn for each layer of the retina (GCL, IPL, INL and PhR) to measure the TrkC.T1 positive staining using ImageJ. Data are shown as the average area (in pixels) ± SEM or as normalized area values ± SEM, with WT being set to 1 (100%).

Table 3.1. **Details of antibodies used for immunohistochemistry**

Primary antibodies

Specificity	Source	Clone	Company	Dilution
Protein Kinase C	Mouse	MC5	Sigma	1:100
CRALBP	Mouse	B2	Cedarlane	1:200
Glutamine synthetase	Mouse	Monoclonal	Millipore	1:500
p44/p42 MAPK (Erk1/2)	Rabbit	Polyclonal	Cell Signaling	1:25
Phospho p44/p42 MAPK (Erk1/2) (Thr202/Tyr204)	Rabbit	Polyclonal	Cell Signaling	1:200
Phospho-Akt (Ser473)	Rabbit	D9E	Cell Signaling	1:100
Akt	Rabbit	Polyclonal	Cell Signaling	1:1000
TrkCT1	Rabbit	Polyclonal	Rockland	1:100
2B7 (anti-TrkC-FL)	Mouse	Monoclonal	Dr. Saragovi	1:1000
Actin	Rabbit	Polyclonal	Sigma	1:1000
NT-3	Rabbit	Polyclonal	Santa Cruz	1:100

Secondary antibodies

Specificity	Source	Clone	Company	Dilution
Rabbit IgG	Goat	Alexa Fluor 488	Invitrogen	1:200
Mouse IgG	Goat	Alexa Fluor 594	Invitrogen	1:200
Mouse IgG	Donkey	Rhodamine-Red-X	ImmunoResearch	1:200
Rabbit IgG	Goat	Peroxidase	Sigma	1:5000

Retinal organotypic cultures

Whole eyes were enucleated and whole retinas dissected from wild-type and RHOP347S mice at PN day 18. Retinas were used for organotypic culture experiments in 24 well plates

containing 500 µl of culture medium (DME/F12 supplemented with 10 mM $NaHCO_3$, 100 µg/ml Transferrin, 100 µM Putrescine, 20 nM Progesterone, 30 nM $Na2SeO_3$, 0.05 mg/ml Gentamicin, 2 mM L-Glutamine, and 1 mM Sodium Pyruvate). Under sterile conditions, the media was gently removed and replaced with fresh media containing the treatments or controls, and incubated at 37°C and 5% CO_2 for 24 hours.

TUNEL staining

Staining was performed using the DeadEnd Fluorometric TUNEL system (Promega). Vehicle or KB1368 treated RHOP347S retinas in culture (n=6) were first fixed in 4% PFA in PBS and kept at 4°C overnight. Then, the sections were washed with PBS-0.2% BSA and permeabilized using 2% Triton-X in PBS. Retinas were then incubated with 20µg/mL Proteinase K in PBS for 15 minutes, briefly re-fixed in PFA for 30 minutes and washed again with PBS-0.2% BSA before being transferred into Eppendorf tubes. Samples were incubated with 50µL of equilibration buffer for 20 minutes, then 25µL of TdT reaction mixture for 2.5 hours at 37°C. The reaction was terminated using a 30-minute incubation of 2XSSC solution. The retinas were washed and mounted between two coverslips with the ganglion-cell layer facing up using Vectashield with DAPI as this was easier to achieve given the natural curvature of the retina. The cover-slipped samples were then flipped over and taped to microscope slides to have the photoreceptor-side facing up. For image acquisition, the retinas were divided into 4 quadrants, and 2 pictures with a 20X objective were taken in each area (one central and one peripheral) for a total of 8 images of the outer-nuclear layer (ONL) per retina. Total TUNEL-positive cells were counted in each image semi-automatically (ImageJ) by 3 independent blinded examiners. Wild-type retinal flat mounts were used as negative controls.

Western blots

Whole retinas either from culture or freshly dissected were collected and added to 200µL lysis buffer (20mM Tris-HCl pH 7.5, 137mM NaCl, 2mM EDTA, 1% Nonidet P-40) containing a protease inhibitor cocktail (Roche). Samples were sonicated briefly and left on ice for 30 minutes before centrifuging and obtaining the supernatant. Protein quantities were assessed using the Bradford assay (BioRad), and 40µg of total protein was mixed with Laemmli buffer, boiled

for 5 minutes and loaded onto 10% gels. After transferring to PVDF membranes, a blocking step of 1 hour in 2% BSA was done, followed by an overnight incubation at 4°C with the primary antibodies. Membranes were washed repeatedly then incubated for 1 hour with secondary antibody, washed again and developed using Western Lightning Plus ECL (PerkinElmer). Blots were scanned and quantified using ImageJ software. All primary antibodies were used at a 1:2000 dilution and secondary antibodies at a 1:10000 dilution. To detect total protein for loading controls, membranes were stripped with 62.5 mM Tris-HCl pH 6.8, 2% SDS, and 0.7% 2-Mercaptoethanol at 55°C for 15 minutes, followed by extensive washing, blocking, and re-incubation with the primaries as just described.

Statistical Analysis

Results are presented as mean ± SEM for all studies. One-way analysis of variance with significance $\alpha=0.05$ or higher were used for processing data. Bonferroni post-hoc analysis was used for calculating significance between groups. Two-tailed student t-test was used to test for significance between two means.

Results

Rhodopsin mutation causes progressive thinning of the ONL

The thinning of the ONL is detectable as early as PN day 18, and rapidly decreases by ~33% ($p<0.001$) at PN day 24, and by ~60% ($p<0.001$) at PN day 28, compared to wild-type retinas (**Figure 1A**). NGI measurements were 46.13 μm ± 0.727 in wild-type mice, and 46.71 μm ± 0.98 in RHOP mice at PN day 24. Therefore, these retinal layers are not affected in RP. These data corroborate that rhodopsin mutation causes progressive thinning exclusively in the ONL, but not in rhodopsin–unrelated retinal layers such as the NGI. The PN day 28 was the experimental endpoint because the ONL is no longer measurable unbiasedly beyond this time point.

TrkC.T1 heterozygosity delays thinning of the ONL in RHOP mice

We previously demonstrated that deletion of TrkC.T1 reduces RGC death in glaucoma, a model where RGCs are stressed and degenerate [8]. Thus, we examined whether TrkC.T1 has an impact on the degeneration of the ONL in RP.

FD-OCT data showed that there is a significant delay in ONL thinning in RHOP:T1 mice compared to their RHOP littermates, from PN day 18 to PN day 24 (**Figure 1A and 1B**). However, at PN day 28, the ONL thickness was similar in both RHOP and RHOP:T1 retinas (**Figure 1A**). Similar results were obtained using quantitative histochemical techniques. (**Figure 1C and 1D**).

These data indicate that the deletion of TrkC.T1 has a temporary protective role in RP, and that 50% reduction of TrkC.T1 is sufficient to delay degeneration of the ONL in RHOP:T1 retinas.

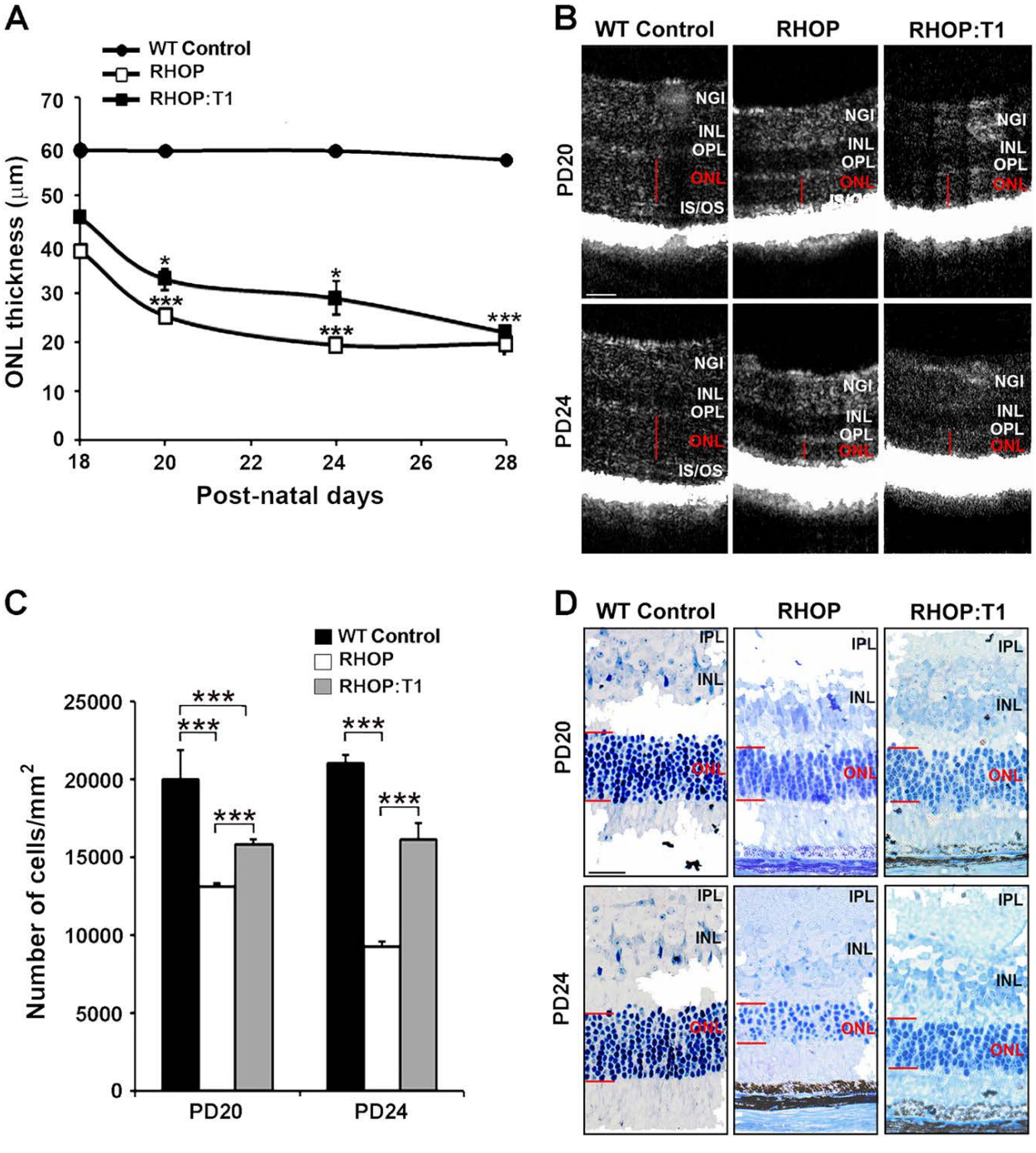
A
WT Control
RHOP
RHOP:T1
ONL thickness (μm)
70
60
50
40
30
20
10
0
18
20
22
24
26
28
Post-natal days
*
***
*
***
***
B
WT Control
RHOP
RHOP:T1
PD20
PD24
NGI
INL
OPL
ONL
IS/OS
C
WT Control
RHOP
RHOP:T1
Number of cells/mm2
25000
20000
15000
10000
5000
0
***
***
***
***
***
PD20
PD24
D
WT Control
RHOP
RHOP:T1
PD20
PD24
IPL
INL
ONL

Figure 2.1. TrkC.T1 depletion delays degeneration of the ONL during RP

(A) ONL average thickness measurements (± SEM) from FD-OCT images at PN days 18, 20, 24 and 28. The ONL thickness decreases over time in RHOP retinas compared to WT control. Note that the thinning of the retina is delayed in RHOP:T1 retinas compared with RHOP, n= 8-10 mice per group, ***p< 0.001 (RHOP *versus* WT) and *p< 0.05 (RHOP *versus* RHOP:T1). **(B)** FD-OCT representative retina images from WT, RHOP and RHOP:T1 mice at PN days 20 and 24, scale bar = 30 µm. **(C)** Quantification of the number of photoreceptors per mm^2 (average ± SEM) in ultrathin retinal sections. A total of 18 images were taken from n=2 retinas per group, ***p<0.001. Images were taken at 40X. **(D)** Representative images of ultrathin retinal sections at PN days 20 and 24, scale bar = 60 µm. Note that photoreceptor cells are stained in blue. NGI: Nerve fiber layer-Ganglion cell layer-Inner plexiform layer; IPL: inner plexiform layer; INL: inner nuclear layer; ONL: outer nuclear layer; IS/OS: internal/external segment.

TrkC.T1 is upregulated in retina glia Müller cells of RHOP mice

We have shown that TrkC.T1 is upregulated in glial cells in glaucoma, and in mouse and human ALS [8, 10]. Hence, we studied TrkC.T1 localization of mRNA and protein in wild-type and RP mice. In wild-type retinas there are low levels of TrkC.T1 mRNA, in the GCL and INL. In RHOP retinas, there was an increase of TrkC.T1 mRNA ($p \leq 0.01$) in the GCL and INL (**Figure 2A quantified in 2B**). In RHOP:T1 retinas there was a significant reduction of TrkC.T1 mRNA by ~50% in the GCL ($p \leq 0.01$) compared to RHOP mice, and a reduction of TrkC.T1 mRNA by ~25% in the INL (not statistically significant). There were no reductions in the IPL and the PhR layer, suggesting that there may be a preferential accumulation of TrkC.T1 mRNA in these anatomical sites. Control hybridization with TrkCT1 antisense mRNA in RHOP retinas fully depleted of TrkC.T1 (RHOP:T1 KO) and hybridization with sense TrkC.T1 mRNA in wild-type and RHOP retinas were negative (**data not shown**).

RHOP retinas had a robust increase of TrkC.T1 immunoreactivity in the IPL, and a moderate increase in the GCL, INL and PhR layers, compared with wild-type retinas. Interestingly, TrkC.T1 staining was detected surrounding the cell somata in the GCL, and intermingled with photoreceptors in the PhR layer. In RHOP:T1 mice, TrkC.T1 immunoreactivity was partially reduced in the GCL, IPL, INL and PhR layer ($p<0.01$), compared to RHOP retinas (**Figure 2C quantified in 2D**). TrkC.T1 signal was completely absent in RHOP retinas with full knock-out TrkC.T1, confirming the specificity of the TrkC.T1 antibody.

There were no significant differences in TrkC-FL protein between wild type retinas and any of the RHOP genotypes (**Figures 2E quantified in 2F**). TrkC-FL protein was present in neuronal retinal layers.

The TrkC.T1 immunohistochemistry results were consistent with the *in situ* mRNA hybridization data with the exception that the TrkC.T1 protein was strongly expressed in the IPL and PhR (**Figure 2C and 2D**), whereas TrkC.T1 mRNA levels were low in these areas. This observation suggests that TrkC.T1 protein may be transported from the Müller cell soma to the Müller fibers contacting neurons in the inner and the outer nuclear layers of RHOP mice.

These results demonstrate that TrkC.T1 is upregulated in glia during RP and that this upregulation takes place mainly in the INL and in the projections of Müller cells towards the IPL and PhR layers where photoreceptors reside. This change is TrkC.T1 happens without obvious alterations in TrkC-FL expression.

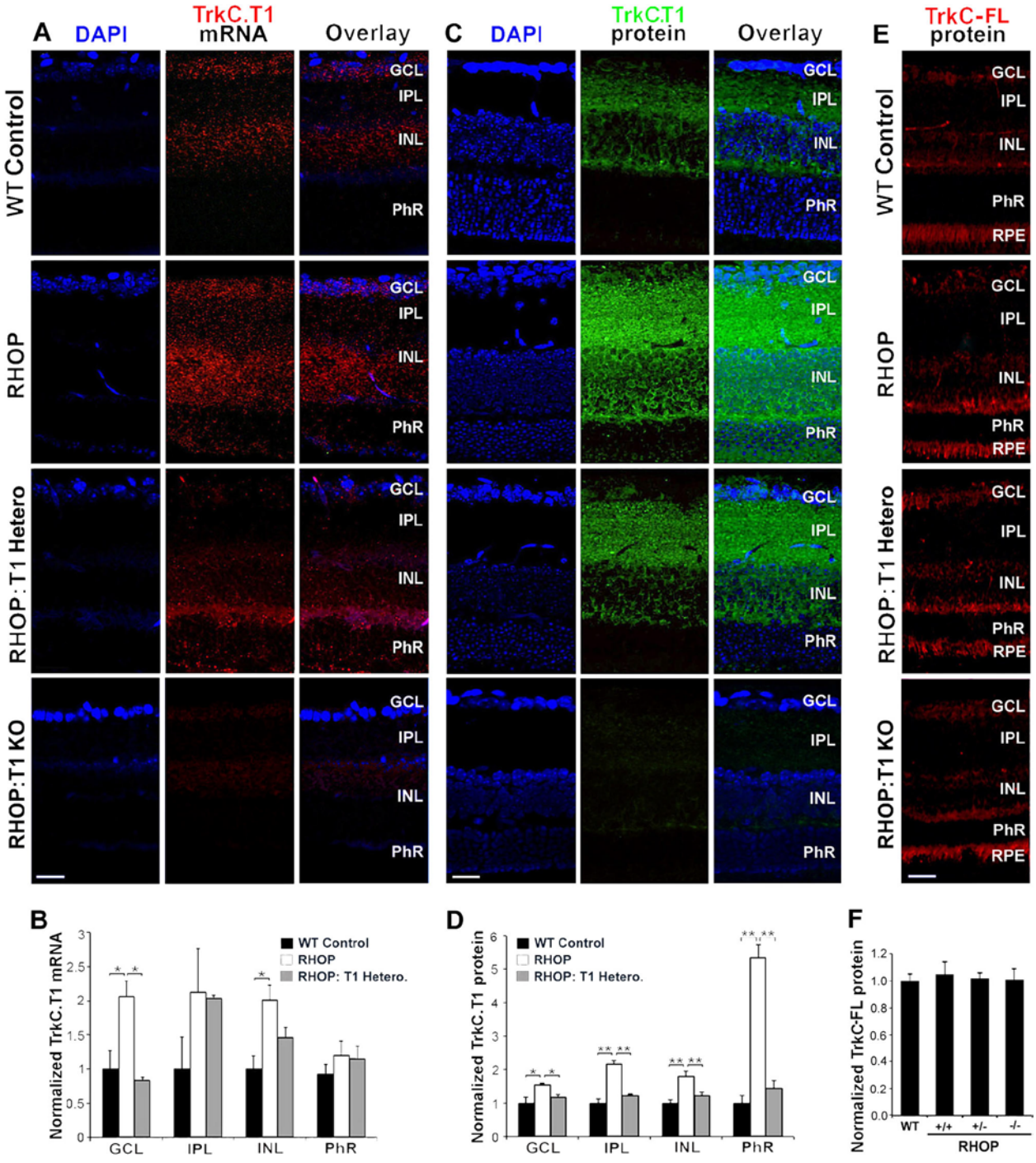

Figure 2.2. TrkC.T1 mRNA location and protein expression in healthy and RHOP retinas

(A) Fluorescence "In situ" hybridization (FISH) with TrkC.T1 mRNA antisense in WT, RHOP, RHOP:T1 heterozygote and RHOP:T1 KO (full TrkC.T1 knock-out) mice at PN day 24. **(B)** Histogram shows the quantification of the area of TrkC.T1 mRNA signal in the different retina layers. TrkC.T1 was markedly increased in the GCL and INL in RHOP retinas and

partially decreased in RHOP:T1. Data are represented as normalized TrkC.T1 mRNA area values (± SEM) relative to WT control values in each retina layer. A total of 18 images were taken from an n=3-4 retinas per group. **(C)** TrkC.T1 immunoreactivity in WT, RHOP, RHOP:T1 heterozygote and RHOP:T1 KO (full TrkC.T1 knock-out) mice at PN day 24. **(D)** Quantification of TrkC.T1 immunoreactivity in the different retina layers. TrkC.T1 immunoreactivity was increased in the GCL, IPL, INL and PhR of RHOP mice retinas whereas TrkC.T1 was decreased in RHOP:T1 eyes. Data are shown as normalized TrkC.T1 protein area values (± SEM) relative to WT control in the different retina layers. A total of 30-40 images were taken from an n=3-4 retinas per group. (**E**) TrkC-FL immunoreactivity in WT, RHOP, RHOP:T1 heterozygote and RHOP:T1 KO (full TrkC.T1 knock-out) mice. (**F**) Histogram shows the quantification of the area of TrkC-FL protein in the retina. No changes were observed among the different groups. Data are shown as normalized TrkC-FL protein area values (± SEM) relative to WT control. RHOP +/+: RHOP, wild-type TrkC.T1; RHOP +/-: RHOP, TrkC.T1 heterozygote; RHOP -/-: RHOP, full TrkC.T1 knock-out. A total of 10 images were taken from n=3 retinas per group. * $p< 0.01$ and ** $p<0.001$. Images taken at 20X. Scale bar = 25 µm. GCL: ganglion cell layer; IPL: inner plexiform layer; INL: inner nuclear layer; ONL: outer nuclear layer; PhR: photoreceptor layer.

The Neurotrophin-3 (NT-3) is up-regulated in RHOP mice

NT-3 binds and activates TrkC-FL and TrkC.T1 with equal affinity [5]. Thus, we analyzed the NT-3 mRNA expression and its distribution.

In wild-type retinas, we found low levels of NT-3 mRNA in the GCL, INL and PhR layer (**Figure 3A and 3B**). In RHOP and RHOP:T1 retinas at PN day 16 and more noticeably at PN day 20, the levels of NT-3 mRNA were increased to a similar degree and significantly over wild type retinas ($p < 0.001$) (**Figure 3C and 3D**). The elevation of NT-3 mRNA levels was detected most prominently in the PhR layer (**Figure 3A and 3B**), and was also detectable in the GCL, INL.

In wild-type retinas, there was a weak expression of NT-3 protein in the GCL, INL; and undetectable levels in the PhR layer (**Figure 3E**). In RHOP retinas (**Figure 3F**) and RHOP:T1 retinas (**Figure 3E**) there was a significant increase of NT-3 protein in the IPL, INL and even more robustly in the PhR; compared to wild type retinas ($p<0.001$). The increased NT-3 signal in RP co-localized with Müller cells, predominantly in Müller cell fibers intermingled with photoreceptors.

These results indicate that NT-3 is specifically elevated early after eye opening in RHOP mice, regardless of the TrkC.T1 genotype, and that the increase takes place mainly towards the damaged photoreceptors, but sparing GCL.

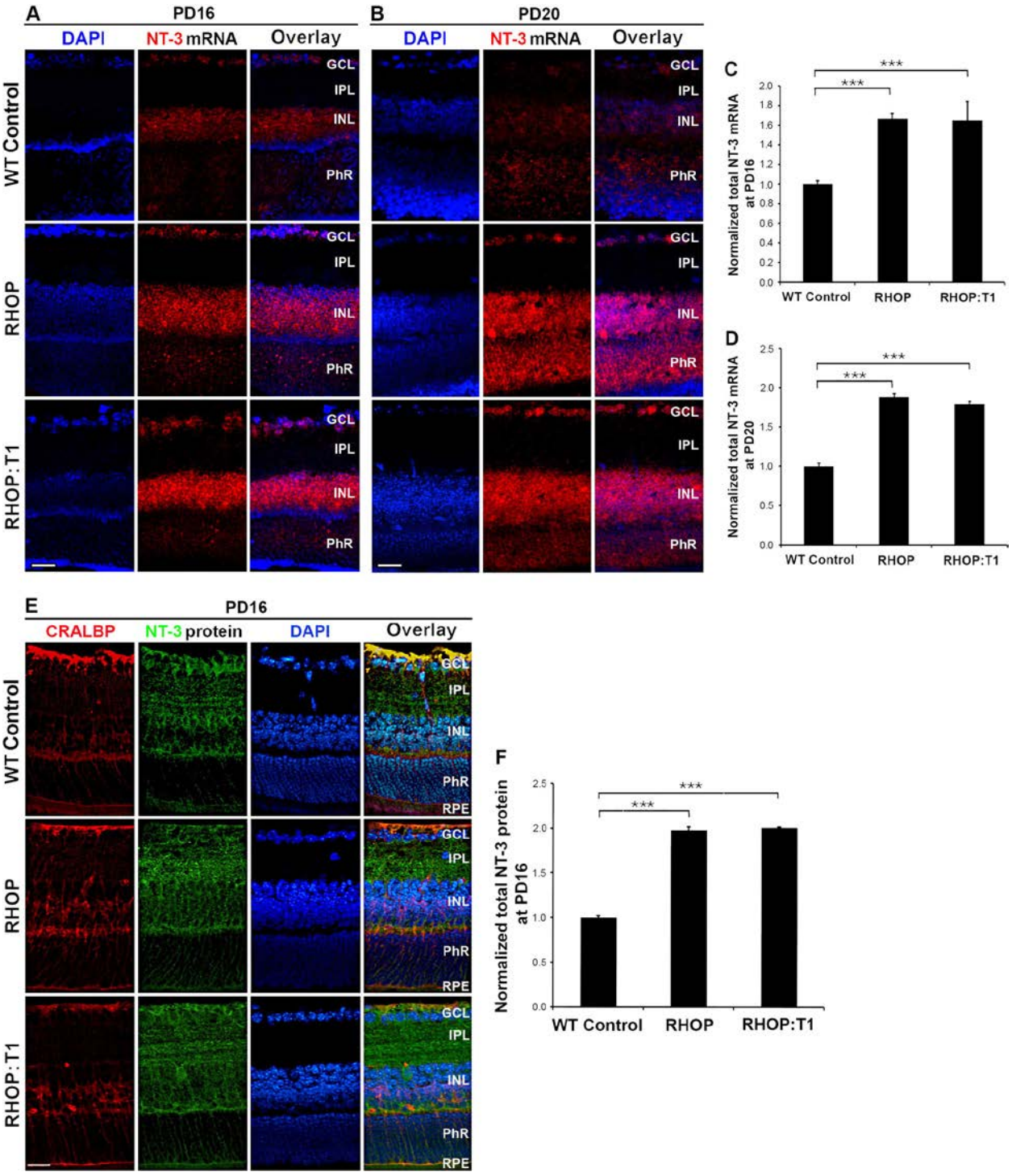

Figure 2.3. NT-3 is up-regulated in RHOP mice

(A) Representative image of "in situ" mRNA hybridization with NT-3 (red) antisense probe in WT, RHOP and RHOP: T1 mice at PN day 16 and **(B)** at PN day 20. NT-3 mRNA was

increased in the GCL, INL and more prominently in the PhR layer of both, RHOP and RHOP:T1 retinas compared to WT control. **(C)** Quantification of NT-3 mRNA in total retina at PN day 16 and **(D)** at PN day 20. Note that the NT-3 mRNA levels in RHOP and RHOP:T1 retinas are not significantly different. Data are shown as normalized area values (± SEM) relative to WT control. A total of 16-20 images were taken from an n=2 retinas per group, *** $p<0.001$ **(E)** Representative images of double immunofluorescence with NT-3 (green) and the Müller cell marker CRALBP (red) in WT, RHOP and RHOP:T1 mice at PN day 16. NT-3 immunoreactivity was increased in the IPL, INL and more prominently in the PhR layer of RHOP and RHOP:T1 mice retinas, but not in the GCL. Note that NT-3 immunostaining was detected in the somata of Müller cells, basal-end feet and mostly in the fibers projected towards the photoreceptors. Images were taken at 20X. Scale bar = 25 µm. **(F)** Quantification of NT-3 immunoreactivity in total retina. Data are shown as normalized area values (± SEM) relative to WT control. A total of 16-20 images were taken from an n=2 retinas per group, * $p< 0.05$, **$p<0.01$ and *** $p<0.001$. GCL: ganglion cell layer; IPL: inner plexiform layer; INL: inner nuclear layer; ONL: outer nuclear layer; PhR: photoreceptor layer.

TrkC.T1 directly activates the MAPK/Erk signaling pathway in Müller glial cells in RHOP mice

Next, we investigated the underlying signaling mechanisms upon TrkC.T1 up-regulation in Müller glial cells. TrkC.T1 induces Rac1 [5] and p-Erk and p-Akt are targets of Rac1 in the nervous system [59-61]. Hence we investigated whether TrkC.T1 regulates p-Erk and p-Akt in the rMC-1 rat Müller cell line, endogenously expressing TrkC.T1 but undetectable levels of TrkC.FL [10].

The rMC-1 cells were untreated or infected with either PLKO.1$^{TrkC.T1}$ or control PLKO.1^{scrambled}, and each culture was stimulated with vehicle or 4 nM NT-3 for 10 min. In uninfected cells and control lentivirus PLKO.1^{scrambled} infected cells NT-3 stimulation induced a ~2-fold increase and a ~1.8-fold increase in p-Erk, respectively. However, there was no NT-3–stimulated increase in p-Erk in cells infected with PLKO.1$^{TrkC.T1}$ (**Figure 4A and 4B**). As control, the levels of p-Akt did not change under any culture condition (**Figure 4A and 4C**). Overall, these results support the view that the MAPK/Erk signaling cascade is activated in a ligand-dependent manner by TrkC.T1 in Müller glial cells.

Next, we investigated whether TrkC.T1 regulates p-Erk *in vivo* early during RP. In healthy wild-type retinas, a very weak p-Erk signal was detected in the INL and GCL. In RHOP retinas, there was a sustained increase of p-Erk clearly co-localized with Müller glial (**Figure 4D, 4E, 4F**). In the early RHOP retinas, at PN day 20, the p-Erk signal was found predominantly in the soma of Müller glial cells, and in Müller cells fibers and Müller cells end-feet in the direction of and spanning the PhR layer (**Figure 4D**). In the RHOP retinas at PN day 24, relatively late in disease, p-Erk was even more robust in Müller cell bodies and fibers projected towards the PhRs and in their processes ending in basal end-feet (**Figure 4E**). In the RHOP retinas at PN day 28, the p-Erk immunoreactivity was decreased (**Figure 4F**).

In RHOP:T1 retinas at PN days 20 and 24 there was a reduction of p-Erk signal in the somata and Müller cell fibers compared with RHOP retinas ($p<0.01$). However the p-Erk levels were still higher in RHOP:T1 than in wild type retinas. In RHOP:T1 retinas at PN days 28, there were no significant differences in p-Erk compared to RHOP retinas (**Figure 4G**). These genetic and anatomical data demonstrate that during RP progression, upregulated TrkC.T1 stimulates p-Erk activity specifically in Müller cell fibers pointing towards stressed photoreceptors.

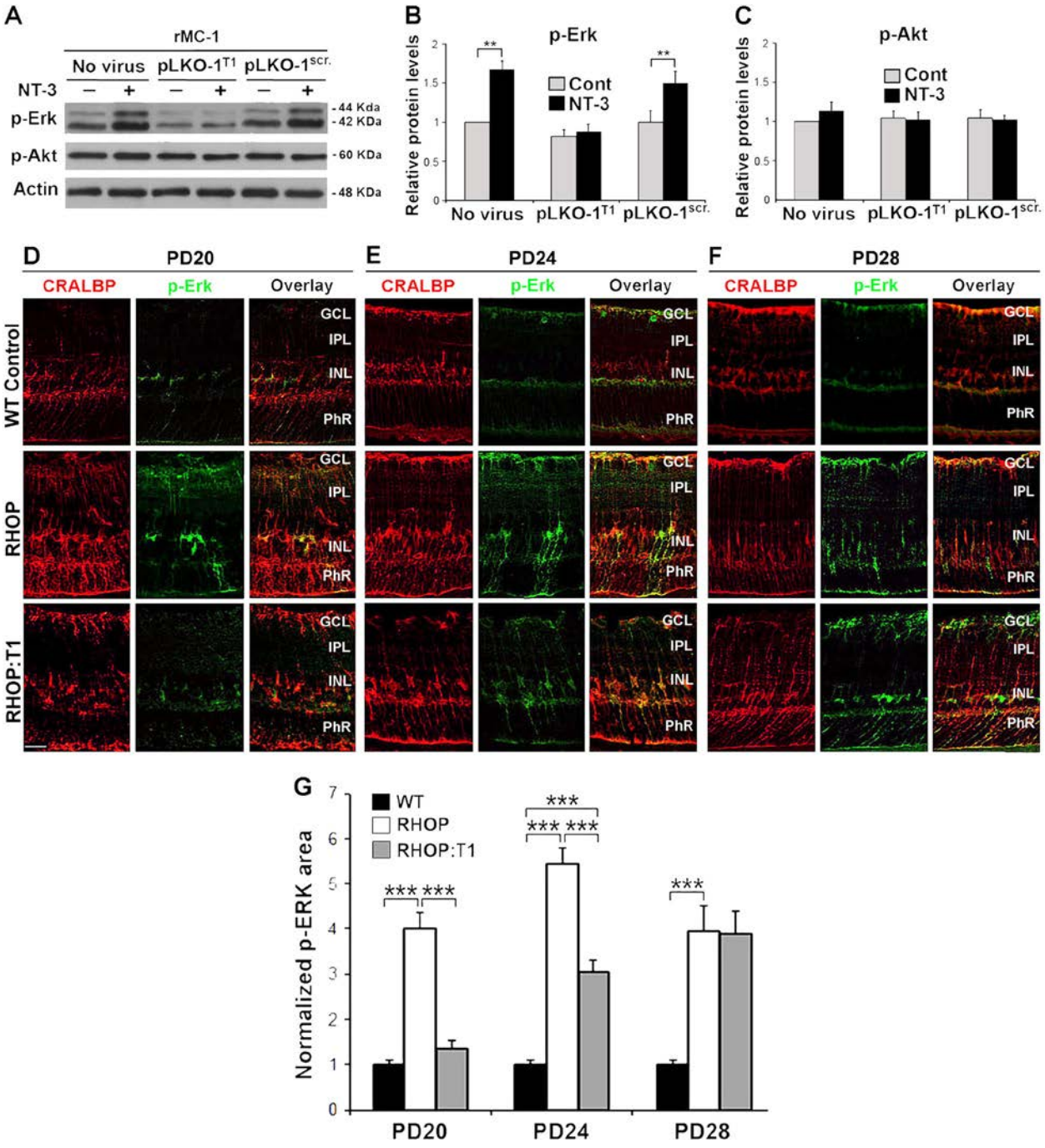

Figure 2.4. TrkC.T1 directly activates MAPK/Erk in Müller cells

(A) Representative western blots showing the levels of TrkC-FL (140 KDa), TrkC.T1 (110 kDa), p-Erk 1/2 (44 and 42 KDa) and p-Akt (60 KDa) in non-infected r-MC1 cells and rMC-1 cells infected with PLKO.1$^{TrkC.T1}$ or lentivirus PLKO.1^{scrambled}; with or without stimulation of 4nM NT-3 for 10 min. All membranes were stripped and re-probed with anti-actin

as a loading control. **(B, C)** Densitometric quantification of p-Erk and p-Akt signal standardized to untreated controls (arbitrary value of 1). Note that in rMC-1 cells, silencing TrkC.T1 prevents p-Erk activation. The data represent relative protein levels ± SEM. n=3 independent experiments. * $p<0.05$, ** $p<0.01$ and ***$p<0.001$. **(D-F)** p-Erk immunoreactivity in WT, RHOP and RHOP:T1 at PN days 20 **(D)**, 24 **(E)** and 28 **(F)**. The p-Erk signal was markedly increased in Müller cells in RHOP retinas at all PN days, as revealed by co-localization with the specific Müller cell marker CRALBP. Note that p-Erk immunostaining was detected in the somata of Müller cells, basal-end feet and in the fibers projected towards the outer retinal layers. The p-Erk immunoreactivity was partially decreased in RHOP:T1 retinas. (**G**) Quantification of p-Erk area in WT, RHOP and RHOP:T1 at PN days 20, 24 and 28. Data are shown as normalized area values vs. WT p-Erk area values (± SEM). Area was significantly increased in RHOP retinas at all PN days tested. Note that RHOP:T1 retinas showed a significant reduction of p-Erk area at PN days 20 and 24. No difference in area values were observed between RHOP and RHOP:T1 at PN day 28. Thirty images taken from n=3 retinas per group, ***$p<0.001$. Images taken at 20X. Scale bar = 25 µm. GCL: ganglion cell layer; IPL: inner plexiform layer; INL: inner nuclear layer; ONL: outer nuclear layer; PhR: photoreceptor layer.

TrkC.T1 regulates the production of TNF-α mRNA in RHOP mice

Next, we sought to examine whether TrkC.T1 regulates TNF-α mRNA production in RHOP glia. In wild-type retinas, a weak expression of TNF-α and TrkC.T1 was detected in the GCL and INL. At PN day 16, in RHOP retinas, there were increased levels of TNF-α mRNA and TrkC.T1 mRNA in the GCL, and more prominently in the INL and PhR layer. TNF-α and TrkC.T1 mRNAs were almost completely co-localized.

In RHOP:T1 retinas, there was a reduction of TrkC.T1 mRNA accompanied by a reduction in TNF-α mRNA, mostly in the INL (**Figure 5A, quantified in 5B, 5C**). Negative controls by double *in situ* hybridization with sense mRNAs of TrkC.T1 and TNF-α had no signal, as expected (**data not shown**). These results were corroborated by analysis of TNF-α protein, by immunofluorescence. TNF-α protein was increased in RHOP sections and that increase was thwarted in T1 heterozygotes at all time points tested (**Figure 5D and data not shown**). TNF-α receptors are highly expressed in ganglion cells, and are expressed also in photoreceptors. This explains why the staining for TNF-α protein is more apparent in the GCL than in the PhR layer, since soluble TNF-α binds to the receptors in neurons.

These data indicate that there is an anatomical overlap for TrkC.T1 and TNF-α mRNAs, in Müller glial cells. Upregulation of TrkC.T1 drives TNF-α mRNA and protein overexpression at early stages of disease in RHOP mice. Partial genetic depletion of TrkC.T1 impedes TNF-α mRNA and protein overexpression. High levels of TNF-α are well-known to trigger neuronal cell death in the retina [8, 37, 62, 63], hence we evaluated whether TNF-α is up-regulated in Müller cells downstream of TrkC.T1 and pErk activity.

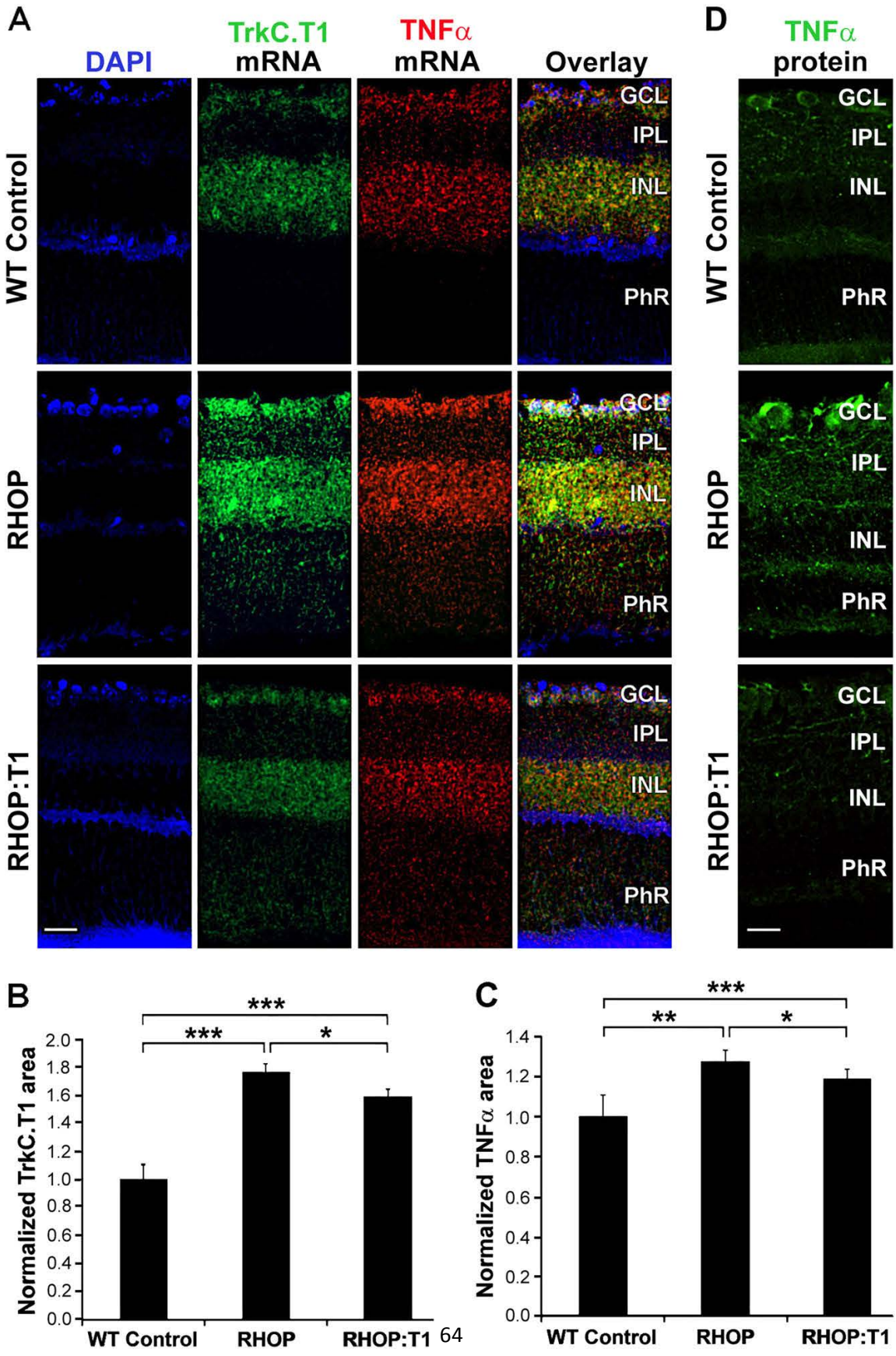
A
DAPI
TrkC.T1 mRNA
TNFα mRNA
Overlay
WT Control
RHOP
RHOP:T1
GCL
IPL
INL
PhR
D
TNFα protein
B
Normalized TrkC.T1 area
***
***
*
WT Control
RHOP
RHOP:T1
C
Normalized TNFα area
***
**
*
WT Control
RHOP
RHOP:T1

Figure 2.5. TrkC.T1 mediates TNF-α mRNA up-regulation in RHOP mice

(A) Double "in situ" mRNA hybridization with TrkC.T1 (green) and TNF-α (red) antisense probes in WT, RHOP and RHOP: T1 mice at PN day 16. TNF-α mRNA was up-regulated in the GCL, INL and PhR layer in RHOP retinas. TNF-α up-regulation shared the same anatomical distribution of TrkC.T1 mRNA expression, as shown by substantial co-localization between both probes. Note that TNF-α mRNA expression was partially reduced in RHOP:T1 mice. **(B)** Quantification of TrkC.T1 and **(C)** TNF- α mRNAs at PD16. Data are represented as normalized TrkC.T1 or TNF-α area values (± SEM) relative to WT control. A total of 10 images were taken from an n=3 retinas per group, *p < 0.05; **p< 0.01; ***p<0.001. (**D**) TNF-α immunoreactivity in WT, RHOP and RHOP:T1 at PN day 24. Images were taken at 20X. Scale bar = 25 μm. GCL: ganglion cell layer; IPL: inner plexiform layer; INL: inner nuclear layer; PhR: photoreceptor layer.

In RP pharmacological antagonism of TrkC prevents pERK activation and TNF-α elevation, and delays retinal degeneration.

We tested the hypothesis that pharmacological antagonism of TrkC may ablate the degenerative phenotype in RHOP retinas, leading to neuroprotection.

First, we tested this hypothesis using organotypic retinal explants cultured *ex vivo.* In organotypic cultures of RP retinas the photoreceptors continue to die at the same rate as *in vivo*. The retinal explants were treated with KB1368, a small molecule antagonist of TrkC [8, 64, 65] or control vehicle and photoreceptor death was quantified in TUNEL assays. RHOP retinal explants treated with KB1368 had significantly reduced photoreceptor death compared to vehicle ($p< 0.01$) (**Figure 6D**) demonstrating a protective role for TrkC antagonism. RHOP retinas cultured with KB1368 TrkC antagonist had a significant reduction of p-Erk, p-Akt, and TNF-α protein ($p< 0.01$) compared to vehicle (**Figure 6E**).

Similar data were obtained *in vivo* (**Figure 6A**). In RHOP retinas the ONL of KB1368-injected eyes (at PN day 17) was significantly thicker than the vehicle-injected eyes, at PN days 22, 24 and 28. These data demonstrate a significant preservation of the photoreceptor structures. In further controls, injection of vehicle or KB1368 in wild-type eyes caused no significant changes in ONL structure (**data not shown**).

Quantification showed a reduction of p-Erk (~40%, $p< 0.01$), p-Akt (~50%, $p< 0.01$) and TNF-α (~60%, $p< 0.01$) in KB1368–treated RHOP eyes compared to vehicle-injected contralateral eyes (**Figure 6B**). Immunohistochemistry demonstrated that reduction of p-Erk resulting from KB1368 treatment occurs primarily in Müller cells (**Figure 6C**).

These pharmacological data are consistent with the data obtained using RHOP:T1 as a genetic TrkC.T1 ablation strategy. The only phenotypic difference between RHOP:T1 ablation and the pharmacological inhibitor KB1368 is a reduction in p-Akt. The decrease in retinal p-Akt may be due to TrkC-FL inhibition by KB1368, because KB1368 can antagonize both TrkC.T1 as well as TrkC-FL [65] and p-Akt is downstream of TrkC-FL.

Together, these results indicate that in RP Müller cells upregulate TrkC.T1 and NT-3; and that genetic ablation or pharmacological inhibition of TrkC.T1 reduces p-Erk and TNF-α that are otherwise increased in Müller cells. Hence, TrkC.T1 appears to be upstream of p-Erk and TNF-α. The next question was whether p-Erk is upstream of TNF-α and induces its expression.

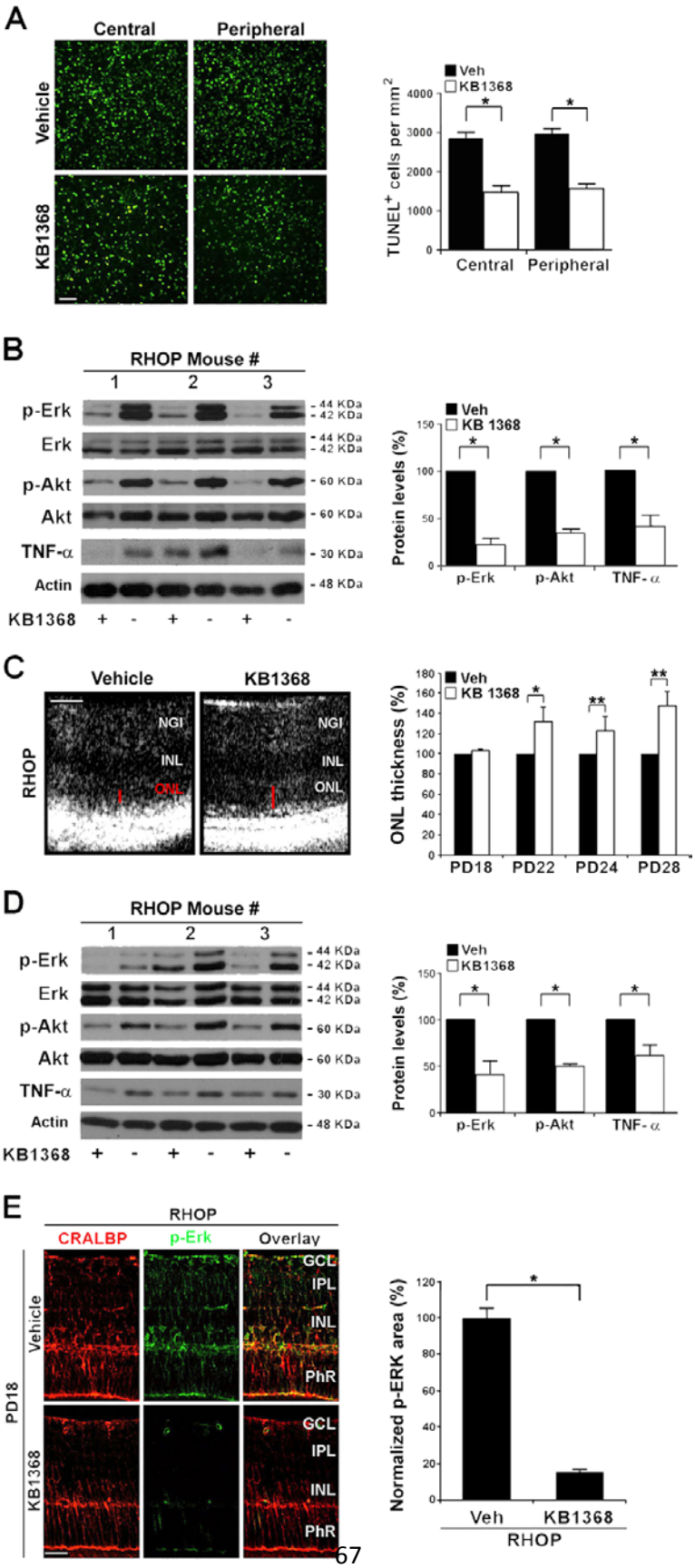
A
Central
Peripheral
Vehicle
KB1368
Veh
KB1368
TUNEL+ cells per mm2
4000
3000
2000
1000
0
Central
Peripheral
B
RHOP Mouse #
1
2
3
p-Erk
Erk
p-Akt
Akt
TNF-α
Actin
44 KDa
42 KDa
60 KDa
30 KDa
48 KDa
KB1368 + - + - + -
Veh
KB 1368
Protein levels (%)
150
100
50
0
p-Erk
p-Akt
TNF-α
C
Vehicle
KB1368
RHOP
NGI
INL
ONL
Veh
KB 1368
ONL thickness (%)
180
160
140
120
100
80
60
40
20
0
PD18
PD22
PD24
PD28
D
RHOP Mouse #
1
2
3
p-Erk
Erk
p-Akt
Akt
TNF-α
Actin
44 KDa
42 KDa
60 KDa
30 KDa
48 KDa
KB1368 + - + - + -
Veh
KB1368
Protein levels (%)
150
100
50
0
p-Erk
p-Akt
TNF-α
E
RHOP
CRALBP
p-Erk
Overlay
PD18
Vehicle
KB1368
GCL
IPL
INL
PhR
Normalized p-ERK area (%)
120
100
80
60
40
20
0
Veh
KB1368
RHOP

Figure 2.6. TrkC antagonist KB1368 blocks the expression of p-Erk and p-Akt, decreases TNF-α production, inhibits ONL degeneration and PhR cell death in RP

(A-B) KB1368 treatment of organotypic retinal cultures. Retinas were dissected at PN day 17 and cultured for 24 hr with KB1368 (10 µM, 2µl) or vehicle (Veh) (5% DMSO, 2 µl). Explants were processed for TUNEL or Western blots. **(A)** Representative images of TUNEL staining of central and peripheral areas of RHOP mice retinas. Histogram shows TUNEL data quantification of both retina areas, TUNEL positive cells per mm^2 (±SEM), *p<0.01, n=6. KB1368-treated retinas had decreased photoreceptor apoptosis compared to vehicle. **(B)** Expression of p-Erk and p-Akt protein in RHOP retinas. Histogram shows densitometric analysis of Western blots. The signal for each eye was respectively adjusted to total Erk or total Akt, and the ratio of right/left eye was calculated. In each mouse, the KB1368-treated eye was compared to the vehicle-injected eye standardized to 100% (±SEM), *p<0.01, n=3. The TrkC antagonist reduced p-Erk signal by 70% and p-Akt by 40%. **(C-E)** Effect of KB1368 *in vivo*. KB1368 (1 mM, 2µl) (right eye) or vehicle control (Veh) (5% DMSO, 2µl) (left eye) were injected intravitreally at PN day 17**. (C)** FD-OCT images (PN day 24) from RHOP mice. In RHOP eyes KB1368-treatment resulted in ONL thicker than in vehicle-treated from postnatal day 22 to PN day 28 (red bars). Histogram shows FD-OCT data quantified for RHOP retinas at PN days 18, 22, 24, and 28. For each mouse the vehicle-injected eye was standardized to 100%, n=3 animals per group, *p<0.01, scale bar= 60 µm. **(D)** Western blots of RHOP retinas 24 hours after intravitreal injections. Histogram shows densitometric quantification of p-Erk, p-Akt and TNF-α. The signal for each eye was respectively adjusted to total Erk, total Akt, or actin, and the ratio of right/left eye was calculated. For each mouse, the KB1368-treated eye was compared to the vehicle-injected eye standardized to 100% (±SEM), *p<0.01, n=4. The TrkC antagonist reduced p-Erk signal by 40%, p-Akt by 50% and TNF-α by 60% **(E)** Representative images of p-Erk immunoreactivity in RHOP retinas at PN day 18. KB1368 abolished p-Erk immunostaining compared with the vehicle-injected retinas. Histogram shows quantification of p-Erk area in pixels (±SEM), *p<0.001. Scale bar = 25µm. NGI: Nerve fiber layer-Ganglion cell layer-Inner plexiform layer; IPL: inner plexiform layer; INL: inner nuclear layer; ONL: outer nuclear layer; IS/OS: internal/external segment.

Inhibition of MAPK/Erk activity prevents TNF-α elevation and delays retinal degeneration in RP retinas in vivo

We examined whether direct interference with the MAPK/Erk signaling cascade could reduce TNF-α and prevent photoreceptor degeneration in the RHOP mouse *in vivo*. An intravitreal injection of the MAPK/Erk inhibitor PD90859 (right eye, treated) or control vehicle (left eye, control) were done at PN day 17, and p-Erk was examined by immunohistochemistry 24 hr later (at PN day 18).

Treatment significantly blocked p-Erk in Müller cells ($p<0.01$) compared to control contralateral eye. The p-Erk signal was abolished in Müller cell, most of which contact the photoreceptor layers (**Figure 7A**). Inhibition of p-Erk in RHOP mice significantly reduced TNF-α levels, indicating that in the RHOP model TNF-α elevation is p-Erk–dependent (**Figure 7B**).

Reduction of p-Erk and TNF-α in RHOP mice significantly preserved retinal structure and photoreceptor neurons (**Figure 7C**). In PN day 24 RHOP mice the ONL was thicker in PD98059-treated eyes, compared to vehicle-treated contralateral eyes. This indicates significant preservation of retinal structure ($p<0.01$). ONL protection was still evident at PN day 28 ($p<0.001$) (note that the higher significance is due to continued degeneration in the vehicle-treated control eyes). In wild type control mice the ONL was the same whether eyes were injected with PD98059 or vehicle.

Together, these data demonstrate that in the RHOP model of RP a TrkC.T1–dependent activation of p-Erk in Müller glia, which is vectorial towards photoreceptors, contributes to local TNF-α increases by Müller glia. Elevated local TNF-α causes selective photoreceptor death. Direct inhibition of TrkC.T1 or MAPK/Erk activity prevents local TNF-α increases and delays photoreceptor cell death and degeneration of the ONL.

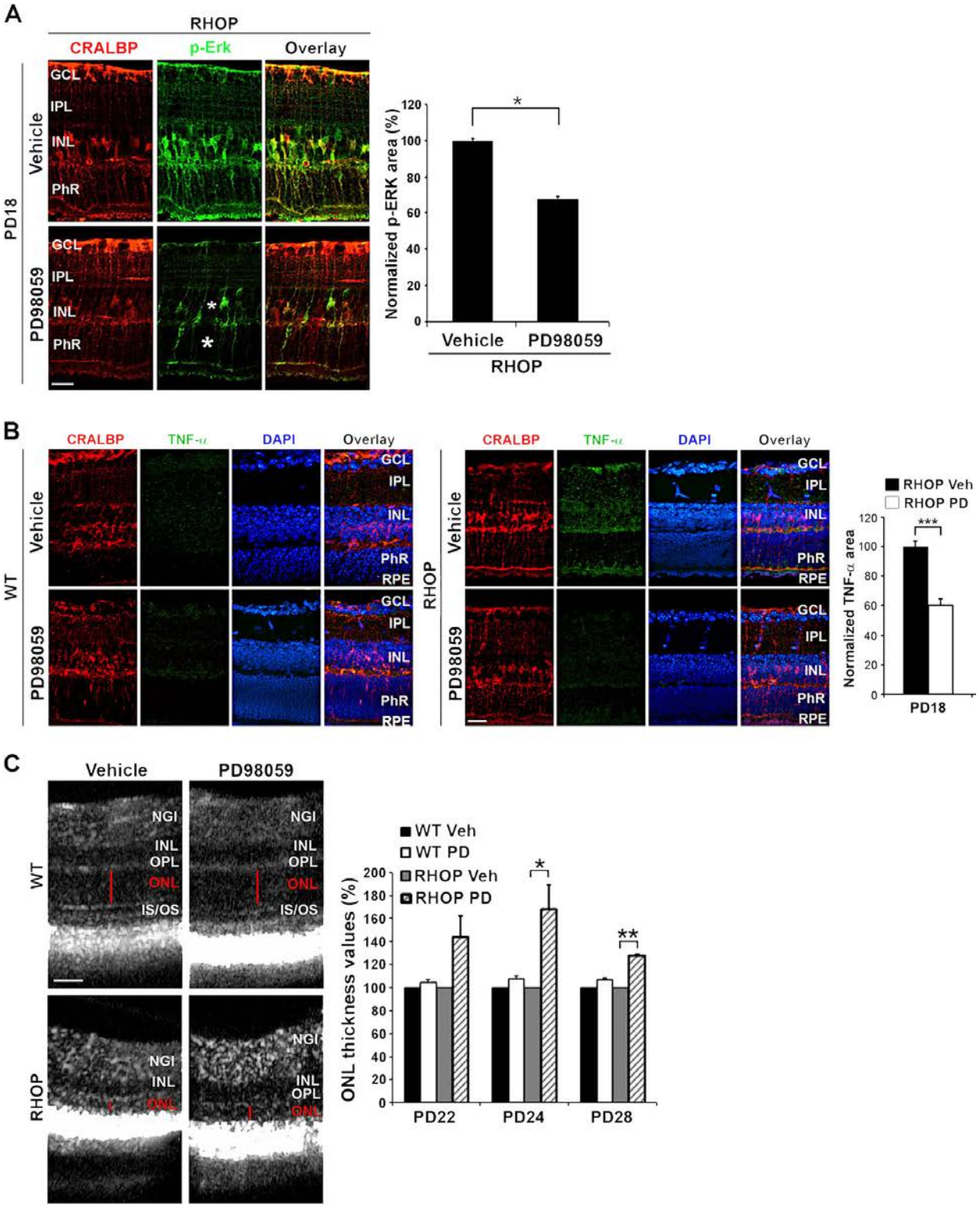
A
RHOP
CRALBP
p-Erk
Overlay
PD18
Vehicle
PD98059
GCL
IPL
INL
PhR
Normalized p-ERK area (%)
Vehicle
PD98059
RHOP
B
CRALBP
TNF-α
DAPI
Overlay
WT
RHOP
Vehicle
PD98059
GCL
IPL
INL
PhR
RPE
RHOP Veh
RHOP PD
Normalized TNF-α area
PD18
C
Vehicle
PD98059
WT
RHOP
NGI
INL
OPL
ONL
IS/OS
WT Veh
WT PD
RHOP Veh
RHOP PD
ONL thickness values (%)
PD22
PD24
PD28

Figure 2.7. MAPK/Erk inhibition delays ONL degeneration in RP

PD98059 (100 µM, 2µl) (right eye) or vehicle (Veh) (50% DMSO, 2 µl) (left eye, control) were injected at PN day 17. **(A)** Representative images of p-Erk immunoreactivity in RHOP retinas at PN day 18. P-Erk signal was clearly reduced in the cell bodies and mostly in the fibers of Müller cells projected towards the PhR layer (asterisk) in RHOP eyes treated with PD98059, scale bar = 25 µm. Histogram represents the quantification of the p-Erk area in pixels (±SEM), *p<0.001. **(B)** Representative images of TNF-α immunoreactivity in RHOP retinas at PN day 18. TNF-α signal was reduced in RHOP eyes treated with PD98059. Histogram shows TNF-α immunofluorescence quantification. Data are shown as normalized TNF-α area values (± SEM) vs. area values in Vehicle-injected RHOP retinas. **(C)** FD-OCT representative images (PN day 24) from WT and RHOP mice animals injected with vehicle or PD98059. In PD98059-injected RHOP eyes, ONL was thicker than in vehicle-injected eyes (red bar) at postnatal days 24 and 28. In control WT mice no ONL changes were observed in PD98059-injected compared with vehicle-injected eyes. Histogram shows the quantification of FD-OCT images from WT and RHOP retinas at PN days 22, 24, and 28. In each animal regardless of the genotype, the vehicle-injected eye was standardized to 100%, n=3 animals per group, *p< 0.05 and **p<0.01, scale bar= 60 µm. NGI: Nerve fiber layer-Ganglion cell layer-Inner plexiform layer; IPL: inner plexiform layer; INL: inner nuclear layer; ONL: outer nuclear layer; IS/OS: internal/external segment.

Discussion

We report the mechanism of action of TrkC.T1 in a retinal dystrophy mouse model of RP. In disease, TrkC.T1 mRNA and protein are expressed in Müller cells predominantly in an anatomical location proximal to stressed photoreceptors. TrkC.T1 signals are NT-3–dependent, and in disease NT-3 mRNA and protein are expressed predominantly in an anatomical location proximal to stressed photoreceptors. TrkC.T1 is implicated in the sequential activation of MAPK/Erk signaling pathways, with local promotion of TNF-α production in glia. These subsequent events are also vectorial towards stressed photoreceptors, and culminate in their selective death. These data explain a novel mechanism of photoreceptor death in RP, as well as how death signals are selectively delivered to photoreceptors in RP.

It has been challenging to explain how a neuronal population can be affected *selectively* by a paracrine mechanism common to many degenerative diseases, and by a Müller cell that can contact multiple neuronal populations. We provide evidence supporting the "vectorial hypothesis" of Müller cells being activated directionally towards the injured neurons. In addition, we discuss a paired "two hit hypothesis" where Müller cells provide the terminal blow by local delivery of TNF-α which is known to be toxic to an already wounded neuron. In the case of photoreceptors, the first hit is a dystrophic mutant Rhodopsin protein.

Increased TrkC.T1 in Müller cells in RP

The degeneration of ONL in the retina is a hallmark of RP and reflects the progressive death of photoreceptors [33-35]. In the RHOP model, it takes place during the two weeks following eye-opening. In the RHOP model the production of NT-3 is increased and TrkC.T1 is upregulated prior to or at the time of eye-opening, primarily in Müller cells.

TrkC.T1 and TNF-α mRNAs were increased and were anatomically co-localized in RHOP mice in retinal layers where Müller glial cell bodies reside; at early stages of the disease. These data strongly suggest a correlation between TrkC.T1 and TNF-α upregulation in RP. Here, we also show the molecular mechanism. In Müller cells TrkC.T1 activates p-Erk, which causes exacerbated TNF-α production, which causes photoreceptor death and degeneration of the

ONL. These events are ameliorated *in vivo* by genetic reduction of one TrkC.T1 allele, by pharmacological antagonism of TrkC, or by pharmacological inhibition of pErk. However, the protective effect of each of these treatments was temporary, most likely due to the complex nature of RP disease, and the convergence of other mechanisms that promote the pathology, such as the neurotoxic activity of $p75^{NTR}$ [43].

Role of p-Erk in Müller cells

In a glial cell line and in RP *in vivo* pErk was regulated by TrkC.T1. The activation of p-Erk in Müller cells has been previously reported in other models of RP [67-69] and has been identified as a marker of Müller cell proliferation and differentiation [70], and as an early marker of retinal stress [71-73]. However, there were no data on the mechanism causing p-Erk activation, which we show is TrkC.T1–mediated.

Pharmacological inhibition of the MAPK/Erk cascade reduced TNF-α and delayed photoreceptor death and ONL degeneration in RHOP retinas, indicating that p-Erk activation could ultimately trigger PhR cell death through TNF-α. Our data are consistent with reports showing that specific blockade of TNF-α up-regulation reduces photoreceptor cell death in the *rd10* mouse model of RP [37] and other models of photoreceptor degeneration [74].

How do Müller cell neurotoxic signals injure photoreceptors selectively?

Müller cells expand throughout the retina and are layered between the RGCs in the inner retina and the photoreceptors in the outer retina. Given their anatomical position and design, Müller cells sense a healthy state and support neuronal function, or react to neuronal stress or disease ultimately becoming arbiter and executioner [10, 36, 75]. The selective death of a type of neuron in each disease model (RGCs in glaucoma; photoreceptors in RP), using a single TrkC.T1 mechanism, might be explained by a combination of strategies.

First, Müller cell p-Erk activation is TrkC.T1–dependent and "vectorial" towards the injured neurons. How this may be controlled remains unknown but it could be due to local presence and activation of TrkC.T1, by its ligand NT-3, on the injured side of the retina. Perhaps there is a gradient of factors or signals stemming from the injured neuron to inform the Müller cell of a stress.

Second, Müller cells may exert a "second hit" on the stressed neuron that tilts the balance towards death. In the case of photoreceptors a "first hit" may include the Rhodopsin mutation that causes dysfunction of light transmission and structural malformations in Rod outer segments. In the case of RGCs in glaucoma a "first hit" may include high intraocular pressure stressing RGC fibers, causing impaired transport, and reducing synaptic density. The use of common mechanisms to achieve selective cellular death is not an unusual biological strategy [37].

Other models of RP and mechanisms of disease

Our data regarding the role of TNF-α in the RHOP model are consistent with reports of the deleterious effect of glial TNF-α in different RP models [36, 37, 76, 77]. Although RP is primarily a photoreceptor disease, retinal changes beyond photoreceptors have been reported to occur late in disease.

Loss of sensory rod and cone input to the neural retina constitutes deafferentation that results in remodeling at the cellular level and reprogramming at the molecular level and progressive neural degeneration (for review see Jones et al., 2016). Interestingly, bipolar cells undergo anatomical changes that include, among others, the Akt/mTOR pathway. Akt/mTOR is a key regulator of neuronal structure, function and plasticity [78] and dysregulation is associated with neurodegenerative states [79].

Hypothetical model

This study shows the implication of TrkC.T1 in one of the most common inherited retinal diseases and uncovers the novel signaling mechanism of TrkC.T1–p-Erk–TNF-α production during disease progression. This represents a non-cell autologous mechanism driven by Müller glia, oriented predominantly towards the injured side of the retina. How glia resolves the *selective death* of a specified neuronal population is paradoxical. Here we postulate a "vectorial hypothesis", and a "two hit hypothesis" (**Figure 8)**.

In RP, increased production of NT-3 and local up-regulation of TrkC.T1 in Müller cells on the injured side of the retina are the earliest molecular events right after eye-opening. In Müller cells, TrkC.T1 activity mediated through NT-3 triggers vectorial expression of p-ERK

towards the stressed PhR layer, which in turn promotes the expression/release of TNF-α. Up-regulated TNF-α will eventually provoke the cell death of photoreceptors ("vectorial and two hit hypothesis").

The etiological implication of TrkC.T1 in RP provides a starting point for exploring a shared mechanism in a disease family where more than 200 gene mutations [33-35] have been identified. Along with our previous evidence in glaucoma, we suggest that TrkC.T1 may be a therapeutic target for the treatment of retinal neurodegenerative diseases.

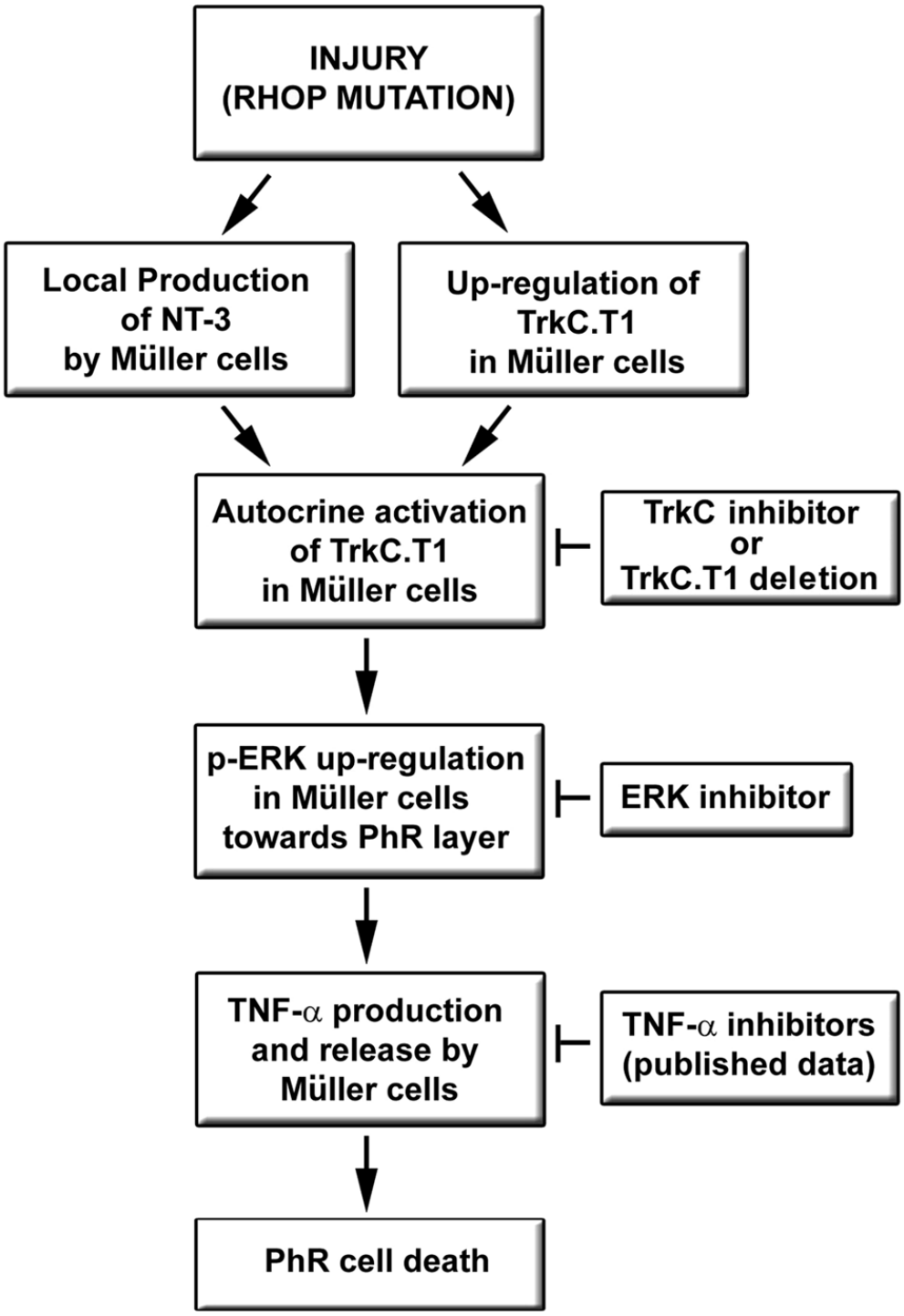

Figure 2.8. Hypothetical model leading to PhR cell death in RP

In RP, photoreceptor stress triggered by the rhodopsin mutation induces the early production of NT-3 and up-regulation of TrkC.T1 in Müller glial cells on the injured side of the retina. In Müller glial cells, autocrine activation of TrkC.T1 triggers vectorial expression of p-

ERK towards the stressed photoreceptor layer, which in turn promotes the production and release of TNF-α. Genetic ablation of one single copy of TrkC.T1 or intravitreal injections of PD98059 (p-ERK inhibitor) or KB1368 (TrkC antagonist) significantly diminished p-ERK activation, decreased TNF-α production and prevented photoreceptor cell death. All these findings represent novel mechanisms. Up-regulated TNF-α provokes (and inhibitors of TNF-α delay) photoreceptor cell death (as per literature).

Conflict of Interest

The authors declare no conflict of interest.

Acknowledgements

We are thankful to Dr. Tiansen Li who kindly donated the "RHOP347S" (RHOP) rhodopsin mutant transgenic mice. We are thankful to Dr. Mario Maira (Lady Davis Institute) for valuable discussions, and to Lucia M. Saragovi (Lady Davis Institute) for counting and analyses of TUNEL assays. This work was supported by the Foundation Fighting Blindness and CIHR-PPP grants to HUS.

p75NTR antagonists attenuate photoreceptor cell loss in murine models of retinitis pigmentosa

María Platón-Corchado[1,3], Pablo F Barcelona[2,3], Sean Jmaeff[2], Miguel Marchena[1], Alberto M Hernández-Pinto[1], Catalina Hernández-Sánchez[1], H Uri Saragovi[2,4] and Enrique J de la Rosa*[1,4]

[1]Centro de Investigaciones Biológicas, CSIC, Madrid, Spain and [2]Lady Davis Institute-Jewish General Hospital, McGill University, Montreal, QC, Canada

*Corresponding author: EJ de la Rosa, Centro de Investigaciones Biológicas, CSIC, C/Ramiro de Maeztu 9, Madrid 28040, Spain. Tel: +34 91 8373112, ext. 4375;

Fax: +34 91 5360432; E-mail: ejdelarosa@cib.csic.es

[3]These authors contributed equally to this work.

[4]These authors contributed equally to this work.

Abstract

ProNGF signaling through p75NTR has been associated with neurodegenerative disorders. Retinitis Pigmentosa (RP) comprises a group of inherited retinal dystrophies that causes progressive photoreceptor cell degeneration and death, at a rate dependent on the genetic mutation. There are more than 300 mutations causing RP, and this is a challenge to therapy. Our study was designed to explore a common mechanism for p75NTR in the progression of RP, and assess its potential value as a therapeutic target. The proNGF/p75NTR system is present in the dystrophic retina of the rd10 RP mouse model. Compared with wild-type (WT) retina, the levels of unprocessed proNGF were increased in the rd10 retina at early degenerative stages, before the peak of photoreceptor cell death. Conversely, processed NGF levels were similar in rd10 and WT retinas. ProNGF remained elevated throughout the period of photoreceptor cell loss, correlating with increased expression of α2-macroglobulin, an inhibitor of proNGF processing. The neuroprotective effect of blocking p75NTR was assessed in organotypic retinal cultures from rd10 and RhoP mouse models. Retinal explants treated with p75NTR antagonists showed significantly reduced photoreceptor cell death, as determined by the terminal deoxynucleotidyl transferase-mediated dUTP nick-end labeling (TUNEL) assay and by preservation of the thickness of the outer nuclear layer (ONL), where photoreceptor nuclei are located. This effect was accompanied by decreased retinal-reactive gliosis and reduced TNFα secretion. Use of p75NTR antagonist THX-B (1,3-diisopropyl-1-[2-(1,3-dimethyl-2,6-dioxo-1,2,3,6 tetrahydropurin-7-yl)-acetyl]-urea) in vivo in the rd10 and RhoP mouse models, by a single intravitreal or subconjunctival injection, afforded neuroprotection to photoreceptor cells, with preservation of the ONL. This study demonstrates a role of the p75NTR/proNGF axis in the progression of RP, and validates these proteins as therapeutic targets in two different RP models, suggesting utility irrespective of etiology.

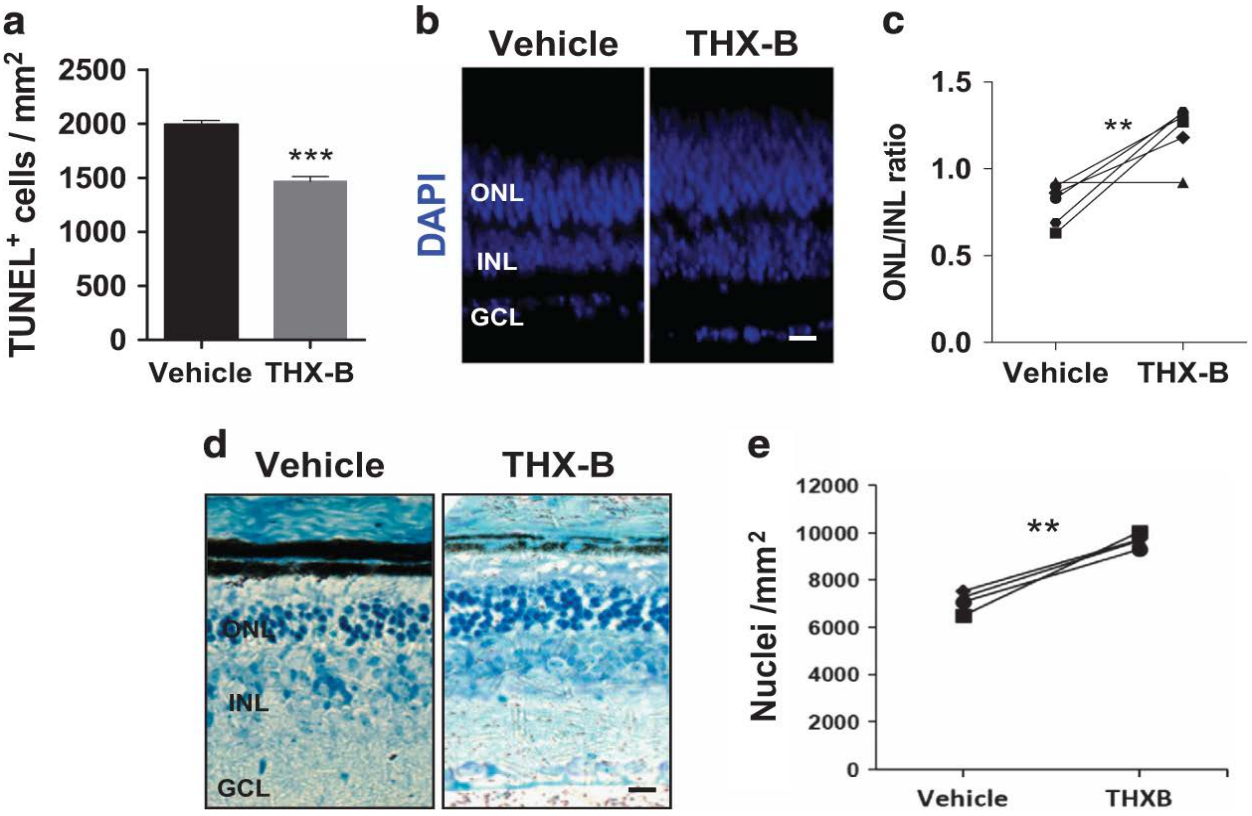

Figure 2.9. Effect of the P75NTR antagonist THX-B, both *ex vivo* and *in vivo*, in the RhoP retina

(A.) P18 RhoP retinas were cultured for 24 h in the absence (vehicle) or presence of the THX-B. Photoreceptor cell death was visualized by TUNEL and quantified. **(B.)** P17 RhoP mice were intravitreally injected with THX-B in one eye and with vehicle in the contralateral eye, and analyzed at P22. Nuclei in whole-mount retinas were counterstained with DAPI. Representative cryosections. **(C.)** Comparison of the ONL/INL thickness ratio between the THX-B-treated eye and the vehicle control eye. Paired eyes are individually represented. **(D.)** P18 RhoP mice were subconjunctivally injected with THX-B in one eye and with vehicle in the contralateral eye and analyzed at P24. Representative cryosections stained with toluidine. **(E.)** Comparison of the density of nuclei in the ONL between the THX-B treated eye and the vehicle control eye. Paired eyes are individually represented. Bars represent the mean±S.E.M.; n≥3; **P<0.01; *** P<0.001. Scale bar: 20 μm. GCL, ganglion cell layer; INL, inner nuclear layer; ONL, outer nuclear layer

Connecting Text Between Chapters 2 and 3

In Chapter 2, we addressed some of the aberrant mechanisms at work in diseases like RP and identified two anti-neurotoxic targets for therapy, TrkC.T1 and p75. We verified that TrkC.T1 was indeed upregulated in the retina and contributed to neurotoxicity through an Erk-dependent pathway, leading to TNFa production in glia. Using a small molecule antagonist, we demonstrated that blockade of this pathway was disease-modifying in both retinal cultures and longitudinally *in vivo*. In a separate work, p75 was examined and was found to play a similar role in the pathogenesis of RP. Small molecule blockade of p75 showed therapeutic efficacy.

Both receptors are worthy of further exploration, and the work lends strong support for the 'trophic imbalance' hypothesis of neurodegeneration. Here, we have intervened on one side of the balance, attempting to restore harmony by reducing the toxic burden of mediators like TNFa. This was achieved through the use of small molecules, and as such the work also serves to generate interest in the importance of drug development as a catalyst for progress in disease research. In the next chapter we continue with this purpose in mind, interrogating the RET receptor and attacking neuronal loss from the other side of the balance, through pro-survival pathways.

Chapter 3

Small molecule ligands that bind the RET receptor activate neuroprotective signals independent of but modulated by co-receptor GFRα1

Sean Jmaeff [1,2], Yulia Sidorova [3], Hayley Lippiatt [1], Pablo F. Barcelona [1], Hinyu Nedev [1], Lucia M. Saragovi [1], Mark A. Hancock [4], Mart Saarma [3], H. Uri Saragovi [1,2]

[1] Lady Davis Institute - Jewish General Hospital. McGill University. Montreal, CANADA.

[2] Pharmacology and Therapeutics. McGill University. Montreal, CANADA.

[3] Institute of Biotechnology. HiLIFE. University of Helsinki. Helsinki, FINLAND.

[4] SPR-MS Facility, McGill University, Montreal, CANADA

Abstract

Glial cell line-Derived Neurotrophic Factor [80] binds the GFRα1 receptor, and the GDNF–GFRα1 complex binds to and activates the transmembrane RET tyrosine kinase to signal through intracellular Akt/Erk pathways. To dissect the GDNF–GFRα1–RET signaling complex, agents that bind and activate RET directly and independently of GFRα1 expression are valuable tools. In a focused naphthalenesulfonic acid library from the NCI database, we identified small molecules that are genuine ligands binding to the RET extracellular domain. These ligands activate RET tyrosine kinase and afford trophic signals irrespective of GFRα1 co-expression. However, RET activation by these ligands is constrained by GFRα1, likely via an allosteric mechanism that can be overcome by increasing RET ligand concentration. In a mouse model of retinitis pigmentosa, monotherapy with a small molecule RET agonist activates survival signals and reduces neuronal death significantly better than GDNF, suggesting therapeutic potential.

Introduction

Glial cell line-derived neurotrophic factor [80], a distant member of the TGF-beta superfamily, mediates pro-survival signaling in neuronal populations [81-83]. Indeed, GDNF has been tested in animal models of neurodegeneration, notably Parkinson's Disease (PD) , Amyotrophic Lateral Sclerosis, neuropathic pain [84], and eye diseases such as retinitis pigmentosa (RP) and glaucoma [85-87].

In human clinical trials for PD, the therapeutic efficacy of GDNF and related factor neurturin has been controversial, with post hoc analysis showing clinically significant motor improvement [31, 88]. In part, GDNF therapy remains a challenging strategy due to the limited understanding of the physiology of its receptors, varying receptor/co-receptor expression patterns, and binding or functional interactions with other factors or matrix proteins *in vivo* [89-91]. GDNF can bind to extracellular matrix and transmembrane heparan sulfate proteoglycans and neuronal cell adhesion molecules NCAM [22, 92], affecting its bioavailability [25]. These issues could be solved using RET agonists that are not bound/trapped, and which may exhibit more favorable kinetics and avoid the need for invasive delivery methods.

GDNF binds first to the GPI-anchored GDNF Family Receptor alpha 1 (GFRα1) receptor, and the resulting GDNF/GFRα1 complex then activates the RET receptor tyrosine kinase (RTK). There appears to be a functional cross-regulation between RET and GFRα1, as reported for another receptor family, the neurotrophin receptors [93]. However, the required concomitant presence of GFRα1 and RET receptors to activate measurable GDNF-induced signals limits biological and pharmacological studies.

For example, studies of cross-regulation are difficult, and access to receptor-specific ligands would be useful to probe this question. Moreover, the pharmacological utility of GDNF may be limited to indications where both receptors are present in the same tissue in disease. However, there are indications where RET is expressed without GFRα1, for example, in the retina [94]. Selective, small molecule RET agonists may provide a broader range of tissue targets and activities.

Here we report chemical biology studies to develop small molecules that selectively activate RET-pY^{1062}, which activates Akt and Erk pathways leading to cell survival-promoting

signals. Activity is dependent on RET-expression, but independent of GFRα1-expression. We used these small molecules as tools to demonstrate regulation of RET by GFRα1, a process which is likely allosteric. A RET agonist, compound 8, was used as a therapeutic lead in an animal model of retinitis pigmentosa, to validate the RET receptor as a druggable target in this disease.

Materials and Methods

Cell Lines

MG87 RET are murine MG87 fibroblasts stably transfected with RET proto-oncogene cDNA [21], and were cultured in DMEM containing 10% FBS, 2 mM L-Glutamine, 10 mM HEPES, 100 U/ml Penicillin/Streptomycin, and 2 μg/ml puromycin. MG87 RET cells were transfected with a GFRα1 cDNA construct containing Blasticidin resistance gene to generate the MG87 RET/GFRα1 cell line, and were cultured in the same media with the addition of 5 μg/ml Blasticidin S. MG87 TrkA cells were transfected with human NGF receptor TrkA cDNA, and cultured in DMEM 10% FBS supplemented with 250 μg/ml G418. MG87RET/GFRα1 cell lines were stably transfected with PathDetect Elk-1 system (Stratagene) harboring Luciferase reporter under the control of Erk activity. Cells were cultured in DMEM, 10% FBS, 15 mM HEPES pH 7.2, 100 μg/ml normocin (Invivogen), 2 μg/ml puromycin, 500 μg/ml G418 [95]. Growth factors GDNF and NGF were purchased from Peprotech (catalogue 450-10, 450-01) and FGF2 from Sigma Aldrich (catalogue F0291). Cell lines were routinely tested and verified to be free of mycoplasma (Venor GeM Mycoplasma Detection Kit).

Luciferase assay

Initial screening of a chemical library was performed in MG87RET/GFRα1 cells with luciferase reporter controlled by Erk [95]. 20000 cells per well were plated in 96-well plates in DMEM, 10% FBS, 15 mM HEPES pH 7.2, 100 μg/ml normocin, 1% DMSO and incubated overnight under standard conditions. Cells were treated with tested compounds dissolved in DMEM, 15 mM HEPES pH 7.2, 1% DMSO to achieve final concentration of 5 and 20 μM for 24-30 hr. Afterwards, cells were lysed with 25 μl of cell lysis buffer (Promega) per well and frozen and thawed once. Five μl of lysate was combined with 20 μl of luciferase assay reagent (Promega) on ice. Luminescence was measured using MicroBeta 2 instrument (PerkinElmer) twice. Results of the second run were used for analysis.

RET phosphorylation assays

Phosphorylation of RET was assessed as previously described [96]. MG87 RET cells were plated on 35 mm tissue culture dishes, left to attach to the surface overnight and then transfected with 4 μg/dish of GFRα1-expressing plasmid using Lipofectamine 2000 (Invitrogen) for DNA delivery as described by manufacturer. Next day cells were starved for 4 hr in serum-free DMEM containing 15 mM HEPES, pH 7.2 and 1% DMSO and stimulated with 5-100 μM compounds or GDNF (200 ng/ml) for 15 min diluted in serum-free DMEM containing 15 mM HEPES, pH 7.2 and 1% DMSO. Afterwards, cells were washed once with ice-cold PBS containing 1 mM Na_3VO_4 and lysed on ice in 0.5 ml per well of RIPA-modified buffer (50 mM Tris-HCl, pH 7.4, 150 mM NaCl, 1 mM EDTA, 1% NP-40, 1% triton-X100, 10% glycerol, EDTA-free EASYpack, protease inhibitor cocktail (Roche), 1 mM Na_3VO_4, 2.5 mg/ml of sodium deoxycholate). Plates were incubated on horizontal shakers for 30 min with vigorous shaking, lysates were collected in Eppendorf tubes and centrifuged for 10 min at 6000g at 4°C to precipitate cell debris. Supernatants were incubated overnight with 2 μg/ml of anti-RET C-20 antibodies (Santa-Cruz Biotechnology, Inc., sc-1290) and protein G-conjugated beads (Thermo Fisher Scientific, Cat # 10004D). Beads were washed 3 times with 1x TBS (50 mM Tris-HCl, pH 7.4, 150 mM NaCl) with 1% triton X-100, bound proteins were eluted by 50 μl of 2x Laemmli loading buffer, resolved on 7.5% SDS-PAGE and then transferred to a nitrocellulose membrane. Total phosphorylated residues were then probed using the 4G10 antibody (1:1,000, Millipore, Cat # 05-321) followed by anti-mouse antibodies conjugated with horse radish peroxidase (1 : 1,500, DAKO, Cat# P0447) in TBS-T containing 3% skimmed milk. To confirm equal loading, membranes were stripped, washed, blocked, and re-probed with anti-RET C-20 antibodies (1:500, Santa-Cruz Biotechnology, Inc.) followed by anti-goat antibodies conjugated with horse radish peroxidase (1:1,500, DAKO, Cat# P0449) in TBS-T containing 3% skimmed milk. Stained bands were visualized with ECL or femptoECL reagent (Pierce) using LAS-3000 imaging system (Fuji).

Surface Plasmon Resonance (SPR)

Binding interactions between the small molecules (4 mM stocks of Compounds 8 and 9 in 5% (v/v) DMSO) and human RET protein (R&D Systems #1168-CR/CF) were examined at 25°C using a BIACORE T200 system (GE Healthcare Bio-Sciences AB, Upsala, Sweden;

Control software v2.0 and Evaluation software v1.0). Protein-grade Tween 20 and Empigen detergents (Anatrace #APT020 and #D350, respectively), anhydrous DMSO (Sigma #276855), Pierce Gentle Ag/Ab Elution buffer (Thermo Fisher #21027) and all other chemicals were reagent grade quality. The carrier-free proteins were immobilized to S-series CM5 sensors (10 μg/ml RET in 10 mM sodium acetate pH 5.5) using the Biacore Amine Coupling Kit as recommended by the manufacturer (1500 – 5000 RU final density) in PBS-T running buffer (10 mM phosphate, pH 7.4; 150 mM NaCl; 0.05% (v/v) Tween-20). Corresponding reference surfaces were prepared in the absence of protein. The immobilized surfaces were active as confirmed by binding of specific anti-Ret monoclonal antibodies (0.25 mg/ml stock, Abcam ab134100) in dose-dependent binding. Between titration series, the surfaces were regenerated at 50 μl/min using two 30 sec pulses of solutions I (0.1% (v/v) Empigen in Pierce Gentle Elution buffer), II (1.0 M NaCl and 0.1% (v/v) Empigen in 50 mM HCl), and III (1.0 M NaCl and 0.1% (v/v) Empigen in 50 mM NaOH).

Using PBS-T containing 5% (v/v) DMSO, fixed 100 μM concentrations of Compound 9 (negative) and compound 8 (positive) were injected in-tandem over reference and protein-immobilized surfaces at 25 μl/min (60 sec association, 60-180 sec dissociation) to establish binding specificity. To examine binding kinetics and affinity, compound 8 was titrated in single-cycle (25 μl/min x 1 sec association + 60-600 sec dissociation) and multi-cycle (10 μl/min x 10 min association + 20 min dissociation) mode. Between titration series, the surfaces were regenerated at 50 μl/min using two 30 sec pulses of solutions I (1.0 M NaCl and 0.1% (v/v) Empigen in PBST-DMSO), II (1.0 M NaCl and 0.1% (v/v) Empigen in 50 mM NaOH), and III (50 mM NaOH).

Biochemical Assays

For biochemical assays, cells were seeded onto 6-well plates (0.4×10^6 cells/well) and cultured overnight. Cells were serum-starved for 2 hr and then stimulated with compounds for 20 minutes before preparation of cell lysates in 100 μl lysis buffer (20 mM Tris-HCl pH 7.5, 137 mM NaCl, 2 mM EDTA, 1% Nonidet P-40) containing a protease inhibitor cocktail. Lysates were centrifuged at 4°C for 10min at 6000g prior to protein quantification using the Bradford assay (BioRad). After SDS-PAGE, Western transfer to PVDF membranes, and blocking steps, an

overnight incubation at 4°C with the primary antibodies pAkt, pErk, total Akt, total Erk (Cell Signaling, catalogue #4060, #4370, #9272, #9102), Actin (Sigma Aldrich, catalogue A2066), RETpY^{1062} (a gift from Dr. Brian Pierchala) were used at a 1:2,000 dilution, with secondary 1:10,000. Signals were developed using Western Lightning Plus ECL (PerkinElmer), films were scanned and quantified using ImageJ software. Controls for protein loading for each sample were standardized to total Akt, total Erk or Actin.

Primary Cultures

E18 primary cortical neurons from mouse were purchased frozen (BrainBits LLC). For biochemical assays, 0.25 x 10^6 cells were plated in 12-well plates coated with poly-D-lysine, and cultured for 5 days in commercial neurobasal media (NbActiv1). Half of the media was exchanged every 2 days. Following the culture period, the media was removed and replaced with serum-free DMEM for a 3-hour starvation. Treatments were 20 minutes, and lysates were prepared as described above.

Cell Survival Assays

Cell survival was measured by the MTT assay using optical density readings as the endpoint. 2000-5000 cells were plated in 96-well format in serum-free media (SFM) (HCell-100, Wisent) and vehicle or test agents at concentrations of 5 μM and 10 μM were added. The positive control growth factors (GF) were used at optimal concentrations (30 ng/ml GDNF for MG87 RET/GFRα1, 25 ng/ml FGF2 for MG87 RET, 30 ng/ml NGF for MG87 TrkA). FGF2 was used for MG87 RET cells as they do not respond to GDNF in the absence of GFRα1. Assay time was typically 72 hr, at which point MTT reagent (Sigma Aldrich) was added. Assays were repeated at least 3 times. MTT optical density (OD) data were standardized to growth factor = 100%, and SFM = 0%, using the formula $[(OD_{test} - OD_{SFM})*100 / (OD_{GF} - OD_{SFM})]$.

Compounds

Test compounds were acquired from the NCI/DTP repository (http://dtp.cancer.gov), through searches of the PubChem Compound database [97]. Upon receipt, structures were coded for simplicity. The original identifiers and IUPAC names are: 4-amino-8-hydroxynaphthalene-2,6-

disulfonic acid (NSC37051) **compound 7 (CAS 6271-90-5)**; 5-amino-4-hydroxynaphthalene-1,6-disulfonic acid (NSC37052) **compound 8 (CAS 6271-89-2)**; (3Z)-6-amino-4-oxo-3-(phenylhydrazinylidene)naphthalene-2,7-disulfonic acid (NSC45189) **compound 9 (CAS 6222-38-4)**; 5-amino-3-[[4-[4-[(4-amino-2-methylphenyl)diazenyl]phenyl] sulfanylphenyl]hydrazinylidene]-6-[(4-nitrophenyl)diazenyl]-4-oxonaphthalene-2,7-disulfonic acid (NSC65571) **compound 15 (CAS 6950-40-9)**; 4-amino-3-[(2,5-dichlorophenyl)diazenyl]-5-oxo-6-[[4-[4-[2-(4-oxocyclohexa-2,5-dien-1-ylidene)hydrazinyl]phenyl] sulfanylphenyl]hydrazinylidene]naphthalene-2,7-disulfonic acid (NSC75661) **compound 23**; (3E)-5-amino-3-[[4-[4-[(4-amino-6-sulfonaphthalen-1-yl)diazenyl]phenyl] phenyl]hydrazinylidene]-6-[(4-nitrophenyl)diazenyl]-4-oxonaphthalene-2,7-disulfonic acid (NSC77520) **compound 24**; 4-amino-3-[(4-nitrophenyl)diazenyl]-5-oxo-6-[[4-[4-[2-(4-oxocyclohexa-2,5-dien-1-ylidene)hydrazinyl]phenyl]sulfanylphenyl]hydrazinylidene] naphthalene-2,7-disulfonic acid (NSC79723) **compound 28**; (3Z)-5-amino-3-[[4-[4-[(2,4-diamino-5-methylphenyl)diazenyl]phenyl]phenyl]hydrazinylidene]-6-[(2,5-dichlorophenyl)diazenyl]-4-oxonaphthalene-2,7-disulfonic acid (NSC79730) **compound 29**; 4-amino-3-[[4-[4-[(1-amino-5-sulfonaphthalen-2-yl)diazenyl]phenyl]phenyl]diazenyl]-5-oxo-6-(phenylhydrazinylidene)naphthalene-2,7-disulfonic acid (NSC79745) **compound 35 (CAS 6486-54-0)**; (3Z)-5-amino-3-[[4-[4-[(2,4-diamino-3-methyl-6-sulfophenyl)diazenyl]phenyl] phenyl]hydrazinylidene]-6-[(3-nitrophenyl)diazenyl]-4-oxonaphthalene-2,7-disulfonic acid (NSC80903) **compound 36**.

SU5416 was purchased from Tocris (Cat. # 3037), and XIB4035 was purchased from Sigma (Cat. # SML1159).

Synthesis and structural characterization of compounds

See **Supplemental** information (**Appendix I)**. **Compound 8** was misannotated in the NCI library, and the correct structure is reported here. Other compounds were annotated correctly.

Animal models

All animal procedures respected the IACUC guidelines for use of animals in research, and to protocols approved by McGill University Animal Welfare Committees. All animals were housed

12 hr dark-light cycle with food and water *ad libitum*. We used the "RHOP347S" transgenic mouse (expressing the human Rhodopsin mutated at amino acid position 347) in a C57BL/6J (B6) background (kindly donated by Dr. T. Li) [98]. This model of RP faithfully replicates the features of disease progression in humans. Both male and female animals were used in the experiments. For retinal cultures, animals at post-natal day 18 weighing between 10-12 g were used. For intravitreal injections and histochemical studies, animals 8 weeks of age were used, weighing between 20-25 g.

Retinal Organotypic Cultures

Whole eyes were enucleated and whole retinas dissected from wild-type and RHOP347S mice at post-natal day 18 were used for organotypic culture experiments. Roughly 50% loss of photoreceptors occurs at this time point, making it ideal for observing signs of neuroprotection. Following enucleation, eyes were placed in a petri dish with PBS. The cornea was perforated and cut away along the ora serrata, leaving room to remove the lens. Whole intact retinas were then freely dissected away from the sclera and immediately transferred into 24 well plates containing 500 µl of culture medium (DMEM/F12 supplemented with 10 mM $NaHCO_3$, 100 µg/ml Transferrin, 100 µM Putrescine, 20 nM Progesterone, 30 nM $Na2SeO_3$, 0.05 mg/ml Gentamicin, 2 mM L-Glutamine, and 1 mM Sodium Pyruvate). Under sterile conditions, the media was gently removed and replaced with fresh media containing the treatments or controls, and incubated at 37°C and 5% CO_2 for 24 hr. Compounds were tested at a concentration of 20 µM, GDNF at 500 ng/ml. Cell grade DMSO was used for vehicle treatments and was 0.5% by volume. Retinas were then used for TUNEL staining.

TUNEL staining

Staining was performed using the DeadEnd Fluorometric TUNEL system (Promega). RHOP347S retinas in culture (n=4 for GDNF treatments, n=3 for test compounds) were first fixed in 4% PFA in PBS and kept at 4°C overnight. Three quick washes in PBS-0.2% BSA were done the next day, followed by three 30-minute permeabilization steps using 2% Triton X-100 in PBS. Retinas were then incubated with 20 µg/mL Proteinase K in PBS for 15 minutes, briefly re-fixed in 4% PFA in PBS for 30 minutes and washed again with PBS-0.2% BSA before being

transferred into Eppendorf tubes. Samples were incubated with 50 µl of equilibration buffer for 20 minutes, then 25 µl of TdT reaction mixture for 2.5 hr at 37°C. The reaction was terminated using a 30 minute incubation of 2X SSC solution. The retinas were mounted with the ganglion-cell layer facing up using Vectashield with DAPI.. For image acquisition, the retinas were divided into 4 quadrants, and 3 pictures with a 20X objective were taken in each area (central, mid, peripheral) for a total of 12 images of the outer-nuclear layer (ONL) per retina. Total TUNEL-positive cells were counted in each image semi-automatically (ImageJ). Counts were verified by at least one other person blinded to the experimental conditions. Wild-type retinal flat mounts were used as negative controls.

Immunohistochemistry

After enucleation, the eyes were immersed overnight in fixative composed of 4% PFA in PBS at 4°C, followed by cryoprotection by soaking in 30% sucrose overnight at 4°C. Eyes were frozen in O.C.T tissue TEK and cryostat sections were cut and mounted onto gelatin-coated glass slides. Sections (14 µm thick) were washed with PBSand then incubated in PBS containing 3% normal goat serum, 0.2% Triton X-100 and 3% bovine serum albumin (BSA) for 2 hr. After, sections were incubated overnight at 4°C with primary antibody (1:250 p-MAPK, Cell Signaling #4370; 1:250 p-Akt, Cell Signaling #4060; 1:400 CRALBP, Abcam ab183728). The sections were rinsed and incubated with secondary antibody for 1 hr at room temperature. Then, sections were washed and coverslipped using Vectashield mounting media with DAPI.

Image acquisition (fluorescence microscopy) and data analysis

Pictures were taken as Z-stacks of confocal optical sections using a Leica confocal microscope at a 20X objective. Images were equally adjusted using Adobe Photoshop CS 8.0 to remove background signals.

For each experimental condition, a minimum of 6 images were acquired from 3 sections cut from different areas of the retina (n=3 retinas per group). The area of the profiles of the cells expressing pErk and pAkt was measured using ImageJ software.

Intravitreal injections

Mice were anesthetized with isoflurane, delivered through a gas anesthetic mask. The treatments were delivered using a Hamilton syringe. Injections were done using a surgical microscope to visualize the Hamilton entry into the vitreous chamber and confirm delivery of the injected solution. 3 μl of a 2 mM stock solution composed of 50% DMSO in PBS were delivered. 1-3 μl injections are typically reported in the literature, with 3 μl chosen to improve accuracy of delivery and minimize the impact of any loss upon syringe withdrawal. After the injection, the syringe was left in place for 30 seconds and slowly withdrawn from the eye to prevent reflux. Experimental right eyes were injected with the test agents and left eyes served as the vehicle-injected internal control.

Statistical analyses

The quantitative data were subjected to statistical analyses using GraphPad Prism 5 software, and are presented as mean ± SD for all studies. The differences between groups were determined by ANOVA (multiple groups) followed by Dunnett's or Bonferroni-corrected t-tests. Student t-tests were performed to compare two groups. p-values below 0.05 were considered to indicate statistically significant differences between groups. The number of experimental replicates was pre-determined based on the level of variation observed in previous work, and each experiment was reproduced the number of times indicated. The nature of the experiments are exploratory, and as such are not testing a pre-specified null hypothesis. P-values are therefore meant to be descriptive in their interpretation.

Results

In vitro screening: Identification of selective RET agonists

Initial hits emerged and were identified by a luciferase-reporter assay [95] monitoring Erk activation in cells expressing GDNF receptors. Selected compounds (NCI/DTP chemical repository, and the PubChem database) [97] were screened at 5 and 20 μM concentrations (**Supplemental, Appendix I: Table 1**). A small family of compounds that increased luciferase activity >1.5 times, consistently in more than three independent luciferase-reporter assays, were considered candidates for further study.

Candidates, coded 15, 23, 24, 28, 29, 35, and 36, were tested in biochemical assays for stimulation of RET phosphorylation (pRET), and downstream phosphorylation of Akt (pAkt) and Erk (pErk) using transfected MG87 fibroblasts stably expressing either RET only or RET/GFRα1 (untransfected or TrkA-transfected MG87 cells were used as controls). Structures are shown in **Supplemental, Appendix I: Figure 1**. Cells were treated with compounds, DMSO vehicle (negative control), or GDNF (positive control), and lysates were analyzed by Western blot for pRET (specific antibody to RET-pY^{1062}), pAkt and pErk.

Compounds 15, 24, 28, 29, 35, and 36 were active and generated pAkt and pErk signals in MG87 RET/GFRα1 cells. The RET-pY^{1062} does not yield a quantifiable signal (**Figure 1A**), but pAkt and pErk quantifications are shown (**Figure 1B**). Biochemical activation by compounds was comparable to the optimal dose of GDNF. Compound 23 was not active, though it is a structural analog of the active compounds.

In MG87 RET cells compounds 15, 24, 28, 29, 35, and 36 also activate RET in the absence of GFRα1 (**Figure 1C**, quantified in **Figure 1D**); but, as GDNF requires the presence of GFRα1 receptor, GDNF was not active in these cells. Note that the compounds activate RET in the absence of GFRα1, but GFRα1 expression dampens RET activation by some compounds (especially at the lower concentrations of 5-10 μM). An example of dose-dependent activation of RET, Akt and Erk is shown for compound 29 (**Figure 1E**).

To evaluate RET selectivity and RET dependence, counter-screens were performed using the MG87 TrkA cell line expressing the TrkA receptor tyrosine kinase. In MG87 TrkA cells the positive control is Nerve Growth Factor (NGF), and vehicle and compound 23 were used as

negative controls. Compound 35, an agonist of RET, did not activate any signals in MG87 TrkA cells. There were no increases in pErk, pAkt or pTrkA compared to negative control compound 23 or to vehicle (**Figure 1F**). In positive controls, NGF increased pTrkA, pAkt and pErk levels. Hence, compound 35 appears to be RET-selective or dependent on RET-expression. Compound 35 was selected for further studies.

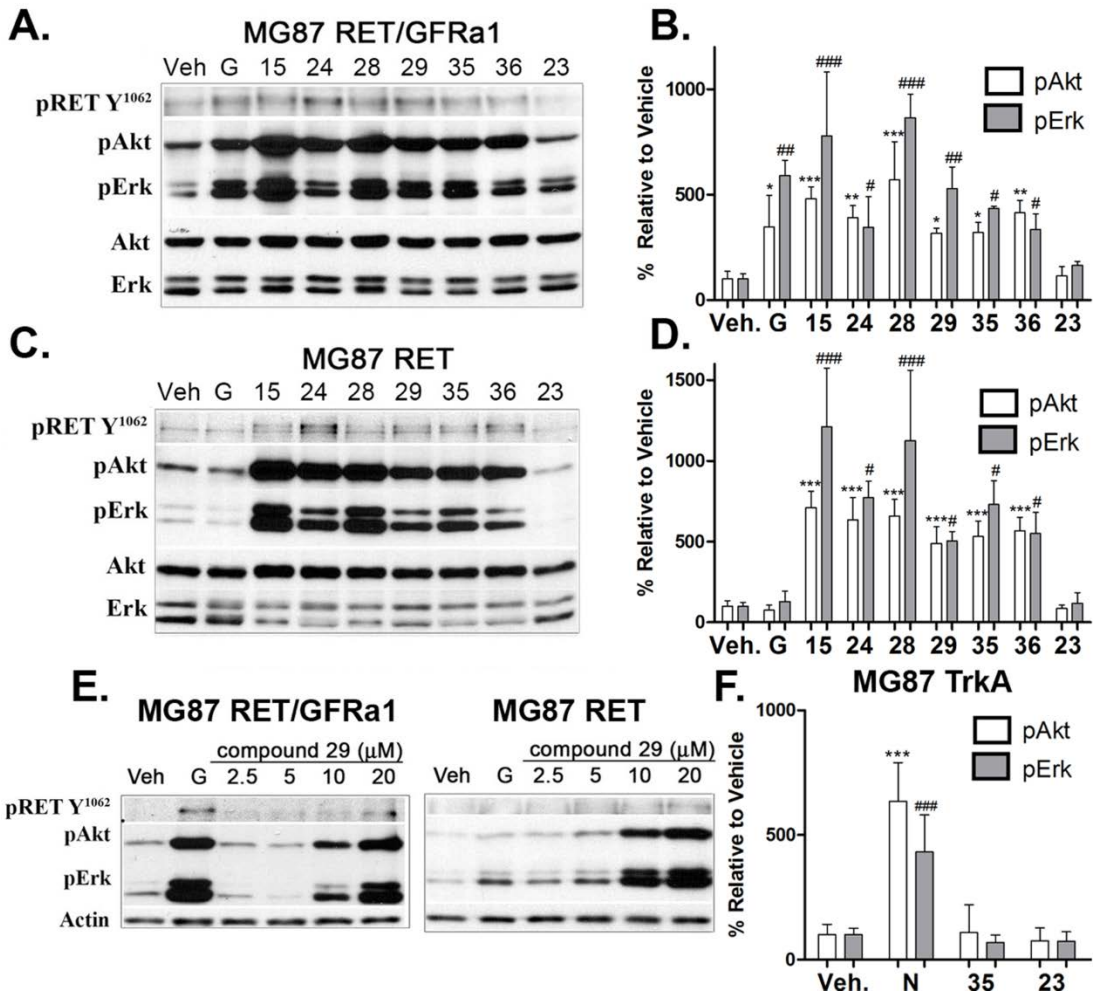

Figure 3.1. Characterization of RET agonists

A-B. Biochemical studies of RET activators in MG87 RET/GFRa1 cells. Following serum deprivation, cells were treated with DMSO vehicle (V), 10 ng/ml GDNF (G), or 20 μM compounds for 20 min. Representative blot shown, cell lysates were probed for pRET-Y^{1062}, pAkt, and pErk. Total Akt and Erk used as loading controls. Increases in pRET-Y^{1062} were seen, however compounds generated large increases particularly in pAkt and pErk, with the exception of compound 23. **C-D**. Biochemical studies of RET activators in MG87 RET cells, lacking GFRa1. Representative blot shown, demonstrating relevant signaling by this panel of compounds. Note that GDNF is inactive in this cell type, and compound 23 remains inactive. **E**. Western blots showing dose-dependent RET activation by compound 29 (2.5-20 μM) in both

MG87 RET/GFRa1 and MG87 RET cells, further suggesting GFRa1 independence. **F**. Counter screens for selectivity in MG87 TrkA cells. Western blot quantification of NGF (N) at 30 ng/ml (positive control), or the selected compound 35 at 20 μM. Compound 23 was used as a negative control. Compound 35 demonstrated the most favorable selectivity as it did not activate Akt or Erk in MG87 TrkA cells lacking RET.

Western blot data were quantified from 3 independent experiments, expressed as mean ± SD and standardized to Vehicle control. For pAkt *$p<0.05$, **$p<0.005$, ***$p<0.0005$. For pErk, #$p<0.05$, ##$p<0.005$, ###$p<0.0005$, Dunnett's test.

Optimization of selective RET agonists

Analogs of compound 35 yielded compounds 7, 8, and 9 from the NCI database (structures are listed in **Supplemental, Appendix I: Figure 1**). In MG87 RET/GFRα1 cells, compound 8 acted as a RET agonist and significantly increased pAkt and pErk, (**Figure 2A**, quantified in **2B**). Compound 7 also appeared to exhibit some activity, with a biased trend for pErk. Compound 9 was inactive.

In MG87 RET cells (lacking GFRα1) compound 8 activated RET and significantly increased the levels of RET downstream targets pAkt and pErk, and all other compounds and GDNF were inactive (**Figure 2C**, quantified in **2D**). While remaining non-significant, the same biased pErk signaling profile for compound 7 was observed in these cells as well.

RET selectivity was tested in counter-screens using MG87 TrkA cells. Compounds 7, 8, and 9 did not generate pAkt or pErk or pTrkA signals, while positive control Nerve Growth Factor (NGF) activated these signals (**Figure 2E**, quantified in **2F**). These data indicate that compound 8 (like parental compound 35) remains RET-selective or RET-dependent, and does not require co-expression of GFRα1, while compounds 7 and 9 are negative controls.

Signaling was further evaluated in E18 mouse primary cortical neurons which endogenously express RET and GFRα1, and respond to GDNF [99, 100]. Increases in pAkt were detectable following treatment with GDNF (200 ng/ml) or compound 8 (10 and 20 μM) (**Figure 2G**). These data confirm RET activation by compound 8 in primary neurons.

Agonism by compound 8 requires the RET kinase to be active. In MG87 RET/GFRα1 cells, the pAkt and pErk induced by GDNF or by compound 8 are completely ablated when cells are pre-treated with RET kinase inhibitor SU5416 [101] (**Figure 2H**).

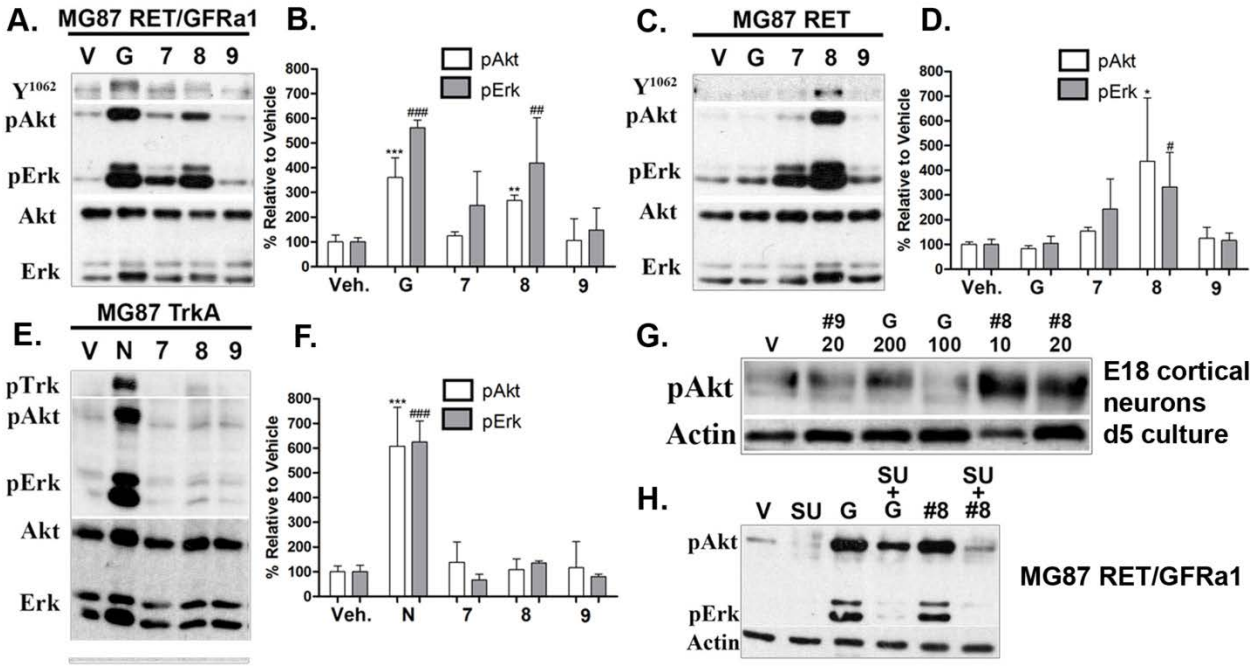

Figure 3.2. Lead optimization

A-B. Biochemical studies with compound 35 derivatives in MG87 RET/GFRa1 cells assayed 20 μM concentrations of compounds 7, 8, and 9 with a 20 min exposure time. Representative Western blot shown for RET-pY^{1062} and its effectors pAkt and pErk. GDNF (G) is GDNF positive control and vehicle (V) is the DMSO negative control. Compound 8 displayed a signaling profile which mirrored that of the parent compounds, while compound 7 generated a pErk biased signaling trend. Compound 9 was completely inactive. **C-D**. Biochemical studies with compound 35 derivatives tested in MG87 RET cells. Representative Western blot shown for RET-pY^{1062} and its effectors pAkt and pErk. GDNF (G) is GDNF positive control and vehicle (V) is the DMSO negative control. Signaling profiles of compounds 7,8, and 9 were similar to those observed in MG87 GFRa1/RET cells, indicative these derivatives maintained GFRa1 independence. **E-F**. Selectivity screens in MG87 TrkA cells, using 20 μM concentrations of compound 35 derivatives, stimulated for 20 min. Representative blot for pTrkA and its effectors pAkt and pErk. NGF (N) is positive control and vehicle (V) is the negative control. Compounds 7,8, and 9 were all inactive in these assays. **G**. Compound 8 signaling in E18 mouse cortical neurons. Neurons were treated with compound 9 at 20 μM, GDNF at 100 and 200 ng/ml, and compound 8 at 10 μM and 20 μM, for 20 min. Representative blot showing pAkt increases observed with both treatments of compound 8. Actin was used as loading control. **H**. RET

inhibition blocks compound 8 signaling. MG87 RET/GFRa1 cells were first treated with the RET antagonist SU5416 at 10 μM for 20 min, and then additionally for 20 min with GDNF (G) or compound 8. Vehicle (V) and SU5416 (S) alone are controls. SU5416 pre-treatment resulted in clear reductions in the signaling capacity of both GDNF and compound 8.

Representative blot showing pAkt and pErk, with Actin as loading control. Vehicle (V) is the negative control. In panels **B**, **D**, and **F**, quantification of western blot data was standardized to total Erk or total Akt and expressed as mean ± SD from 3 independent experiments. For pAkt *p<0.05, **p<0.005, ***p<0.0005. For pErk #p<0.05, ##p<0.005, ###p<0.0005 versus Vehicle, Dunnett's test.

Compound 8 is a RET ligand

We examined the kinetics and affinity of RET-compound 8 interactions using real-time surface plasmon resonance (SPR). Recombinant human RET extracellular ectodomain was amine-coupled to SPR sensors, with reference sensor having no protein. A fixed concentration (100 μM) screening of compound 8 to RET-coated surfaces showed substantial binding with slow dissociation kinetics (**Figure 3A**). Under the same binding conditions and on the same chip, inactive compound 9 failed to interact with RET (**Figure 3A**).

Dose-dependent titrations (**Figure 3B**) showed that on low-density RET surfaces compound 8 generated signals (e.g. 150 RU at 12.5 μM and 230 RU at 25 μM, see arrows). Complementary multi-cycle analyses indicated that compound 8 has sub-micromolar affinity for RET (**Figure 3C**). After the binding studies using titrations of the compound, we verified that immobilized RET protein was still present on chip surfaces as it was bound by anti-RET monoclonal antibodies (mAb). The anti-RET mAb generated signals correlating binding to the low-density and the high-density RET-loaded chip surfaces (**Figure 3D**). These data indicate that compound 8 is a genuine ligand of the RET ectodomain.

Compound 8 induces signals through RET phosphorylation

Taken together, the data strongly support RET as the main target for the panel of molecules tested. Moreover compound 8 binds to RET directly.

Compound 8 and compound 9 (negative control) were selected for dose-dependent studies in MG87 RET/GFRα1 cells. From lysates prepared from treated or control cells, RET was immunoprecipitated, and total pTyr was quantified by western blotting.

This technique allows the direct detection and quantification of pRET. The data show dose-dependent induction of pRET by compound 8, comparable to GDNF, while compound 9 was inactive over the full concentration range (**Figure 3E**, quantified in **3G**). Similar experiments in MG87 RET cells showed that compound 8 induces detectable increases in pRET whether or not cells express GFRα1 (**Figure 3F**).

These data demonstrate that RET is a pharmacological target for compound 8, and corroborate the biochemical findings that GFRα1 is not necessary for the compound to induce signaling. However, we note that the 50-100 μM concentrations that induce significant pRET

levels are higher than the 5-20 μM concentrations that afford detection of pAkt and pErk. This can be explained by signal amplification, and by the transient nature of pRET which reportedly is difficult to detect because it is rapidly targeted for degradation [102]. Therefore, small, undetectable changes in phospho-RET may lead to much larger increases in the effectors pAkt and pErk.

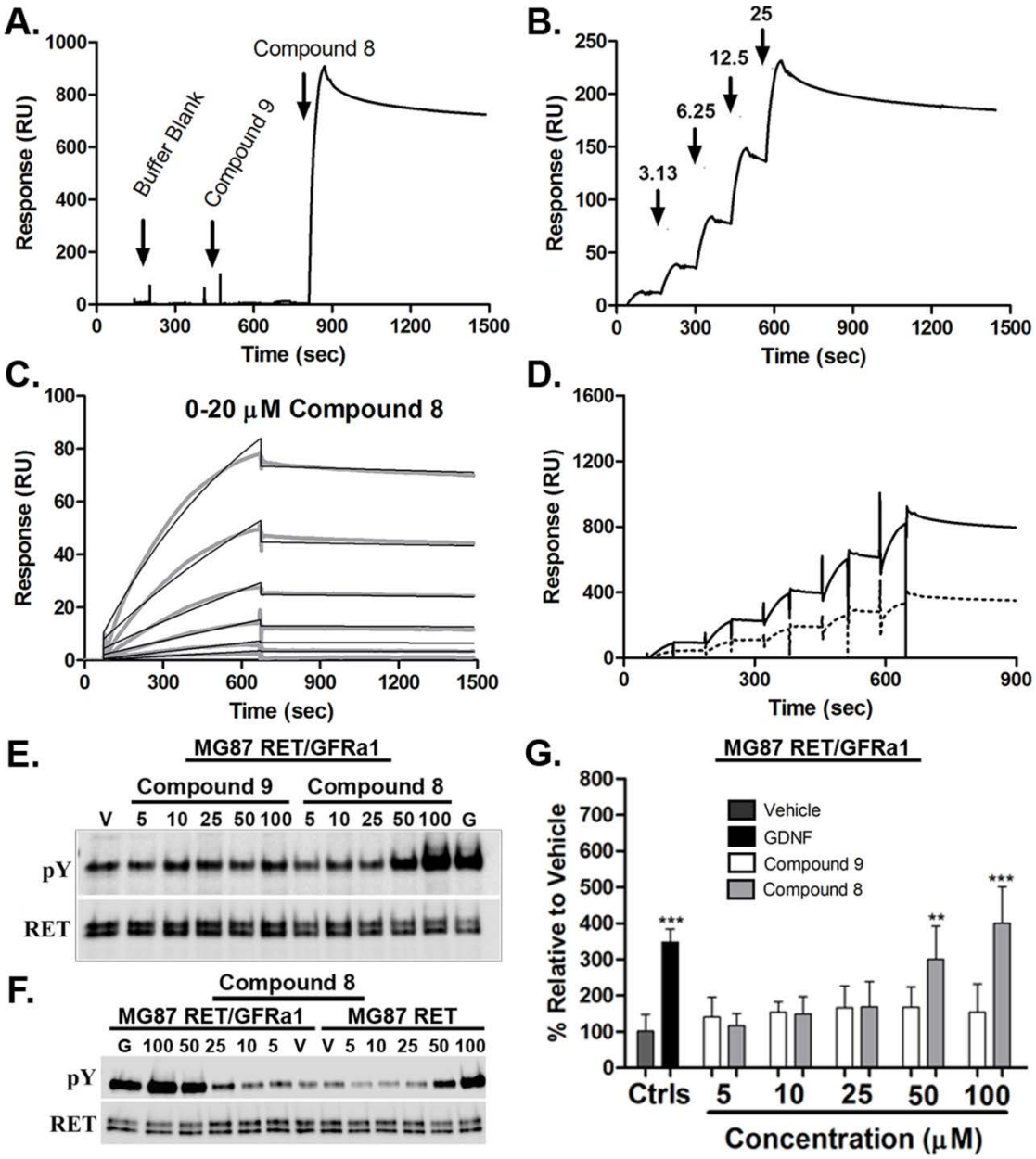

Figure 3.3 Compound 8 is a RET ligand that induces RET tyrosine phosphorylation

A. Surface Plasmon Resonance, real-time binding to recombinant human RET ectodomain. Representative, reference-subtracted SPR for sequential injections of buffer (PBS-T containing 2% (v/v) DMSO), compound 9 (100 μM, negative control), and compound 8 (100 μM) over amine-coupled high-density RET (4600 RU, *solid black line*) at 25 μL/min (60 sec association). **B**. Representative single-cycle SPR data for compound 8 (0 – 25 μM; 2-fold dilution series) injected over amine-coupled low-density RET (1650 RU, *solid black line*) at 25 μL/min (60 sec association +/- 60-600 sec dissociation). Arrows indicate injection times. **C**.

Representative multi-cycle SPR data for compound 8 (0 – 20 μM; 2-fold dilution series) injected over 1650 RU RET surface at 25 μL/min (600 sec association + 900 sec dissociation); experimental titration series (*grey lines*) were fit globally to "1:1 kinetic" model in BIAevaluation software (*black lines*). **D**. Representative single-cycle SPR data for anti-RET monoclonal antibody (0 – 210 nM; 2-fold dilution series) injected over 4600 RU RET (*solid black line*), and 1650 RU RET (*dashed black line*) surfaces at 25 μL/min (60 sec association +/- 60-600 sec dissociation). **E-G**. Compound 8 induces RET phosphorylation in a dose-dependent manner. MG87 RET/GFRa1 or MG87 RET cells were treated for 15 min with compound 8, or control compound 9, at a concentration range of 5-100 μM, or controls GDNF (G) at 200 ng/ml, or vehicle (V). RET protein was immunoprecipitated and probed with 4G10 mAb (detecting phosphotyrosine). Compound 9 was inactive at all concentrations, whereas compound 8 induced a marked increase in phosphorylated RET whether or not cells express GFRa1. In MG87 RET/GFRa1 cells compound 8 at 50 μM was as effective GDNF at 200 ng/ml.

Quantification in panel G was standardized to total RET protein and expressed as mean ± SD from 3 independent experiments. **$p<0.005$, ***$p<0.0005$ versus Vehicle, Dunnett's test.

Small molecule RET activation does not require GFRα1 expression but is regulated by GFRα1 likely via an allosteric mechanism

Given that compound 8 induces RET-pY^{1062}, a phosphotyrosine linked to the survival promoting effect of GDNF in neurons [81, 82] we quantified in MTT assays the cell survival / active metabolism as a biological correlate of the biochemical data.

MG87 RET, MG87 RET/GFRα1, and MG87 TrkA cells were treated with test compounds 7 and 8. Inactive compound 9 and vehicle were used as negative controls. As positive controls we used growth factors: FGF2 for MG87 RET (as these cells lacking GFRα1 do not respond to GDNF), GDNF for MG87 RET/GFRα1, and NGF for MG87 TrkA. The growth factors as positive controls were used at their optimal concentrations to afford maximal cell viability, which was set to 100%. Cells were cultured for 72 hr under serum-free conditions ± treatments.

In MG87 RET cells compounds 7 and 8 (5-10 μM) supported viability to a significant ~25% of control FGF2 (**Figure 4A**), and GDNF was inactive because these cells lack GFRα1. In MG87 RET/GFRα1 cells compounds 7 and 8 (5-10 μM) supported viability to ~10% (non-significant) compared to control GDNF (**Figure 4B**). Control compound 9 was inactive in all cell lines, as anticipated.

In MG87 RET/GFRα1 cells, at 10 μM compound 8 does not afford significant cell survival (**Figure 4B**), but signal transduction is significant (**Figure 2**). The discrepancy between biological (cell survival) and biochemical (pTyr) signals may be due to expression of GFRα1 negatively regulating ligand binding or long-term survival. A similar phenomenon was reported for GDNF mutants [21]. Hence, higher concentrations of compound 8 were evaluated in biological assays.

In MG87 RET/GFRα1 cells compound 8 at 40 μM supported viability to a significant ~65% of GDNF levels, while compound 9 remained inactive (**Figure 4B**). In counter-assays using MG87 TrkA cells compounds 7 and 8 (as well as compound 9) were inactive at all concentrations, compared to positive control NGF (N) (**Figure 4C**).

Overall, these biological data demonstrate that compound 8 binds RET, and acts as a selective RET agonist that –unlike GDNF– does not require GFRα1 co-receptors. Compound 8 via RET phosphorylation activates signal transduction pathways that afford neuronal survival independent

of GFRα1 co-receptors. However, expression of GFRα1 co-receptors appear to modulate the long-term survival-promoting action of compound 8. The GFRα1 repression can be overcome with higher concentrations of compound 8, which achieve better cell survival.

Pharmacological modulation of the regulation by GFRα1

To interrogate how GFRα1 regulates compound 8-mediated activation of RET, we used XIB4035, an agent reported to modulate GFRα1 without having intrinsic signaling activity [103].

In MG87 RET/GFRα1 cells, pre-treatment with 4 μM XIB4035 for 20 minutes completely blocked the biochemical signals activated by compound 8, without inhibiting GDNF signals. Cellular controls using MG87 TrkA cells showed that XIB4035 had no effect on either NGF or FGF2 growth factor signaling, demonstrating that the XIB4035 block is selective (**Figure 4D**).

Hence, expression of unbound GFRα1 negatively modulates the RET signals that are activated by compound 8, and this modulation can be overcome with higher concentrations of compound 8. Moreover, the GFRα1 bound by XIB4035 inhibits compound 8 activation of RET even more strongly. Given that compound 8 is a genuine ligand of RET (see SPR studies, **Fig. 3**) we infer that the repression of compound 8 activation of RET by unbound GFRα1 (and the even stronger inhibition by bound GFRα1•XIB4035) likely occurs through an allosteric mechanism.

This concept would be useful for devising screening strategies. While the GFRα1 ligand XIB4035 exacerbates RET inhibition, it is conceivable that there may be GFRα1 ligands that reduce RET inhibition, and potentially could even allow ligand-independent activation of RET.

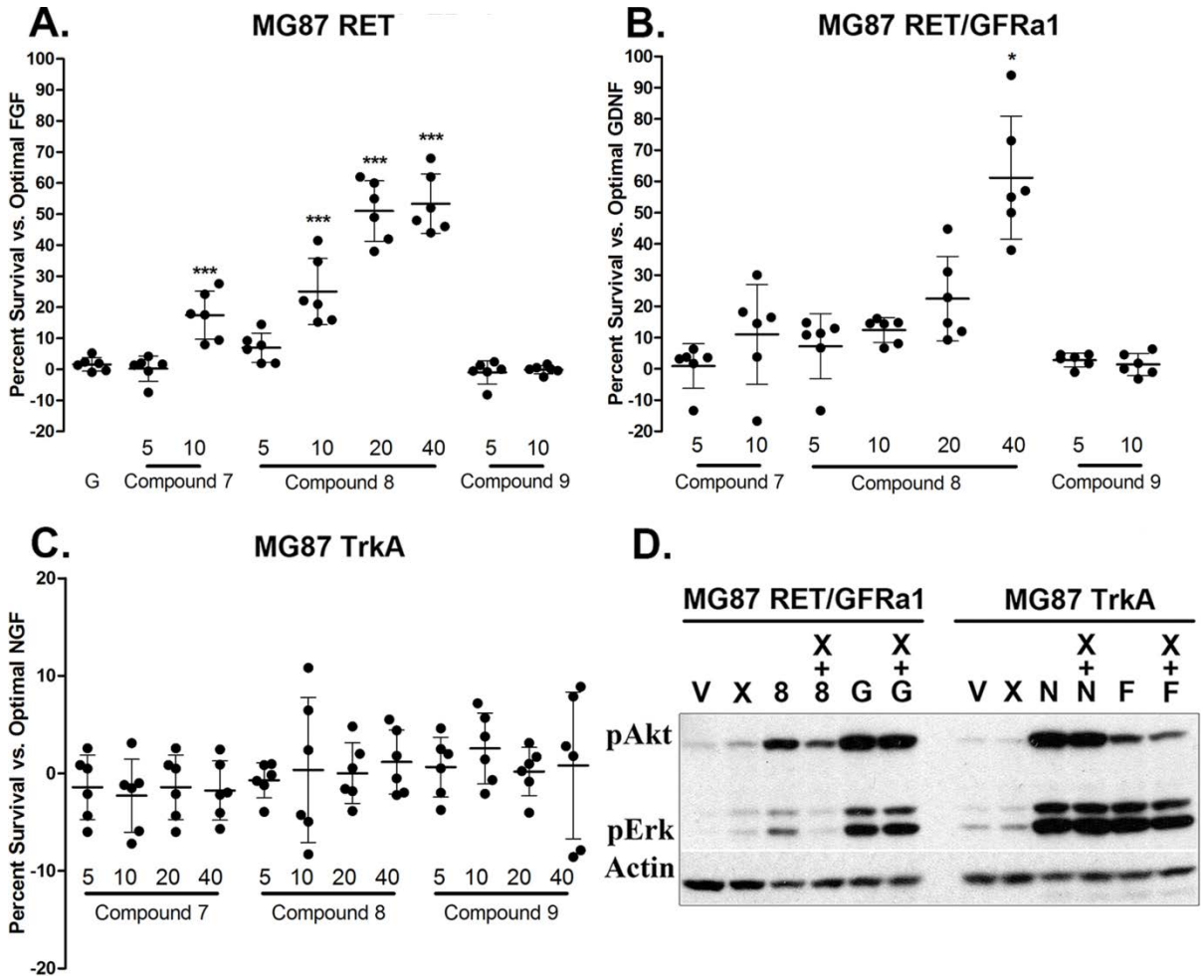

Figure 3.4. RET-trophic signals activated by compound 8 are regulated by GFRa1

A, Compound 35 derivatives mediate survival in MG87 RET cells. Cells under serum starvation for 72 hr were treated with DMSO Vehicle (V), FGF (as these cells are insensitive to GDNF), or compounds 7, 8, and 9; at 5 and 10 μM concentrations. Cell survival/metabolism was assessed via the MTT assay. 10 μM concentrations of compound 7 or compound 8 yielded appreciable survival levels; whereas compound 9 was inactive, as expected. **B**, Compound 35 derivatives do not afford survival in MG87 RET/GFRa1 cells under the same conditions. In these cells, GDNF yielded significant survival while the trophic effects of compounds 7 and 8 diminished, suggesting a negative influence of the GFRa1 receptor. MG87 RET/GFRa1 survival increased with higher concentrations of compound 8, and reached significance at 40 μM, suggesting a negative regulatory role of GFRa1 expression on the functional outcome. **C**. Compound 35 derivatives demonstrate selectivity as measured by cell survival. MTT assays

conducted in the MG87 TrkA cell line, covering the full concentration range of 5 to 40 μM for each compound, were standardized to positive control NGF (N) and compared against Vehicle (V). All compounds were completely inactive in this cell type, including GDNF (G). **D**. Biochemical studies on the influence of GFRa1 and compound 8. MG87 RET/GFRa1 or MG87 TrkA cells were pretreated with 4 μM XIB4035 (a GFRa1 modulator) for 10 minutes before the addition of compound 8 at 10 μM, GDNF (G), NGF (N), or FGF2 (F). XIB4035 blocked the signaling of compound 8, but did not affect GDNF. Control experiments in the TrkA expressing cells showed that XIB4035 did not impact either NGF or FGF2 signals, overall supporting the negative regulatory role of GFRa1 specifically on compound 8 signaling.

MTT Data are expressed as % survival relative to optimal growth factor ± SD from 6 independent experiments (each experiment n=4-8 replicate wells which were averaged). For each cell type, the respective trophic factor was standardized to 100%, and vehicle to 0%. * $p < 0.05$, *** $p < 0.0005$, Dunnett's test versus inactive compound 9.

Compound 8 reduces photoreceptor apoptosis in a retinitis pigmentosa model, and activates pErk and pAkt *in vivo*

Compound 8 was tested for neuroprotective capabilities in the mutant RHOP347S transgenic mouse model of retinitis pigmentosa. This mutation of the *rhodopsin* gene causes a highly aggressive phenotype with ~50% photoreceptor death by post-natal day 18, and nearly complete loss by post-natal day 28 [98].

Organotypic cultures of RHOP347S retinas from post-natal day 18 mice cultured for 24 hr exhibit TUNEL-positive staining in the photoreceptor layer (indicating apoptosis), with other retinal structures remaining free of apoptosis (**Figure 5A**). The PN 18 time point is optimal since significant apoptosis is observed before peak degeneration occurs. Controls using retinal explants from wild-type mice resulted in very low or absent TUNEL signal.

Compound 8 (20 μM) affords a significant ~25% decrease in TUNEL-positive cells indicating neuroprotection in RHOP347S retinas. Representative pictures from the central retina (the region surrounding the optic nerve) demonstrate the reduction in TUNEL-positive cells (**Figure 5A**)**.** In contrast, GDNF (500 ng/ml) did not reduce TUNEL counts compared to vehicle. These data indicate that compound 8 possesses disease-modifying capabilities in the degenerating retina, with an efficacy that is above GDNF under the conditions evaluated. These data highlight the potential utility of using small, selective ligands over large proteins like GDNF as therapeutics.

To further evaluate compound 8 *in vivo*, it was delivered by intravitreal injection in wild-type mice. In each mouse, one eye served as the test eye, and the contralateral eye received control vehicle. Retinal sections were prepared 1 hr later, and pErk and pAkt levels were analyzed by immunohistochemistry.

The effectors pAkt (**Figure 5B**) and pErk (**Figure 5C**) were increased after treatment with compound 8, mainly in Müller cells as confirmed by co-localization with the glial marker cellular retinaldehyde binding-protein (CRALBP). This is consistent with Müller cells expressing RET [104, 105]. High pErk and pAkt were noted particularly in the Müller glial cell processes and fibers projecting towards the photoreceptors. The retinal pErk and pAkt increases were a significant ~3-fold and ~2-fold respectively compared to vehicle (quantified in **Figure 5D**). We were unable to localize pRET in these retinas, as the anti-pRET antibody does not label tissues, and activated pRET is rapidly targeted for degradation [102].

These data indicate that compound 8 is bioactive *in vivo* in the mouse retina, and the neuroprotective effect seen in the experiments above likely derives from Müller glia supporting the photoreceptor population in a paracrine manner.

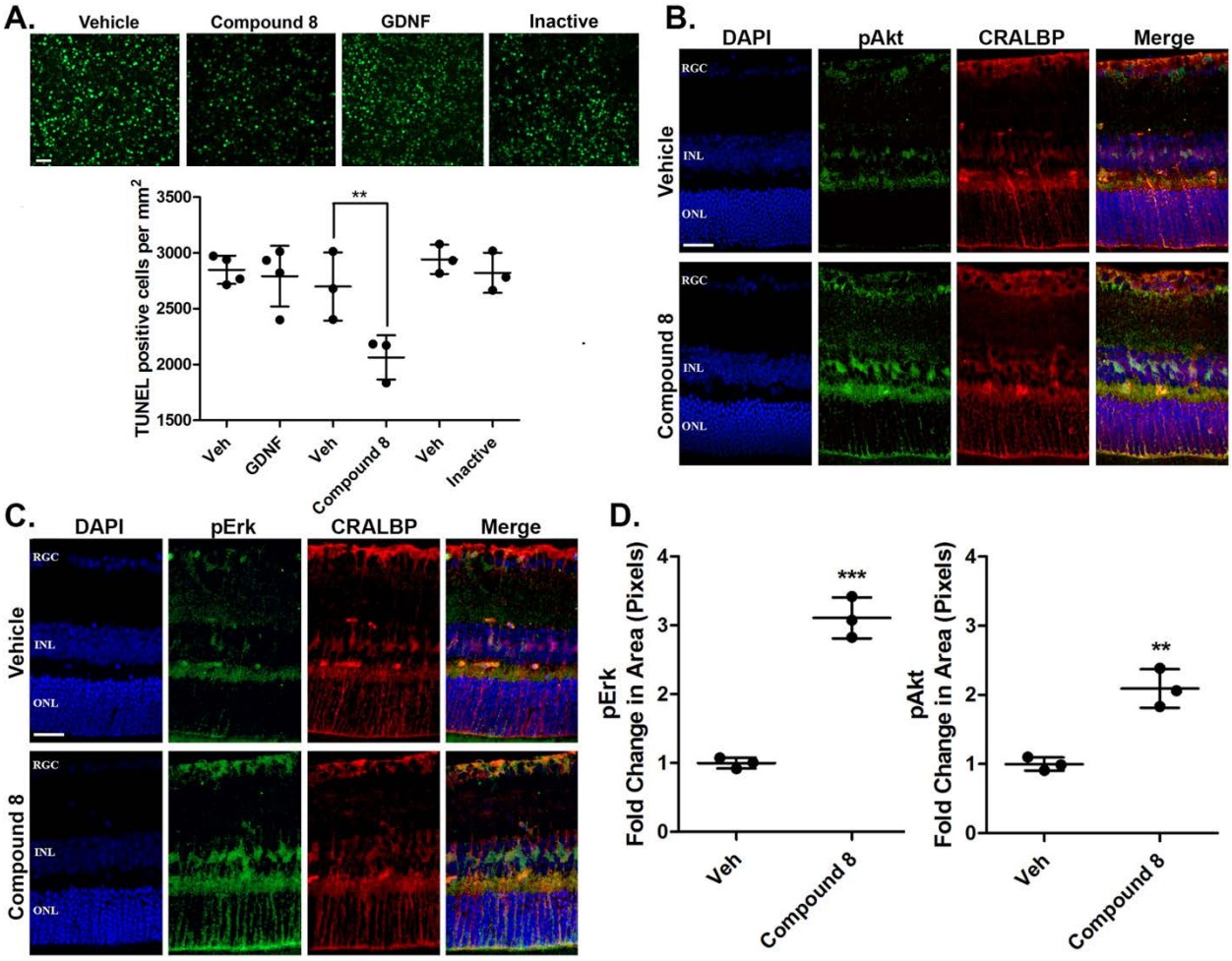

Figure 3.5. Compound 8 is neuroprotective in the RHOP347S model of RP and activates Akt and Erk in retinal Müller Glial cells

A. Compound 8 reduces neuronal death. Whole retinas of post-natal day 18 RHOP347S mice were dissected for organotypic culture. Each paired set of retinas (left and right of the same mouse) were treated with either compound 8 at 20 μM or GDNF at 500 ng/ml in one retina, and DMSO vehicle (V) as control in the other retina. In a separate series of experiments, an inactive compound was also tested as control at 20 μM. Cultures were kept for 24 hr, then TUNEL staining was performed. Representative TUNEL images taken at 20x in the central retina are shown. Scale bar = 25 μm. Quantification of TUNEL-positive photoreceptors in the ONL shows that treatment with 8 reduces apoptosis, while GDNF had no effect.

Data expressed as TUNEL-positive cells per mm^2 ± SD, **p<0.005, Bonferroni-corrected t-test.

B-D. Compound 8 activates signals *in vivo*. Young adult mice (8 weeks old) were injected intravitreally (2 μg) with compound 8 in one eye or DMSO Vehicle in the contralateral eye. Eyecups were collected after 1 hr and sectioned. Compound 8 increased pAkt in the inner nuclear layer, as well as in fibers projecting from cell bodies in the inner nuclear layer (Müller cell bodies). These signals co-localized with the Müller cell marker CRALBP. Compound 8 also increased pErk in the inner nuclear layer, as well as in fibers projecting from cell bodies in the inner nuclear layer (Müller cell bodies) towards the ONL where the cell body of photoreceptors reside. These signals co-localized with the Müller cell marker CRALBP.

Scale bar = 25 μm. RGC = retinal ganglion cell layer, INL= Inner nuclear layer, ONL = outer nuclear layer. Quantification of pAkt and pErk (n=3 per group) expressed as the fold-change in pixel area over vehicle ± SD, ***$p<0.0005$, Student t-test, **$p<0.005$, Student t-test.

Compound 8 is incorrectly curated in the NCI library

In an effort to develop structure-activity relationships, and to generate new chemical entities, we attempted synthesis of analogs of compound 8. Surprisingly, the in-house synthesized compound 8 and its derivatives were inactive.

Thus, we analyzed in detail the identity of compound 8 procured from the NCI, though the amount of material provided was quite limiting. Reverse-phase HPLC analysis revealed that NCI compound 8 has a major peak with 90% of the material, and the remaining material was a mixture (**Supplemental, Appendix I: Figure 2**). The major fraction was isolated and characterized.

The mass of compound 8 (ESI Mass Spec) that we obtained matched that reported by the NCI, however the 1H-NMR spectra revealed an inconsistency with the proposed structure (**Supplemental, Appendix I: Figure 3**). The triplet observed around 7.4ppm suggested an aromatic proton with two neighboring protons. This resonance is not possible given the side-group configuration of compound 8 reported in the NCI database. However, this resonance pattern and the mass are consistent with a positional isomer 4-Amino-5-hydroxy-1,3-naphthalenedisulfonic acid.

We acquired 4-Amino-5-hydroxy-1,3-naphthalenedisulfonic acid commercially (TCI), and this isomer had a mass and 1H-NMR spectra matching that of compound 8. The two agents (NCI-compund 8 and 4-Amino-5-hydroxy-1,3-naphthalenedisulfonic acid) also co-eluted in Reverse-phase HPLC under different buffer conditions, confirming a likely incorrect structural assignment of compound 8 at the NCI database.

Following these findings, we also examined mass spectra of other compounds 15, 23, 29, and 35. The mass of all these agents are reported correctly in the NCI database. Moreover, 1H-NMR spectra of compounds 29 and 35 are consistent with the structures reported in the NCI database, and they are likely correct. While the binding and the bioactivity we report for compound 8 (and other compounds) are conclusive, these findings serve as a cautionary note when screening large chemical databases. Further structural elucidation and synthesis of the bioactive component of compound 8 is under investigation.

Discussion

We have characterized a novel class of small molecules that can activate RET. The small molecules provide improved RET receptor specificity compared to GDNF which requires GFRα1 for activating RET [89-91], and binds to other targets such as heparan sulphate proteoglycans (Bespalov et al. 2011).

RET-selective ligands were useful as a chemical biology tool to evaluate GFRα1•RET functional interactions. We show that expression of GFRα1 (in the unliganded state) dampens the trophic efficacy of compound 8, while in the bound state (with XIB4035) it further inhibits pAkt/pErk signals induced by compound 8. The data highlights the dynamic relationships that exist between RET and GFRα1 receptors.

RET-selective ligands were useful also as neuroprotective agents, and compared to GDNF, are superior therapeutics *ex vivo* and *in vivo*, reducing neuronal death.

RET–dependent signals and selectivity, possible mechanism of action, and the influence of GFRα1

Compound 8 is a genuine ligand of RET ectodomain. Compound 8 and related small drug-like compounds activate the intracellular downstream effectors Akt and Erk. Distinct from GDNF, the compounds activate RET in cells lacking the GFRα1 co-receptor. The agents do not affect GDNF functionally, do not require GDNF or GFRα1 to produce biological effects, and appear to be RET-selective.

There are other reported small molecule "GDNF mimetics" acting as RET agonists, but they have poor pharmacological properties [106-109]. BT13 exists as one of the few other instances of a selective, GFRα-independent agonist, however it suffers from low solubility. Moreover, since these agents compete with GDNF binding, if used as therapeutics they would reduce any benefit provided by endogenous GDNF. Another agent XIB4035 acts as a GFRα1 modulator, but it requires the presence of GDNF and acts only on cells co-expressing RET/GFRα1 [103, 110].

We speculate that the RET-activating agents we report here may be allosteric, though this notion remains unproven. Analysis of the RET/GFRα1 interface revealed a potential allosteric binding site for small molecules [111]. An allosteric mechanism would be consistent with the

ligand-independent regulation of GFRα1 upon RET [112], and observations that mutant forms of GDNF with low affinity for GFRα1 binding can signal through RET but require GFRα1 to be present [21].

RET is a receptor tyrosine kinase (RTK), a family of receptors generally considered to require homodimerization and/or a conformational reorganization of homodimers for activation. It is unlikely that the small molecules would be capable of inducing RET dimerization given their small size and limited surfaces, and the fact that they are asymmetrical and most likely monovalent. However, all RTKs exist at equilibrium between monomeric and dimeric (or oligomeric) forms in the absence ligand, such that a small molecule could induce a conformational change within a preformed receptor complex. This 'dynamic equilibrium' phenomenon has been shown for other neurotrophin RTKs [23, 113, 114], and was suggested for RET [22].

Compound 8 rescues MG87 RET cells from serum-deprivation induced death, but to rescue MG87 RET/GFRα1 cells it required relatively high concentrations, well beyond those needed for pAkt and pErk activation. While the small molecules activate signals in the absence of GFRα1, agonism leading to cell survival can be partially suppressed by the presence of GFRα1. The partial suppression of RET activation by GFRα1 can be overcome by increasing the concentration of compound 8, further suggesting an allosteric impact or an influence on ligand affinity. This is consistent with discrepancies between biochemical signals and biological outcomes reported for GDNF [115]. GDNF-activated RET signaling can be progressively dampened by increasing expression levels of GFRα1 [116].

Since GFRα1 also determines the cellular localization of activated RET to lipid rafts, which in turn can influence signaling, perhaps this is a mechanism for GFRα1 suppression of RET activation by compound 8. The functional antagonism of compound 8 (a RET-activator) by XIB4035 (a reported GFRα1 ligand) further suggests a ligand-dependent allosteric cross-regulation.

Comparable to the functional cross-talk between GFRα1–RET described here, there are reported agonists of Trk receptors [113, 117, 118] whose function can be regulated by $p75^{NTR}$ co-receptors. Regulation can be allosteric, with the ligands promoting Trk-p75 interactions, or with the ligands unmasking a cryptic receptor hot spot [3, 93, 119].

Therapeutic utility

GDNF plays an important neuroprotective role in the developing and the adult retina, supporting neuronal populations. Transgenic mice expressing human rhodopsin with a proline-serine substitution at residue 347 faithfully replicate the RP disease, and were chosen for our studies [98]. Compound 8-induced RET signaling translated into a functional neuroprotective effect, with a significantly reduced number of TUNEL counts in the ONL, compared to vehicle. In contrast, GDNF itself failed to reduce TUNEL counts with concentrations up to 500 ng/ml (using recombinant GDNF produced in *E. coli*, or in mammalian CHO cells).

The reason for the failure of GDNF in our therapeutic experiments is possibly due to the fact that we used a single dose, attempting to evaluate a translational paradigm. Other studies, including those of degeneration due to RP either employ multiple doses or achieve sustained GDNF expression and release [85-87]. GDNF can also fail due to clearance after binding to extracellular matrix and transmembrane heparin sulphate proteoglycans and other proteins upregulated in the degenerating retina [120].

RP is one of the most common forms of inherited visual loss, affecting over a million people worldwide, and is the result of about 400 possible mutations in any one of multiple genes such as rhodopsin. The RP disease is characterized by progressive degeneration of photoreceptors initiated by the mutant rhodopsin, followed by retinal pigmented epithelium stress, and toxic/oxidative/pro-inflammatory damage to the visual system and irreversible blindness [121]. There is no cure or effective treatment. Given that RP is the result of one of many possible mutations in any one of multiple genes, the availability of a small molecule neuroprotective agent would allow treatment of a broad spectrum of patients regardless of disease etiology.

Intravitreal administration of compound 8 induced pErk and pAkt in Müller cells, consistent with other reports using GDNF and related growth factors [105, 122]. Our results support the notion of a non-cell autologous mechanism where neuroprotective signals likely originate from Müller glia acting in a paracrine fashion. This concept is consistent with the fact that ectopic expression of RET on photoreceptors failed to protect them from degeneration [123], and papers suggesting an indirect rescue of photoreceptors either through mitigation of toxic events within

the retina, or by inducing paracrine release of trophic factors which then act on target neurons [104, 105, 124].

Chemical Database Screening: A cautionary tale

Chemical libraries are a valuable resource for research initiatives. However, there continue to be complications. This is especially relevant given the rise of high-throughput screening techniques, when often the data reported are not sufficient for others to interpret and/or replicate [125]. While some chemical repositories do explicitly state that they cannot assure the contents of their libraries, they are also not permitted to provide adequate details in the case of a discrepancy. This is the case for compound 8 and its derivatives where supplier information and storage conditions cannot be provided by the NCI (personal correspondence).

The situation here is similar to the discovery of TIC10/ONC20, an anti-cancer therapeutic agent. TIC10/ONC201 emerged from a screen from the NCI library, and the structure had been only partially documented using mass spectroscopy [126]. Inconsistencies led to the finding that the real active molecule was in fact an isomer of the structure reported by the NCI [127], and both the mixture as well as the correct compound were used for clinical development. In both TIC10/ONC201 and compound 8 the lack of a precise structure does not undermine the biological data reported. However, considerable efforts must be directed at identifying the active component of compound 8 for future studies and reproducibility.

Overall, our work demonstrates the concept that it is possible to develop small molecule RET agonists that do not require GFRα1, and which are devoid of many of the therapeutic hurdles of the GDNF protein. Using small molecules as probes, regulation of agonist-induced RET signals by GFRα1 is demonstrated. The data highlight the utility and advantages small molecules offer with respect to target validation and receptor biology.

Acknowledgements

This work was supported by a CIHR grant to HUS and the Lundbeck Foundation and Sigrid Jusélius Foundation to MS. We are thankful for reagents provided by Dr. Brian Pierchala (pRET antibodies), Dr. Eero Castren (MG87/Trk cell lines), Dr. Carlos Ibanez (MG87/RET cell lines), and Dr. T. Li (RHOP347S transgenic mice). Jenni Montonen assisted with the Ret phosphorylation assays. Dr. Enrique de la Rosa (Spain) assisted with retinal explants and TUNEL assays. The McGill SPR-MS Facility thanks the Canada Foundation for Innovation (CFI grant #228340) for the BIACORE T200 SPR infrastructure.

Disclosures

Patent applications have been filed on behalf of authors (HUS, SJ, MS, and YS).

Connecting Text Between Chapters 2, 3, and 4

In the previous chapters as a whole, we have outlined and demonstrated the two therapeutic approaches in degenerative disease, anti-neurotoxic and pro-survival. The last chapter focused on a screening initiative which led to the discovery of selective RET-activating molecules that signal without reliance on the GFRa1 co-receptor. This also allowed us to test the functional outcomes that may result from RET/GFRa1 cross-regulation, and GFRa1 was shown to exert a negative influence on RET signaling. We further validated RET as a neuroprotective target and provided some insights into how GFRa1 expression may influence the efficacy of a treatment.

We conclude here also with a caveat; that there are concerns when screening compounds from large chemical repositories. Oftentimes these compounds are impure and in the case of compound 8, mislabeled. Attempting to synthesize the 'active' compound 8 led to the startling realization that it was inert in its purest form. Proper isolation and identification of the true active component was met with many obstacles and is the subject of ongoing work.

These discoveries, however demoralizing, formed the hypothesis that the impurities in compound 8 could be by-products of oxidation. As the naphthalene core of compound 8 could readily oxidize to a naphthoquinone, we begin chapter 4 with the screening of some of these derivatives. A new family of RET agonists emerged from these efforts, which possessed some unique biological properties.

Chapter 4

Small-molecule agonists of the RET receptor tyrosine kinase activate biased trophic signals that are influenced by the presence of GFRa1 co-receptors

Sean Jmaeff [1,2], Yulia Sidorova [3], Hinyu Nedev [1], Mart Saarma [3], H. Uri Saragovi [1,2,4,5]

[1] Lady Davis Institute-Jewish General Hospital, [2] Department of Pharmacology, [4] Department of Ophthalmology and Visual Science. McGill University.

[3] Institute of Biotechnology. University of Helsinki.

[5] Corresponding author. H. U. Saragovi (uri.saragovi@mcgill.ca). Lady Davis Institute-Jewish General Hospital. 3755 Cote St. Catherine. E-535. Montreal, Quebec - CANADA H3T 1E2

Abstract

Glial-cell line-derived neurotrophic Factor [80] is a growth factor that regulates the health and function of neurons and other cells. GDNF binds to GDNF family receptor alpha 1 (GFRa1), and the resulting complex activates the RET receptor tyrosine kinase and subsequent downstream signals. This feature restricts GDNF activity to systems in which GFRa1 and RET are both present, a scenario that may constrain GDNF breadth of action. Furthermore, this co-dependence precludes the use of GDNF as a tool to study a putative functional cross-talk between GFRa1 and RET. Here using biochemical techniques, TUNEL staining, and immunohistochemistry in murine cells, tissues, or retinal organotypic cultures, we report that a naphthoquinone/quinolinedione family of small molecules (Q compounds) acts as RET agonists. We found that, like GDNF, signaling through the parental compound Q121 is GFRa1-dependent. Structural modifications of Q121 generated analogs that activated RET irrespective of GFRa1 expression, We used these analogs to examine RET–GFRa1 interactions and show that GFRa1 can influence RET-mediated signaling and enhance or diminish AKT Ser/Thr kinase (AKT) or extracellular signal–regulated kinase (ERK) signaling in a biased manner. In a genetic mutant model of retinitis pigmentosa, a lead compound, Q525, afforded sustained RET activation and prevented photoreceptor neuron loss in the retina. This work uncovers key components of the dynamic relationships between RET and its GFRa co-receptor and provides RET agonist scaffolds for drug development.

Introduction

Naphthoquinones are structurally and biologically diverse molecules of natural and synthetic origin, that have been studied extensively as drug leads [128]. The mechanisms of action are quite varied and the biological outcomes range on a spectrum, with many variables governing the balance between cytotoxicity and cytoprotection [129]. Activities include wide and non-selective inhibition of protein tyrosine phosphatases (PTPs) [130]; but there are examples of selective PTP inhibition [131]. Recent work with the natural quinones shikonin [132] and plumbagin [133] indicated that this class can generate a wide range of cytotoxic or protective effects, from the regulation of inflammatory and stress mediators such as TNFa and pMAPK, to the activation of pro-survival signals through growth factors and their receptors.

Hence, analogs of naphthoquinone scaffolds may be used to potentially generate more selective activity. We focussed on activation of neurotrophic receptors to regulate neuronal health and function after stress or injury [31]. Specifically, we studied mechanisms related to Glial cell line-Derived Neurotrophic Factor [80], a growth factor that was tested in trials for Parkinson's [80]. GDNF therapy has also been proposed for retinal degenerative diseases, and showed early promise in animal models of Retinitis Pigmentosa (RP) [90, 134, 135]. RP is a blinding condition resulting from the progressive loss of photoreceptors. Since over 300 different mutations (e.g. in the *Rhodopsin* gene) can give rise to the RP phenotype, there is a need for a broad-spectrum neuroprotective strategy [136].

So far, GDNF therapy has failed clinically. The reasons for slow therapeutic progress include poor pharmacokinetics, stability, and distribution. This means it must be given continuously in order to be efficacious, and the potential for side-effects is a concern. Another problem is related to the way by which GDNF activates trophic signals. GDNF must bind to a receptor GFRa and only then it can activate a receptor tyrosine kinase RET which mediates the trophic signals. This requirement by GDNF of a co-receptor narrows the breadth of responding cells to those that can access both subunits. A small molecule selective activator of RET, irrespective of GFRa expression, might circumvent all these therapeutic problems. Moreover, such molecules could be used as chemical-biology tools to evaluate RET-GFRa functional interactions.

In the present work we report the development of novel substituted naphthoquinones along with their corresponding quinoline forms, and show that they act as selective agonists for the RET tyrosine kinase receptor, activating the downstream effectors Akt and Erk. Some agents are agonistic regardless of whether or not the GFRa1 receptor is present. For other agents, GFRa1 receptor expression causes biased RET signaling with differential effects upon pAkt and pErk activation, and this can be regulated positively or negatively by the reported GFRa1 modulator XIB4035. A GFRa1–independent RET agonist Q525 was neuroprotective in a mouse model of RP, generating trophic signals i*n vivo* within the Muller glial cell population, thus validating RET as a druggable therapeutic target, and suggesting potential utility for therapy of neurodegenerative diseases.

Materials and Methods

Commercially available compounds

Compounds **Q121** (CAS Registry Number 6956-96-3), **Q128** (CAS Registry Number 1526-73-4) and **Q151** (CAS Registry Number 84348-90-3) are known and described.

Chemistry and synthesis of novel naphthoquinone derivatives

All chemicals were purchased from Aldrich, J&K or Otava. Reactions were monitored by TLC using aluminum backed silica gel plates (Aldrich, silica gel matrix with fluorescent indicator), products visualized under UV light (254 and 365 nm). Flash chromatography purifications were performed in columns using Silica Gel 60A, 230-400 mesh (ACP). NMR spectra were recorded on Bruker 400 MHz spectrometer. Mass spectra were obtained with a Bruker Mass Spectrometer AmaZon SL Direct Infusion and Bruker UltraFlextreme MALDI-TOF. Chemical synthesis, Mass spectrometry (MS), and Nuclear Magnetic resonance (NMR) spectra and other characterization of the compounds are presented in the **Supplemental**, **Appendix II**.

Cell Lines

MG87 RET are murine MG87 fibroblasts stably transfected with RET proto-oncogene cDNA [21], and were cultured in DMEM containing 10% FBS, 2 mM L-Glutamine, 10 mM HEPES, 100 U/ml Penicillin/Streptomycin, and 2 μg/ml puromycin. MG87 RET cells were transfected with a GFRa1 cDNA construct containing Blasticidin resistance to generate the MG87 RET/GFRa1 cell line, and were cultured in the same media with the addition of 5 μg/ml Blasticidin S. MG87 TrkA cells were transfected with human TrkA cDNA, and cultured in DMEM 10% FBS supplemented with 250 μg/ml G418. MG87RET/GFRa1 cell lines were stably transfected with PathDetect Elk-1 system (Stratagene) harboring Luciferase reporter under the control of Erk activity. Cells were cultured in DMEM, 10% FBS, 15 mM HEPES pH 7.2, 100 μg/ml normocin (Invivogen), 2 μg/ml puromycin, 500 μg/ml G418 [95]. Growth factors GDNF and NGF were purchased from Peprotech (catalogue 450-10, 450-01).

RET phosphorylation assays

Phosphorylation of RET was assessed as previously described [96]. MG87 RET cells were plated on 35 mm tissue culture dishes, left to attach to the surface overnight and then transfected with 4 μg/dish of GFRa1-expressing plasmid using Lipofectamine 2000 (Invitrogen) for DNA delivery as described by manufacturer. Next day cells were starved for 4 hr in serum-free DMEM containing 15 mM Hepes, pH 7.2 and treated with 1% DMSO vehicle, compounds, or GDNF (200 ng/ml) for 15 min. Cells were lysed using RIPA-modified buffer (50 mM Tris-HCl, pH 7.4, 150 mM NaCl, 1 mM EDTA, 1% NP-40, 1% TX-100, 10% glycerol, EDTA-free EASYpack, protease inhibitor cocktail (Roche), 1 mM Na3VO4, 2.5 mg/ml of sodium deoxycholate). Cleared lysates were immunoprecipitated with 2 μg/ml of anti-RET C-20 (Santa-Cruz Biotechnology, Inc., sc-1290) and beads conjugated with protein G (Thermo Fisher Scientific, Cat # 10004D). Eluted samples were resolved on 7.5% SDS-PAGE and total phosphotyrosine residues were then probed in Western blots using the 4G10 antibody (Millipore). To confirm equal loading, membranes were re-probed with anti-RET C-20 antibodies (1:500, Santa-Cruz Biotechnology, Inc.).

pAkt, pErk1,2 Biochemical Studies

Cells were seeded onto 6-well plates (0.4 x 106 cells/well) and cultured overnight. Cells were serum-starved for 2 hr, and treated with vehicle, compounds or growth factor (GF) as indicated in the text (generally for 20 minutes). Cell lysates were prepared (20 mM Tris-HCl pH 7.5, 137 mM NaCl, 2 mM EDTA, 1% Nonidet P-40 containing a protease inhibitor cocktail). Protein was quantified in cleared lysates using the Bradford assay (BioRad). After SDS-PAGE, Western blotting was evaluated with the primary antibodies pAkt, pErk1,2 (Cell Signaling, catalogue #4060, #4370), or Actin control for loading (Sigma Aldrich, catalogue A2066). Signals were developed using Western Lightning Plus ECL (PerkinElmer), films were scanned and quantified using ImageJ software.

Phosphatase Inhibition Screens

PTP activity/inhibition assays are as we reported previously [131]. Tagged catalytic domain or full length of the following phosphatases were used for the screen. GST-PTP1B aa 1-321,

GST-LAR-D1D2, GST-Sigma-D1D2, GST-MKPx aa 1-184 and His-SHP-1 aa 1-595. Enzyme reactions were performed in assay buffer 50mM HEPES pH7.0 for PTP1B, LAR, Sigma and MKPx and buffer 50 mM Bis-Tris pH 6.3, 2 mM EDTA for SHP-1. DiFMUP (Invitrogen) was used as substrate for all assays, in black 96-well plates (Corning) in a final volume of 100 µL at 25°C. The reaction was monitored by measuring the fluorescence (excitation wavelength 358 nm/emission 455 nm) with the Varioskan plate reader (Thermo electron). For the kinetic assays, fluorescence was monitored over 10 minutes in 30 seconds intervals and rates were calculated in FU/minutes. Km was determined from rates at various substrate concentrations using Michaelis-Menten equation from GraphPad Prism software. A substrate concentration equivalent to the Km value for each PTP was used for the screening of the compound. Inhibitors were diluted in DMSO, then a dilution to 10 µM or 40 µM was made in assay buffer. Controls contains 1-2% DMSO final. Phosphatases and compounds were pre-incubated 2-5 minutes prior to addition of DiFMUP for enzyme inhibition quantification.

Cell Survival Assays

Cell survival was measured by the MTT assay (Sigma Aldrich) using optical density readings as the endpoint. 2000-5000 cells were plated in 96-well format in serum-free media (SFM) containing 0.03% FBS (HCell-100, Wisent). The indicated test agents, or DMSO vehicle were added to the wells. The respective growth factors (GF, 30 ng/ml GDNF for MG87 RET/GFRa1, 30 ng/ml NGF for MG87 TrkA) at optimal concentrations were added as control. Assay length was typically 72 hr since this time point yields an optimal signal-to-noise ratio between vehicle and growth factor controls. Assays were repeated at least 3 times (each assay n=4-6 wells per condition). MTT optical density data were standardized to growth factor = 100%, and SFM = 0%, using the formula $[(OD_{test} - OD_{SFM})*100 / (OD_{GF} - OD_{SFM})]$.

Animal models

All animal procedures respected the IACUC guidelines for use of animals in research, and to protocols approved by McGill University Animal Welfare Committees. All animals were housed 12 hr dark-light cycle with food and water ad libitum. We used the “RHOP347S” transgenic mouse (expressing the human Rhodopsin mutated at amino acid position 347) in a C57BL/6J

(B6) background (kindly donated by Dr. T. Li). This model of RP faithfully replicates the features of disease progression in humans.

Retinal Organotypic Cultures

Whole eyes were enucleated and whole retinas dissected from wild-type and RHOP347S mice at post-natal day 18 were used for organotypic culture experiments. There is a roughly 50% loss of photoreceptors at this time point, making it ideal for observation of neuroprotection. Following enucleation, eyes were placed in a petri dish with PBS. The cornea was perforated and cut away along the ora serrata, leaving room to remove the lens. Whole intact retinas were then freely dissected away from the sclera and immediately transferred into 24 well plates containing 500 µl of culture medium (DME/F12 supplemented with 10 mM $NaHCO_3$, 100 µg/ml Transferrin, 100 µM Putrescine, 20 nM Progesterone, 30 nM Na_2SeO_3, 0.05 mg/ml Gentamicin, 2 mM L-Glutamine, and 1 mM Sodium Pyruvate). Under sterile conditions, the media was gently removed and replaced with fresh media containing the treatments or controls, and incubated at 37°C and 5% CO_2 for 24 hr. Compounds were tested at a concentration of 20 µM. Cell grade DMSO was used for vehicle treatments and was 0.5% by volume. Retinas were then used for TUNEL staining.

TUNEL staining

Staining was performed using the DeadEnd Fluorometric TUNEL system (Promega) as per manufacturer's instructions and as described by us [9, 137]. RHOP347S retinas in culture were first fixed in 4% PFA in PBS and kept at 4°C overnight, followed by permeabilization using 2% Triton-X in PBS and re-fixed in PFA for 30 minutes. Retinas were incubated with 50 µl of equilibration buffer for 20 minutes, then 25 µl of TdT reaction mixture for 2.5 hr at 37°C, and the reaction was then terminated. The retinas were washed and mounted using Vectashield with DAPI. For image acquisition [9, 43], the retinas were divided into 4 quadrants, and 3 pictures with a 20X objective were taken in each area (central, mid, peripheral) for a total of 12 images of the outer-nuclear layer (ONL) per retina. Total TUNEL-positive cells were counted in each image semi-automatically (ImageJ). Counts were verified by at least one other person blinded to

the experimental conditions. Retinal flat mounts from wild-type mice (where there is no mutation-driven photoreceptor death) were used as negative controls.

Immunohistochemistry

Staining was performed as described by us [9]. After enucleation, the cryoprotected eyes were mounted in Tissue-TEK (Sakura) and cryostat sections were cut and mounted onto gelatin-coated glass slides. Sections (14 μm thick) were incubated in PBS containing 3% normal goat serum, 0.2% Triton X-100 and 3% bovine serum albumin (BSA) for 2 hr. Retinal sections were incubated overnight at 4°C with primary antibody (1:250 p-MAPK, Cell Signaling #4370; 1:250 p-Akt, Cell Signaling #4060; 1:400 CRALBP, Abcam ab183728). The sections were rinsed and incubated with secondary antibody for 1 hr at room temperature. Then, sections were washed and mounted (Vectashield mounting media with DAPI).

Image acquisition (fluorescence microscopy) and data analysis

Pictures were taken as Z-stacks of confocal optical sections using a Leica confocal microscope at a 20X objective. Images were equally adjusted using Adobe Photoshop CS 8.0 to remove background signals. For each experimental condition, a minimum of 6 images were acquired from 3 sections cut from different areas of the retina (n=3 retinas per group). The area of the profiles of the cells expressing pErk and pAkt was measured using ImageJ software.

Intravitreal injections

Briefly, mice were anesthetized with isoflurane, delivered through a gas anesthetic mask. The treatments were delivered using a Hamilton syringe. Injections were done using a surgical microscope to visualize the Hamilton entry into the vitreous chamber and confirm delivery of the injected solution (3 μl of a 2 mM stock solution). 1-3 μl injection volumes are typical in the literature, and 3 μl was chosen to improve accuracy of delivery. After the injection, the syringe was left in place for 30 seconds and slowly withdrawn from the eye to prevent reflux. In each animal the right eyes were injected with the test agents (experimental eye) and the left eyes were untreated (internal control).

Statistical analyses

The quantitative data were subjected to statistical analyses using GraphPad Prism 5software, and are presented as mean ± SD for all studies. The differences between groups were determined by ANOVA (multiple groups) followed by Dunnett's or Bonferroni-corrections as indicated in Legends. Student t-tests were performed to compare two groups. p-values below 0.05 were considered to indicate statistically significant differences between groups.

Data availability.

All data are contained within the article. The complete NMR resonances are available on request to the corresponding author.

Results

Identification of novel naphthoquinone RET activators/modulators

All compounds and structures are summarized in Table 1 in the order that they are mentioned. Biochemical assays revealed that the chlorinated methoxy 1,4 naphthoquinone Q121 activated pAkt and pErk in MG87 RET/GFRa1 cells. Q121 induced RET phosphorylation in a dose-dependent manner (blots were probed using mAb 4G10 for total p-Tyr residues) (**Fig 1A**). Compound Q128 with an (–OH) substituting the (–OCH3) group of Q121 was inactive (**Fig 1A**), indicating the functional relevance of the –OCH3 adduct. These data provide a rationale for further substitutions of the core structure at this position.

To further evaluate RET phosphorylation by Q121 as well as its potential requirement of GFRa1 expression (which GDNF requires), immunoprecipitation experiments were performed. Phospho-RET was significantly increased by treatment of 100 μM. However, in MG87 RET cells lacking GFRa1, there were no increases in RET phosphorylation detected above background vehicle control (**Fig 1C**). These data indicate that Q121, like GDNF, requires GFRa1 to signal through RET.

Compounds coded Q101, Q105, Q112, Q141, Q143, Q151, and Q1047 were then synthesized (See Materials and Methods, Supplemental Data) and evaluated in biochemical assays. Significant increases in pAkt and pErk were observed with compounds Q105, Q112, Q141, Q151, and Q1047, while Q101 and Q143 were inactive (**Fig 1C**). However, counter-assays using MG87 cells expressing the NGF receptor TrkA tyrosine kinase (instead of RET) showed significant activation of pAkt and pErk even though RET is absent. This indicates that these quinone derivatives lack selectivity (**Fig 1D**).

In spite of poor RET selectivity, compounds such as Q151 remained interesting because they induced RET phosphorylation whether or not the GFRa1 co-receptor was present (**Fig 1E**). These data suggest that the modifications to the side-chain of position A (**Table 1)** allows GFRa1-independence.

One concern with these agents is that significant cytotoxicity was observed in the 1-10 μM range when these compounds were screened via the MTT survival assay; this was therefore addressed in further analogs.

Chlorine substitution affects potency and toxicity, and generates GDNF-modulating compounds

To address cytotoxicity, we evaluated substitutions of the chlorine atom at position B (**Table 1)** because the ring-associated chlorine can enhance chemical reactivity and oxidative toxicity [129]. Compounds Q2003 and Q2004, bearing a hydrogen in place of the chlorine, were prepared.

Biochemical assays revealed these compounds to be significantly less potent, with non-significant pAkt/pErk activation even when assayed at a high μM concentration range (data not shown). Moreover, in biological assays measuring cell survival, both Q2003 and Q2004 displayed weak trophic activity which was non-selective and was detectable in MG87 RET/GRFa1 as well as in MG87 TrkA cells. In MTT assays Q2003 and Q2004 supported cell viability to 8-18% of the survival induced by optimal growth factor concentrations (GDNF for RET/GRFa1-expressing cells and NGF for TrkA-expressing cells) (**Fig 1F and 1G**).

While Q2003 and Q2004 lacked potency and selectivity, they remained interesting because their activity was additive in MG87 RET/GRFa1 with sub-optimal doses of GDNF (**Fig 1F**), and this effect was not observed in MG87 TrkA with sub-optimal doses of NGF (**Fig 1G**).

Therefore, although the survival induced by Q2003 and Q2004 can be RET-independent (i.e. the compounds afford survival to MG87 TrkA cells), the RET/GDNF axis is involved in the functional outcome because the agents potentiate GDNF trophic action but they do not potentiate NGF trophic action.

To assess the impact and nature of the compound toxicity, additional MTT assays were performed under full serum conditions for the same 72hr time frame. At 1 μM, both Q2003 and Q2004 lacking the chlorine showed no signs of cell death (**Fig 2**). In contrast, Q1047, identical to Q2003 but including the chlorine, was significantly toxic at the same concentration. Data from both MG87 RET/GFRa1 and TrkA-expressing cells were comparable, and therefore suggest the toxicity arises from a RET-independent mechanism. Knowing that the presence of the chlorine is tied with potency, we directed our efforts into other structural modifications that may allow the atom to be maintained. Q525 was synthesized, significantly less toxic than Q1047, and was pursued further in additional studies.

In summary, simple side-chain substitutions of the naphthoquinone core resulted in RET-activating compounds, and although lacking RET selectivity the compounds did not require GFRa1 co-expression. The chlorine is associated with the potency of the compounds, but also with the toxicity. Removal of the chlorine generated less potent compounds, and while RET selectivity was still not achieved, the compounds were considerably less toxic and had the ability to cooperate with GDNF. These observations prompted further chemical design of the naphthoquinone core in efforts to improve RET selectivity.

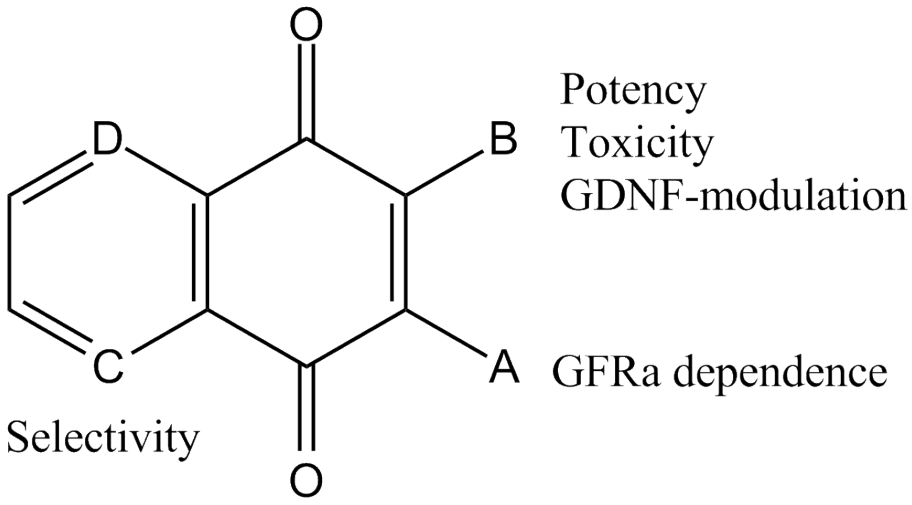

Q#	D	C	B	A
121	C	C	Cl	OCH3
128	C	C	Cl	OH
101[A]	C	C	Cl	NH-CH2-Ph-COOCH3 (p)
105[A]	C	C	Cl	NH-Ph-CH2-COOCH3 (p)
112[A]	C	C	Cl	NH-C(CH2)2-2-Me-Pyrrolidine
141[A]	C	C	Br	NH-Ph-CH2-COOCH3 (p)
143[A]	C	C	Cl	NH-Ph-N=C=S (p)
151[A]	C	C	Cl	NH-Ph-COOCH3 (p)
1047[A]	C	C	Cl	NH-Ph-CH2OH (p)
2003[B]	C	C	H	NH-Ph-CH2OH (o)
2004[B]	C	C	H	NH-C(CH2)2-2-Me-Pyrrolidine
508[C]	C	N	NH-C(CH2)2-2-Me-Pyrrolidine	Cl
525[C]	C	N	NH-Ph-CH2OH (p)	Cl
1041[D]	N	N	H	NH-Ph-CH2OH (p)
1048[D]	N	N	Cl	NH-Ph-CH2OH (p)

Table 4.1. Overview and compound structures, listed as they appear to show SAR progression

Letters A-D denote the position and order in which the modifications took place throughout the paper, and the compounds that resulted. The adjacent text on the core structure describes the parameters that the modification influenced. Starting from Q121 and Q128, side chain substitutions at position A generated compounds that activated RET without GFRa1 expression. Modification at position B through removal of the Cl atom generated compounds

that were much less potent, although toxicity was improved and they potentiated GDNF survival. However, A and B modified compounds exhibited poor selectivity. Modification at position C by N-substitution yielded compounds with improved selectivity for RET and were pursued in further studies. Finally, compounds tested with N-substitutions at both positions C and D were found to be generally inactive.

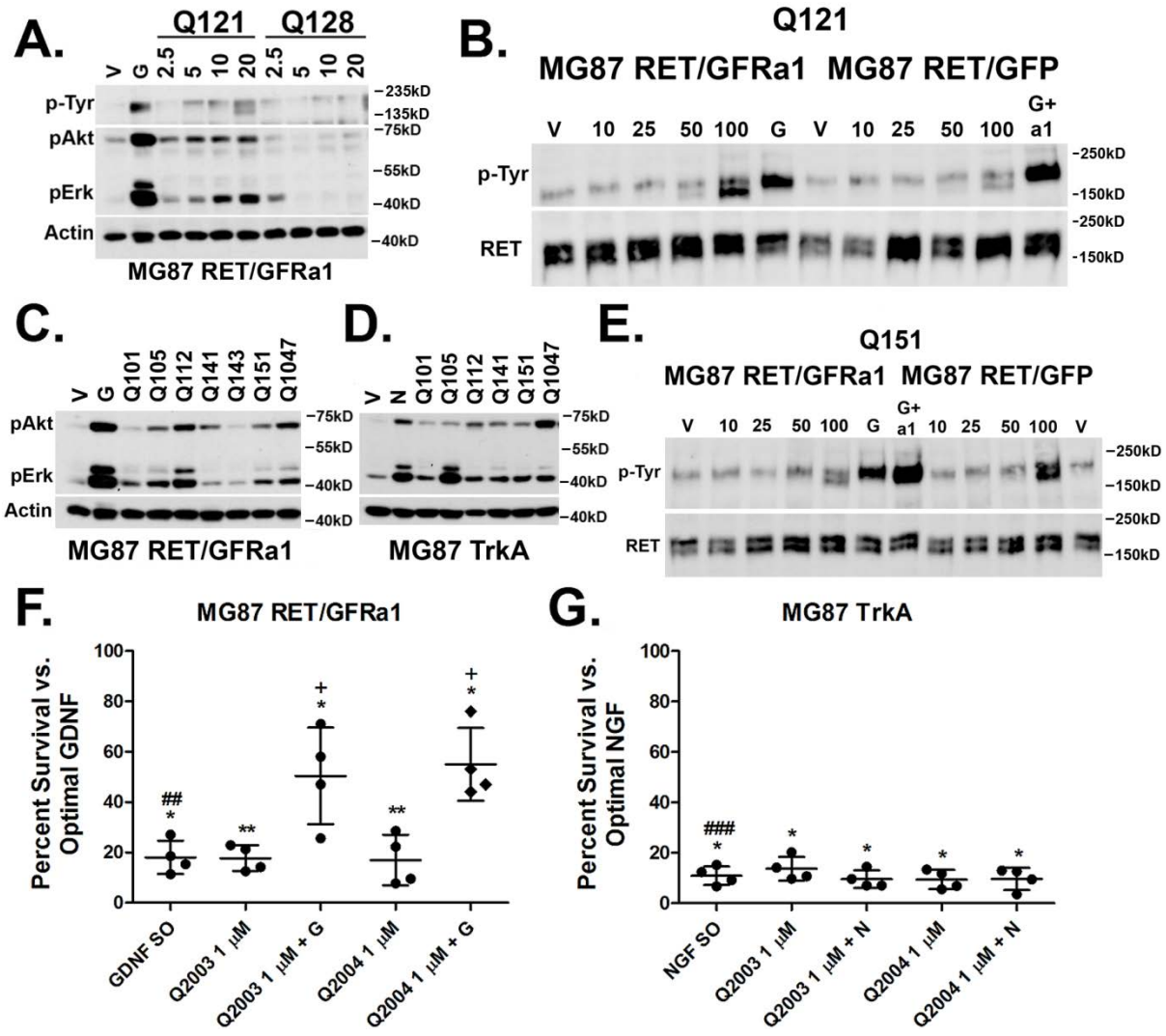

Figure 4.1. Screening and SAR of naphthoquinone RET activators

A. Compounds Q121 and Q128 activity in MG87 RET/GFRa1 cells. Following serum starvation, cells were exposed for 20 min to either vehicle, 10 ng/ml GDNF, or compounds at the indicated μM range. Lysates were collected and probed for pAkt, pErk, and total-phosphotyrosine (4G10). Representative Western blot data are shown. Actin was probed as internal loading standard. **B.** Representative total RET immunoprecipitation from MG87 RET cells transfected with either GFRa1 or GFP control. Q121 treatment results in RET phosphorylation at concentrations of 50 μM and 100 μM in the cells expressing GFRa1. Total RET was probed as internal loading standard. For MG76 RET/GFRa1 cells, G represents GDNF as positive control. For MG87 RET/GFP, G+a1 represents GDNF+GFRa1 co-treatment which is needed to induce RET phosphorylation in these cells lacking GFRa. **C.** Activities of

naphthoquinone derivatives. Side chain modifications generated compounds active in MG87 RET/GFRa1 as demonstrated by the representative Western blot. **D.** The naphthoquinone derivatives are also active in MG87 TrkA cells as demonstrated by the representative Western blot. **E.** Compound Q151 induces RET phosphorylation in both MG87 RET/GFRa1 and in RET/GFP cells lacking GFRa1. **F.** MG87 RET/GFRa1 cells in SFM were treated with Q2003 and Q2004 alone or in combination with sub-optimal GDNF (GDNF SO, 5 ng/ml). Survival was assessed by MTT after 72 hours. Both compounds had low but significantly trophic activity at a concentration of 1 µM. Compounds significantly potentiate GDNF SO. **G.** MG87 TrkA cells in SFM were treated with Q2003 and Q2004 alone or in combination with sub-optimal NGF (NGF SO, 60 pg/ml). Survival was assessed by MTT after 72 hours. Both compounds had low but significantly trophic activity at a concentration of 1 µM, but did not potentiate NGF SO.

Data are expressed as % survival ± SD from 4 experiments, with the respective optimal trophic factor (GF O, 30 ng/ml) standardized to 100%, and vehicle to 0%. Symbol * vehicle versus all treatments. Symbol # sub-optimal GF versus optimal GF. Symbol + sub-optimal GF versus all treatments. One symbol, $p<0.05$, two symbols $p<0.005$, three symbols $p<0.0005$, Bonferroni-corrected t-test.

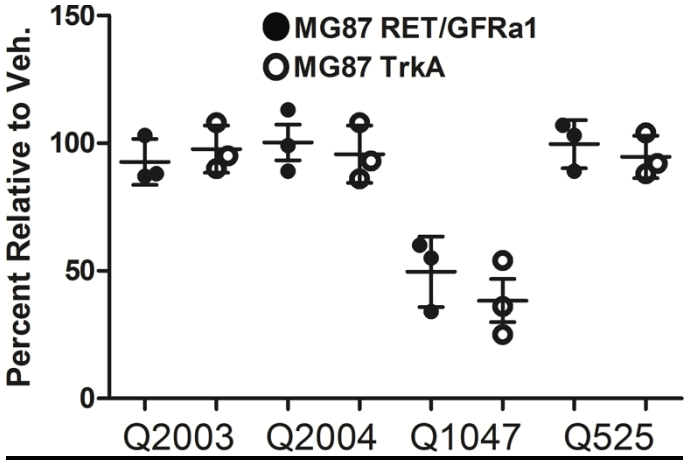

Figure 4.2. Chlorine substitution affects toxicity and directs lead compound development

MG87 RET/GFRa1 and TrkA expressing cells were exposed to 1 μM compounds in regular growth media and assessed by MTT. Q2003 and Q2004 bearing a hydrogen in place of the chlorine were not toxic, indistinguishable from vehicle control. However, Q1047, the chlorine containing analogue of Q2003, showed significant signs of toxicity under the same conditions. Additionally, the lack of toxicity observed by Q525 demonstrated that the chlorine could be maintained, and directed the development of more potent, RET-selective leads. The comparable toxicity between both cell lines indicated that the origin of the toxicity is not due to RET over-activation, but rather a generalized mechanism.

Quinoline analogs are RET activators with improved selectivity and GFRa1-independence

To improve upon this first-generation of molecules, we synthesized quinoline derivatives bearing identical side chains to their naphthoquinone counterparts. This effort generated new chemical entities (NCEs) with a nitrogen at position C (**Table 1)**. These compounds are chemically distinguished from known inhibitors of protein tyrosine phosphatases (PTPases), to exclude this as a possible factor in the poor selectivity of the first-generation molecules.

Q525 (and Q508) were screened in biochemical assays. Q525 was active in MG87 RET/GFRa1 cells across a broad range of concentrations, and generated large and significant increases in pAkt/pErk (**Fig 3A, quantified in 3B**). The compound maintained a high degree of selectivity for RET, as non-significant increases in pAkt and pErk were observed in MG87 TrkA cells (**Fig 3C, quantified in 3D**).

The improved selectivity of the quinoline series (e.g. Q525) is exemplified by lack of selectivity in Q1047 (the naphthoquinone form of Q525) which activates signals in MG87 TrkA cells (**Fig 3C**). Additionally, analogs Q1041 and Q1048 bearing a quinoxaline motif with N-substitutions at both positions C and D (**Table 1)** were synthesized and found to be inactive at all concentrations tested.

Together, these data suggest that the N-substitution in the ring system has a significant impact on compound selectivity, generating agents that maintain RET activity and GFRa1-independence.

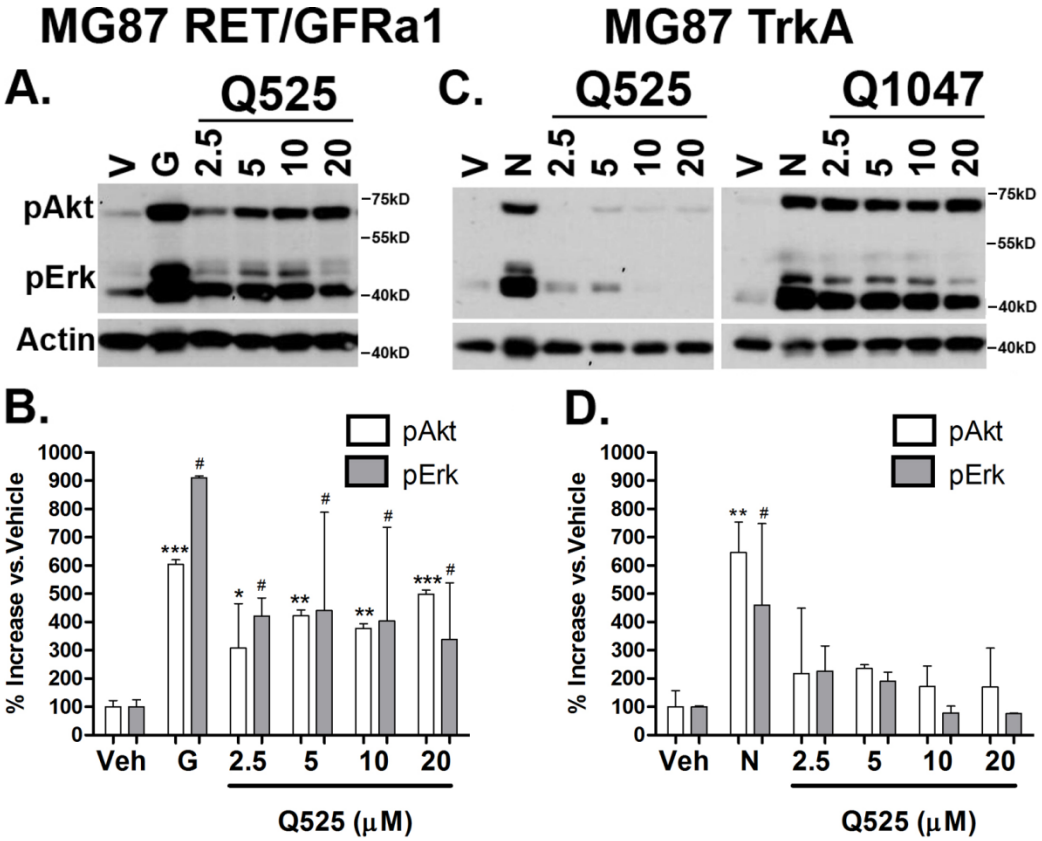

Figure 4.3. Development of Lead Quinoline derivatives

A-B. Biochemical screening of Q525 in MG87 RET/GFRa1 cells. The compound generated large increases in pAkt/pErk within the 5-20 μM range. Western blot data were quantified from 3 experiments and expressed as mean ± SD versus Vehicle, standardized to 100%. For pAkt *p<0.05, **p<0.005, ***p<0.0005. For pErk, #p<0.05, Dunnett's test.

C-D. Counter screens with Q525 were performed in MG87 TrkA cells. Only slight increases in pAkt/pErk were observed within the same concentration range. For comparison, the poorly selective Q1047 bearing an identical side-chain is also shown.

Results were quantified from 3 experiments and expressed as mean ± SD versus Vehicle, standardized to 100%. For pAkt **p<0.005. For pErk, #p<0.05, Dunnett's test.

Differential signaling profiles through pAkt and pErk in combination with the GFRa1 modulator XIB4035

We used the GFRa1-independent RET agonists as chemical-biology tools, to study the influence of the GFRa1 co-receptor upon RET signaling. We evaluated the quinone/quinoline pairs Q1047/Q525, and Q112/Q508 in combination with XIB4035 which is a reported GFRa1 modulator with no agonistic activity on its own [103].

Sub-optimal doses (10 μM) of Q1047 (non-selective agonist) or Q525 (selective RET agonist) generated low but significant increases in both pAkt and pErk, compared to control vehicle or to 4 μM XIB4035 which did not activate signals (**Fig 4A**). Compared to single treatments, a combination of 4 μM XIB4035 + 10 μM of Q1047 or Q525 resulted in significant increases of pErk signals (50% and 100% respectively) (**Fig 4B**), while pAkt levels were unaffected (**Fig 4C**). These data suggest a RET-mediated pErk bias when GFRa1 is modulated by XIB4035.

Sub-optimal doses (10 μM) of Q112 (non-selective agonist) or Q508 (selective RET agonist) generated low but significant increases in both pAkt and pErk, compared to control vehicle or to 4 μM XIB4035. A combination with 4 μM XIB4035 caused a reduction by 50% of the pAkt that was induced by Q112 or Q508 alone (**Fig 4C**) while leaving pErk unaffected (**Fig 4B**).

Hence, a GFRa1 modulator XIB4035 alters the signals induced by RET-agonists, even when these agonists do not require GFRa1 to signal on their own. In one case (Q1047 or Q525) it enhances pErk signals but does not affect pAkt, and in another case (Q112 or Q508) it decreases pAkt signals but does not affect pErk. The end result for both families of compounds is a pErk signaling bias, however this is likely achieved through different mechanisms that involve a ligand-mediated regulation of RET by the GFRa1 receptor. Also, it is of interest that N-substitution in the ring of structurally related quinone/quinoline pairs does not affect regulation of signaling by XIB4035.

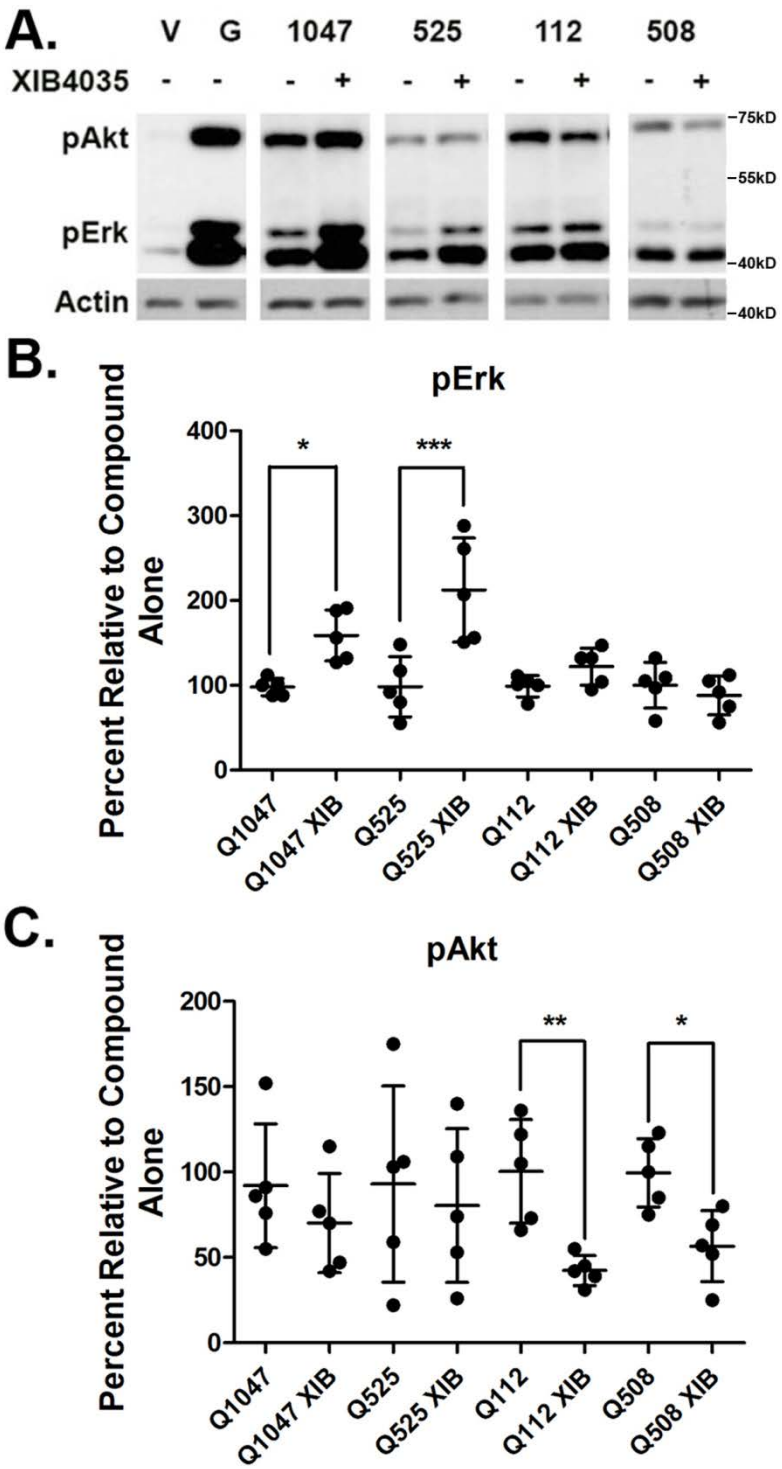

Figure 4.4. Differential signaling through pAkt/pErk is mediated by XIB4035-induced modulation of GFRa1

A. Representative blots taken from separate experiments showing pAkt and pErk signaling of compounds Q1047, Q525, Q112, and Q508 with or without XIB4035 pretreatment.

B. Quantification of pErk signals of compounds Q1047, Q525, Q112, and Q508 in combination with the GFRa1-modulator XIB4035. XIB4035 pretreatment did not affect pErk signals induced by Q112 and Q508. However, Q1047 and Q525 signals were significantly *increased*.

Data are expressed as mean ± SD from 5 experiments, standardized to compound alone which was set at100%. *<p0.05, ***p<0.0005, Bonferroni-corrected t-test.

C. Quantification of pAkt signals of compounds Q1047, Q525, Q112, and Q508 in combination with the GFRa1-modulator XIB4035. XIB4035 pretreatment did not affect pAkt signals induced by Q1047 and Q525. However, Q112 and Q508 signals were significantly *decreased*.

Data are expressed as mean ± SD from 5 experiments standardized to compound alone, which was set at 100%. *<p0.05, **p<0.005, Bonferroni-corrected t-test.

RET activators are not inhibitors of Protein Tyrosine Phosphatases

Several naphthoquinones have been reported as inhibitors of PTPases, some non-selective [130] and some with a degree of selectivity [131]. RET activation could potentially stem from inhibition of PTPases, and we evaluated this possibility.

Select compounds were tested in assays of PTPase activity to evaluate their impact upon the enzymatic activity of five PTPase enzymes (LAR, PTP-sigma, PTP-1B, MKPX, and SHP-1) as described [131]. The compounds did not affect the activity of purified PTPases compared to DMSO vehicle, while the positive control Sodium Orthovanadate showed significant inhibition of >80% (**Table 2**). The 40 μM compound concentrations evaluated in these PTPase assays are at least 3-fold higher than the compound concentrations that induce biological signals in cultured cells, and likely much higher than intracellular compound concentrations, where PTPases are present.

In particular we note lack of inhibition by the quinone/quinoline pairs Q1047/Q525, and Q112/Q508, none of which affected any of the five PTPases tested. Moreover, the fact that XIB4035 (a GFRa1 modulator with no reported link to PTPases) regulates pErk signals induced by Q1047/Q525, and Q112/Q508 (**Fig 4**) is consistent with the notion that these agents are not PTPase inhibitors.

Q#	LARD1D2	SigmaD1D2	PTP1B	MKPX	SHP-1
105	97	98	77	99.5	87
112	91.5	96.5	121.5	97	80
121	96.5	97.5	93	98	90
143	96	99	101	96.5	103.5
508	72	71	92.5	96.5	91
525	97.5	99.5	96	99	94
Na_3VO_4	16.5	24	4	5	
DMSO	99	97.5	99.5	99	93

Table 4.2. Phosphatase inhibition profiles for select compounds.

Select compounds were screened for their ability to inhibit the phosphatases LAR, Sigma, PTP1B, MKPX, and SHP-1 and data are shown as the percent inhibition relative to DMSO control. Sodium Orthovanadate (Na_3VO_4) was used as positive control as a broad spectrum PTP inhibitor.

Q525 is neuroprotective by activation of Müller Glial cells

We selected Q525 for pharmacological evaluation *in vivo* in the transgenic mutant RHOP347S mice (expressing a mutant *rhodopsin* gene that causes Retinitis Pigmentosa). These mice undergo rapid photoreceptor apoptosis which peaks *in vivo* between post-natal days 18-22 [98]. The rate of photoreceptor apoptosis is fully replicated *ex vivo* in cultured whole retinal explants from these mice, allowing rapid testing of many compounds and doses.

Retinal explants were prepared from 18-day old mice and incubated for 24 hours with either compounds or vehicle, followed by quantification of TUNEL staining. Representative confocal images of the central retinal region are shown (**Fig 5A**). Q525 at a 20 µM dose affords robust preservation of the photoreceptors, as indicated by a 40% reduction in $TUNEL^+$ cells in this layer (**Fig 5B**). In controls, the inactive compound Q143, assayed previously (**Fig 1C)** was indistinguishable from vehicle-treated retinas. The data support the notion that RET activation by Q525 may be a disease-modifying strategy for degenerative conditions like RP.

To understand the neuroprotective mechanism of action, we studied activation of biochemical pathways in the retina. Mice (n=3) received intravitreally administered test compound in one eye and control vehicle in the contralateral eye. Eyecups were collected 1 hour later and examined by immunohistochemistry to quantify pErk and pAkt signals. Results show that the Q525 treated eyes had elevated levels of pErk and pAkt by 1.8 and 2.0-fold respectively, while no significant elevations in pErk or pAkt were observed in animals injected with the inactive Q143 (**Fig 5E-F**). This is consistent with biochemical assays using cell lines (**Fig 1 and 3**). The pAkt and pErk signals co-localized with the Müller cell marker CRALBP. This indicates that the Müller glial cells are among the primary cellular targets for the RET agonists, and these cells are known to express RET and to support the health of photoreceptors.

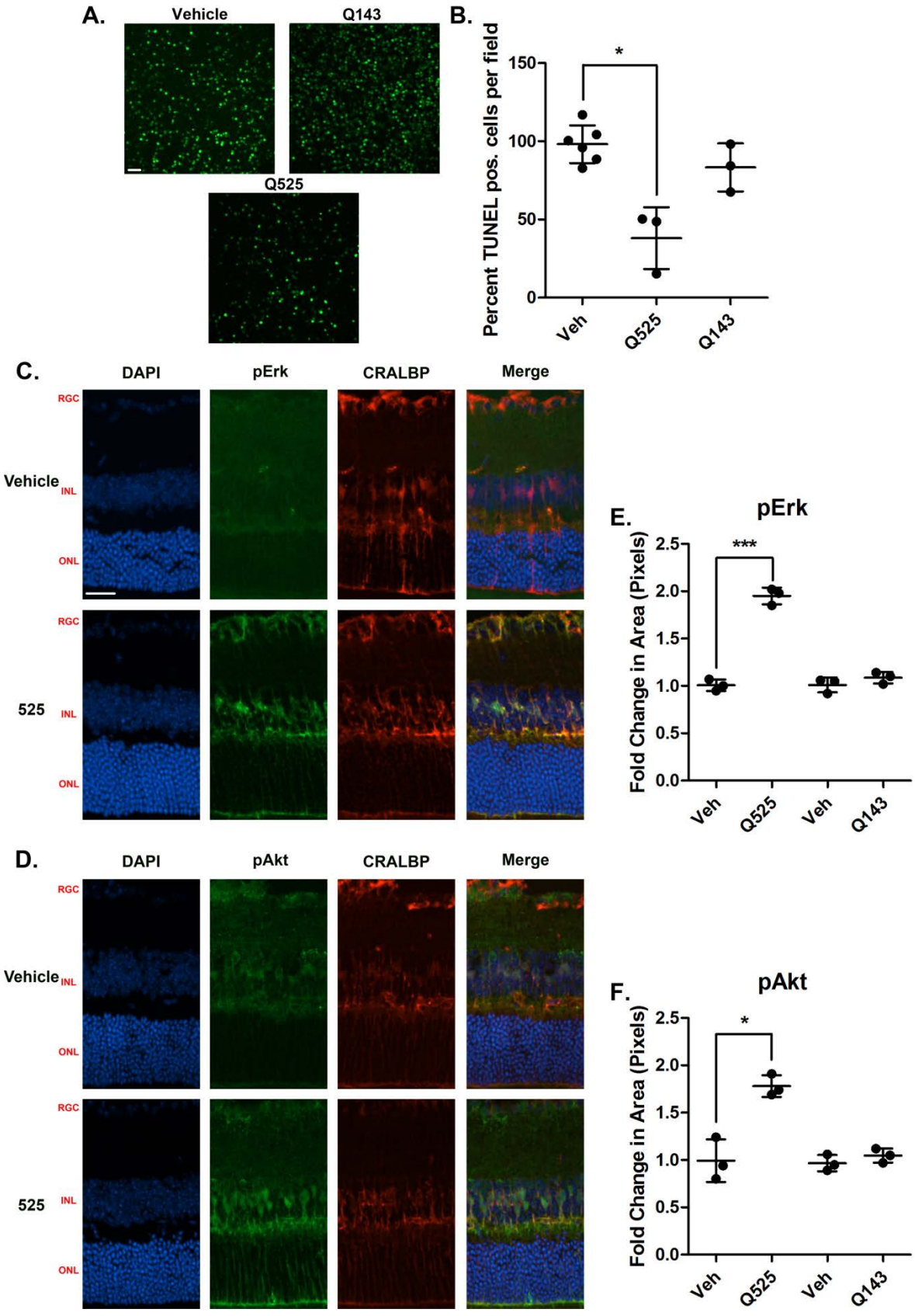
A.
Vehicle
Q143
Q525
B.
Percent TUNEL pos. cells per field
150
100
50
0
*
Veh
Q525
Q143
C.
DAPI
pErk
CRALBP
Merge
RGC
Vehicle
INL
ONL
525
D.
pAkt
E.
pErk
Fold Change in Area (Pixels)
2.5
2.0
1.5
1.0
0.5
0.0
***
F.
pAkt
*

Figure 4.5. Q525 is neuroprotective *ex vivo* in a mouse model of retinal degeneration and activates trophic signals in Muller glial cells

A. Representative confocal images of retinal flat mounts following treatment with Q525 and Q143. Freshly dissected retinas from 18-day old RHOP347S mice were incubated in culture media for 24 hours. One retina with the indicated compounds, and the contralateral retina of the same mouse with vehicle control (e.g. each individual had its own internal control). Tissues were processed for TUNEL staining and flat-mounted, 12 images were taken per retina and quantified semi-automatically. **B.** Quantification of TUNEL-positive cells after treatment. Cell counts from n=3 mice per group were standardized versus vehicle control. Q525 treatment affords a significant reduction in TUNEL staining, while Q143 treatment was comparable to vehicle. *<p0.05, Student t-test. **C. and D**. Images of retinal sections stained for pErk and pAkt following intravitreal injection of compound Q525 *in vivo*. Eyecups were collected 1 hour after injection. Significant increases in staining for pErk and pAkt co-localized with the Muller cell marker CRALBP, suggesting activation within the glial population. RGC = retinal ganglion cell layer, INL= Inner nuclear layer, ONL = outer nuclear layer. **E.** pErk quantification of Q525 and Q143 retinal sections (n=3 per group) expressed as the fold-change in pixel area over vehicle ± SD, *** $p<0.0005$, Student t-test. **F.** pAkt quantification of Q525 and Q143 retinal sections (n=3 per group) expressed as the fold-change in pixel area over vehicle ± SD, * $p<0.05$, Student t-test.

Discussion

We discovered a series of new chemical entities, naphthoquinone/quinoline derivatives with agonistic activity at the RET receptor tyrosine kinase. Employing them as biological tools, we explored functional regulation between RET and its co-receptor GFRa1. A summary of screening and biochemical data is provided in **Table 3.** We demonstrated that although these agents do not require the presence of GFRa1, their signaling profiles can be nuanced by the presence and bound-state of GFRa1. The regulatory functions that the GFRa subunits exert over RET provides additional points to consider when using RET agonists for therapy. We also assessed the efficacy of a compound, Q525, in a model of neurodegeneration and further validated RET as a potential target a disease model of RP.

Screening and optimization of novel derivatives

The finding that a relatively simple naphthoquinone Q121 was a weak RET agonist but required GFRa1 expression was surprising, given its extremely small size in comparison to GDNF and the large surface of interactions of the receptor complex. Large growth factors like GDNF are typically envisioned as mediating a 'bridge' between receptor components, bringing them in close proximity through multiple contact points and stabilizing an active conformation. It is unlikely that small molecules are capable of fully replicating this. Literature suggests that RET and GFRa1 associate in a ligand-independent manner [20], and it is therefore possible that our agents cause RET conformational changes through a preformed receptor complex.

The substitution of the methoxy group for a hydroxyl abrogated RET activity, and clearly implicated this position for synthesis of analogs. However, further screening of these naphthoquinone derivatives, while biochemically interesting, did not possess the RET selectivity worthy of pursuit. It is unclear how the compounds activate pAkt and pErk in non-RET expressing cells, though the molecular targets of the quinone family are quite broad, leaving many possibilities. Their GFRa1 independence was unexpected, but highlights one of the many strengths in small molecule development in that minor structural modifications can have major biochemical impacts. This is again reflected by the impact of the chlorine to hydrogen substitution, yielding mildly pro-survival, GDNF-modulating effects *in vitro*.

In order to differentiate the core structure from those reported previously as being phosphatase inhibitors [131], we made additional modifications to the ring system, generating novel quinolinediones which demonstrated much improved characteristics. The quinoline scaffold has a rich pharmacological background, particularly in regard to anti-cancer therapeutics [138] and in fact a family of RET kinase inhibitors with this motif exists [139]. Others also reported a series of quinolines with neurotrophic activity [140], but their molecular target and signals remain unknown.

Significance of GFRa1-dependent signaling bias

Biased signaling is a relatively new concept in the field of pharmacology, and even more recent is the notion that this property can be exploited to improve therapeutic efficacy [141]. Some of the first biased ligands were synthetically derived and it was largely unknown whether this type of signaling occurred endogenously as an added regulatory mechanism. The chemokines and their receptors are one such example that reveal the presence and utility of signaling bias at the biological level, as a means to fine-tune responses to a wide array of stimuli [142].

Our findings with the compounds in combination with XIB4035 demonstrate a unique aspect of ligand bias working through a co-receptor, and there are few examples of this in the literature [93, 143].

The compounds reported display a balanced activation of both pAkt and pErk pathways through RET by themselves, but become biased in the presence of a GFRa1 modulator. In contrast GDNF activation of the RET tyrosine kinase functions solely in conjunction with a membrane bound or soluble co-receptor GFRa, a feature of this receptor that is conserved among vertebrates [82].

It is tempting to speculate that GFRas may be a gatekeeper of signaling bias. Through shifting their expression levels and patterns, GFRas may allow a single ligand to generate a series of orchestrated responses within the same tissue. Ligand/GFRa complexes may also control RET distribution into and out of lipid rafts, as is the case when comparing persephin versus GDNF [144], and this could dictate which adaptor proteins are most accessible to the activated kinase. It is also known that receptor-receptor interactions on the membrane can create allosteric

regulatory sites at which ligands may bind to alter the functional outcome [3]. Studies with constitutively active p75 mutants reveal that very slight changes in subunit positioning affect the resulting signaling profile, and therefore suggest that different ligands could stabilize unique conformations of the receptor complex to drive signaling bias [145].

Although we did not address this within the present work, soluble GFRas can also be liberated from the membrane surface, and the biological roles of this process are understudied but are likely to be diverse [146-148]. This could provide another way for bias-control via the RET/GFRa complex.

Additionally, there may be other endogenous ligands such as GDF15 [149] or ligands of GFRa that can modulate biased signals through RET to mediate important processes. In that regard, it would be interesting to use GFRa modulators in combination with RET agonists but unfortunately XIB4035 cannot be used *in vivo* in the retina due to poor solubility and high toxicity [103]. There are GFRa modulators under development (e.g. XIB4035 analogs) that eventually can be tested to answer this question.

Our findings have therapeutic relevance, especially in disease where RET expression remains stable, but GFRa levels vary considerably [29, 30]. A RET agonist may provide benefits in some diseases where dynamic changes occurring at GFRa *in vivo* are difficult to assess or control. As more work is done to validate RET and its co-receptors as targets, the ability to take advantage of signaling bias to yield highly specific outcomes with lower side-effects may be a promising strategy.

Test	Potency	Selectivity	GFRa1 dependent	Toxicity
GDNF	+++	+++	**yes**	-
121	++	+	**yes**	++
128	+	+	-	++
101	+	+	-	+++
105	++	+	**no**	+++
112	+++	+	**no**	+++
141	++	+	**no**	+++
143	+	-	-	+++
151	++	+	**no**	+++
1047	+++	+	**no**	+++
2003	+	+	-	+
2004	+	+	-	+
508	++	+++	**no**	+
525	+++	+++	**no**	+
1041	+	-	-	-
1048	+	-	-	-

Table 4.3. Summary of pharmacological profiles

Comparison of signaling (maximal efficacy of activation of Akt/Erk in RET-expressing cells) by the compounds relative to each other and to GDNF. Potency is not indicated (e.g. GDNF is nM and compounds are μM). RET selectivity was gauged by quantification of signaling in cells not expressing RET but expressing other RTKs (negative Akt/Erk activation is wanted). Culture of various cell types with the compounds in serum-containing media gauged general toxicity, and culture in serum-free conditions gauged accelerated or delayed cell death. The use of various cell types in such assays evaluated RET dependence. Q525 is highlighted as a potential lead with the best balance overall. + low/poor ++ moderate +++ high – not tested/not applicable. The summary illustrates the interplay that exists between the different parameters and profiles, and the challenges of choosing a lead agent.

Acknowledgements

We are thankful to Dr. Michel Tremblay and Isabelle Aubry (McGill University) for the Protein Tyrosine Phosphatase assays. This work was funded by a grant from the Canada Institutes of health Research (CIHR), and the Canadian Consortium on Neurodegeneration and Ageing (CCNA) to HUS.

Disclosures

Patent applications have been filed by McGill University (SJ, YS, MS, and HUS, authors).

Chapter 5

General Discussion

Drug development, let alone *successful* drug development, is a monumental undertaking. As a discipline it is extremely broad in scope and demands a careful and continuous assessment of all the variables in motion. Despite the scientific progress we have enjoyed in recent years, the failure rate for new medications entering the market remains extremely high. One reason for this is the lack of a solid foundation from which to build upon. The importance of target validation can never be overstated; not only having an understanding of how that target behaves biologically in a disease, but also having the proper tools to interrogate that target. This is hopefully a resounding point made throughout this work. The clinical failures of the neurotrophins as a whole have cast a shadow over their therapeutic relevance to some extent, but we must keep in mind that this is in part due to a failure to deliver. Small molecules offer us new insights into receptor biology and better strategies to validate disease targets.

In this thesis, the 'trophic imbalance' hypothesis of neurodegeneration has been explored, keeping this dogma in mind. Using RP namely, we have attempted to restore the imbalance from both sides, either through blocking neurotoxic mechanisms, or by facilitating pro-survival pathways. As with many degenerative diseases, including RP, the etiological roots are genetic. For example, the RP phenotype may result from one of many hundreds of possible mutations. Shying away from this fact altogether is preferable, since it allows for a broad-spectrum therapy from which many can benefit. The small molecule approach has allowed us to implicate TrkC.T1, p75, and RET as disease-modifying targets. In the case of the RET work, this approach has also led to some valuable conclusions on the nature of RET/GFRa1 interactions, and provides some food for thought on how these interactions could affect the efficacy of a therapy as well.

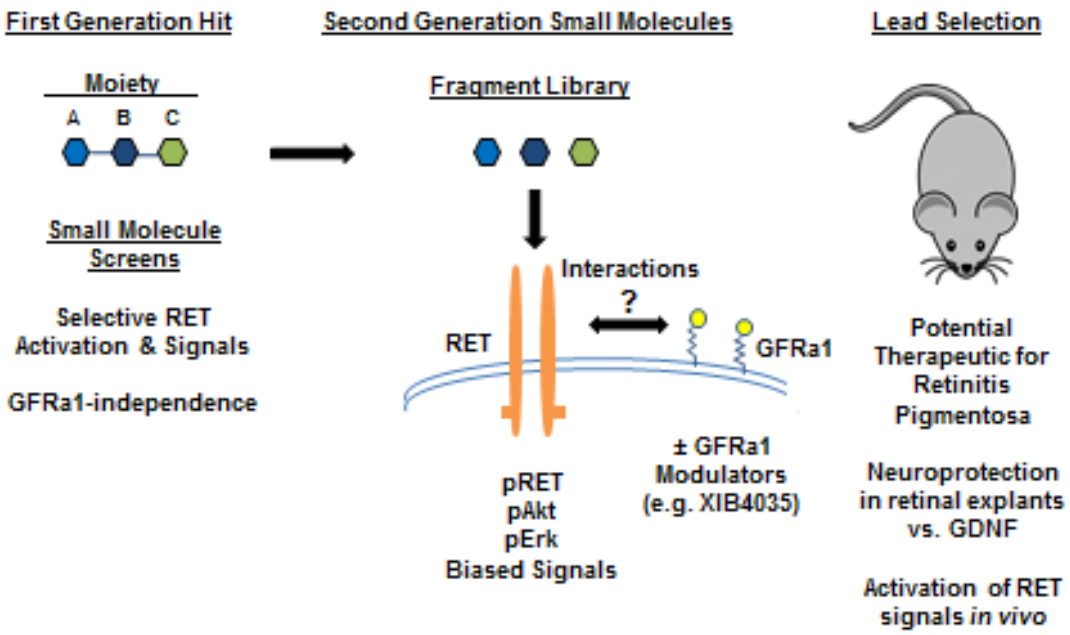

Figure 5.1: Overview scheme of the RET-based small molecule development

Chapters 3 and 4 began with primary screens to identify RET activators with GFRa1-independence, and examine their selectivity. Secondary screens allowed for structural optimizations, and resulted in improved compounds which could be used to explore RET/GFRa1 signaling and their functional outcomes. Lead molecules from both chapters were tested therapeutically in a retinal degeneration model, and revealed the origin of RET-derived signals in the retina.

Anti-neurotoxic strategies and mechanisms in the degenerating retina

The retina is a particularly fascinating tissue in that it is composed of numerous specialized cell-types, each inhabiting discrete layers. The Muller glia cells send out projections spanning the full thickness of the retina, and make intimate contacts with the various neurons along the way. As such, this gives them a privileged vantage on the overall functioning of the retina, and allows them to respond quickly to any stressors. While these responses are meant to be beneficial under normal conditions, we have seen that they may become pathological in diseased states. As RP progresses, we had shown that a truncated form of the TrkC receptor, TrkC.T1, became upregulated in retinal glia, as well as its native ligand, NT-3. Full length TrkC expression levels remained unaltered. This biological consequence sets the precedent for the signaling imbalance, as TrkC.T1 tends to be more highly expressed during nervous system development, and may be considered as a negative counterpart to the full length TrkC. Taken together with our findings that partial ablation of TrkC.T1 expression in RP did indeed preserve the retinal structure, we provided some of the first evidence for validating TrkC.T1 as a therapeutic target in RP, and also that TrkC.T1 overexpression falls nicely in line with the 'trophic imbalance' paradigm.

We further determined that a consistent increase in glial pErk occurred in the disease as well. As TrkC.T1 activation had been previously linked to the adaptor protein Rac1, and pErk downstream, this was a plausible first step through which the receptor may be contributing to the RP phenotype. Knowing also that TrkC.T1 contributes to neurotoxicity via TNFa in other degenerative models, we examined TNFa expression in RP and observed it to coincide with

TrkC.T1 upregulation. These findings outlined the full mechanistic links for TrkC.T1, and now allowed us to test the hypothesis with the use of small molecules as probes.

Our lab had previously published a series of novel TrkC antagonists targeting the ectodomain. As the ectodomains of both TrkC isoforms were thought to be virtually identical, we sought to use these molecules to shut down TrkC,T1 signaling. KB1368 is a broad-spectrum antagonist, and therefore also blocks full length TrkC activation. While this is unwanted, we posited that the higher TrkC.T1/TrkC.FL ratio could favor binding to TrkC.T1 overall, possibly sparing TrkC.FL. Additionally, there is a relatively short residence time for drugs delivered in the eye due to the vitreous fluid being continually replenished. This would mean that any perturbations to TrkC.FL signaling would be transient, and while the TrkC.T1 block would also be brief, it could still yield lasting effects by slowing down the toxic machinery continually at work.

KB1368 treatment of retinal explants from RP mice, and well as *in vivo* by intravitreal injection, corroborated our mechanistic findings and supported TrkC.T1 antagonism as a therapeutic strategy. KB1368 effectively lowered pErk and TNFa levels in both cases, tying the mechanistic components together. In explants, the treatment yielded higher photoreceptor counts, and *in vivo* preserved the retinal thickness long-term. These findings are among the first to attempt TrkC.T1 blockade in disease, and set the precedent for the development of selective small molecules targeting this isoform. Although the general consensus for some time has been that TrkC.T1 and TrkC.FL ectodomains are the same, in that they both bind NT-3 with equal affinity, there is evidence for structural divergence. The 2B7 antibody has planted the seed of doubt, for example. Originally developed to selectively activate TrkC.FL while sparing p75 binding, it was found that it also spared TrkC.T1. Further work suggested that there are in fact subtle differences in disulfide linkages between the isoforms. This could possibly be exploited in efforts to yield TrkC.T1 selective antagonists. Let the games begin.

In a separate collaborative work, the p75 receptor was examined for its etiological role in RP. In striking similarity to the findings surrounding TrkC.T1, p75 also became upregulated in the disease, as well as one of its native ligands, proNGF (analogous to NT-3 increases for TrkC.T1). The presence of elevated glial p75 and its ligand harbors a more toxic retinal

environment which ultimately contributes to photoreceptor loss. Again, to fully address such a question as well as provide some therapeutic relevance, small molecules offer the solution. Fortunately, selective inhibitors of p75 do exist, THX-B being well characterized and among the most efficacious in its class. We found that p75 antagonism by THX-B was able to prevent photoreceptor loss significantly in retinal cultures, as well as histologically in retinal sections from intravitreally injected animals. This cements the deleterious role of p75 in RP, and showcases a novel strategy which is disease-modifying. Moreover, THX-B treated eyes contained lower levels of mRNA transcripts for inflammatory mediators, TNFa unsurprisingly being one of them.

The biological parallels between TrkC.T1 and p75 in RP serve as elegant examples of how the dizzyingly-complex world of degenerative diseases can be tackled with a reductionist approach. That being said, it must be clearly stated that the findings revealed here are not necessarily aimed at curing the disease. It is highly unlikely that there is a 'magic-bullet' of sorts with the ability to halt the disease progression all at once. There are many coinciding mechanisms at work, and therefore finding a common denominator is no simple task. In fact, this work shows that both TrkC.T1 and p75 together are contributing retinal neurotoxicity in RP. It would be worthwhile to examine a combinatorial approach that involves blocking TrkC.T1 and p75 simultaneously. Engaging multiple targets is an underappreciated therapeutic strategy, and it is interesting to speculate that we may be able to make significantly more headway in this fashion, as opposed to proposing the next big monotherapy. Another noteworthy point to make here is that a distinction should be made between the cellular target population and the therapeutic target itself. The retinal work with TrkC.T1 and p75 demonstrate that one does not necessarily need to engage a neuronal target in order to preserve them. While not being a new concept by any means, it does illustrate that the target validation process involves looking at the biological system of interest as a whole. The interplay between neurons and glial cells is certainly relevant, as we are discovering with many other degenerative conditions including ALS, Parkinson's, and Alzheimer's.

Advantages of TrkC.T1/P75 antagonism

Since TrkC.T1 and p75 are similar in their signaling consequences, does their blockade offer improvements over currently adopted strategies which target downstream effectors like TNFa? TNFa, and cytokine biology in general, is highly complex as they play both positive and negative roles in the maintenance of the nervous and immune system [150]. TNF receptors exist in two major subtypes, TNFR1 and TNFR2. Additionally, TNF itself exists as both a soluble and membrane-bound form, each with distinct biological roles. Etanercept, a broad-spectrum inhibitor of both TNF forms, has shown efficacy in disease models of glaucoma for example [151]. However, its effects on normal membrane-bound TNFa functioning may give rise to immune dysfunction, as reflected by a higher incidence of ocular inflammatory disease by the treatment [152]. In response, neutralizing proteins directed specifically at the soluble form of TNFa remain efficacious and offer an improved therapeutic index [62].

While this work validates TNFa specifically as a therapeutic target, it may not fully address the implications of disrupting its normal regulatory functions. Low levels of TNFa are necessary for functioning of both the immune and nervous systems. Disrupting this is a potential concern with TNFa-antagonists. Furthermore, as we show that upregulation of TrkC.T1 and p75 tend to occur early in retinal disease pathology, their blockade allows for a therapeutic intervention at a time point before TNFa-inhibitors would have any efficacy, while sparing the basal levels of TNFa.

In addition to TNFa, there are other inflammatory mediators to consider. For example, upregulation of p75 is also linked to increases in one of its ligands, proNGF, as well as a2m. Together they act in concert to exacerbate pathological conditions [153]. Therefore, p75 antagonism serves as a 'multi-hit' approach, by reducing all of these mediators simultaneously.

Pro-survival strategies in the retina and RET as an emerging target

The next body of work looks at driving trophic signals as a means to correct the RP phenotype. The retina is a highly heterogeneous population of cells, and while the various neurons and glia are intimately connected to process and modulate visual data, they also keep each other alive and functioning properly. The expression patterns within the retina are complex and vary greatly between the developing and adult tissue, as well as after injury or in disease. For example, developing retinal ganglion cells (RGCs) in the rat are TrkA positive [154]; adult

rat RGCs are not but regain this expression after injury [51]. This in fact leads into another important point regarding species differences, and that our findings from animal models must be interpreted cautiously. This is a broad area which is lacking, but we are aware of some fundamental differences in retinal biology that could impact how a therapy translates on a human level. One example is that in mice, only one type of horizontal cell exists, whereas humans have three distinct types. Their general role is to form lateral connections with the photoreceptors and modulate the visual signal before it is passed onto the RGCs and eventually the visual cortex. There is however, clear evidence that these cells also aid in maintaining the photoreceptors, likely through the release of trophic factors [155]. In light of all this, identifying a valid therapeutic target in the retina is particularly challenging.

RET is not exempt from this confusion. There are conflicting reports of where RET protein is expressed in the tissue, as well as the co-receptors GFRa1 and GFRa2. There are also findings to indicate that there is a lack of anatomical overlap between protein levels and mRNA transcripts, suggesting the possibility that different cell types are shuttling RET receptors amongst themselves. Some retinal neurons, and indeed the Muller glia, have been shown to express only RET *in vivo*. The picture becomes muddier still stemming from contradictory findings in cultured retinal cells, cells which are notorious for changing phenotype under such conditions. When it comes to disease, RET is shown to in some cases to be relatively stable, while its GFRa co-receptors vary significantly.

The worthiness of GDNF, given these uncertainties, has been considered dubious. Fortunately, as discussed before, there has been mounting evidence to support its therapeutic value. On the other hand, none of these findings have led to any real progress in the clinic. The foundational base set by GDNF, as well as its poor ability to translate has provided the impetus for our developmental work. We found that both Compound 8 and Q525 were able to rescue photoreceptors in retinal explants, as measured through reduced TUNEL counts. Surprisingly, GDNF had failed under the same paradigm, even when high concentrations were used. We cannot completely rule out the possibility that this was due to kinetic issues; that GDNF was perhaps rapidly degraded or became bound by the extracellular matrix. It may be GFRa1-related as well. Based on our conclusions that the Muller glial cells appear to be the primary cells

targeted by the compounds, this is possible, since RET expression has been shown in these cells while GFRa1 expression is not as clear. What is also unclear is how GFRa1 expression changes during RP progression. Ideally, one might employ a longitudinal study using laser capture microdissection, or something along those lines as a means to isolate specific cell types and assess their receptor content.

Both compounds induced Akt and Erk phosphorylation in the Muller glia, with practically no immunostaining within the photoreceptor population. These data support a paracrine mechanism of photoreceptor protection, and in fact coincide well with our work in Chapter 2. The overall picture here is that the Muller glia play key roles in regulating the environment surrounding the photoreceptors through control of inflammatory mediator and growth factor release. While we did not identify the factors responsible for the neuroprotection, Fibroblast Growth Factor (FGF) is a possibility. Activated Muller glia have been shown to secrete FGF, and FGF receptors have been identified within the photoreceptor outer segments. These are difficult questions to address *in vivo*. A further set of difficult questions arises from the role of pErk when comparing the anti-neurotoxic and pro-survival data. Recall that Erk phosphorylation was shown to be a consequence of TrkC.T1 activation, driving glial production of TNFa. The RET studies however implicate pErk in a neuroprotective cascade of events. The dual nature of Erk in particular has been documented, and has been related to its kinetics of activation, which involve phosphatases. Its microenvironment within the cytoplasm is a determinant of the functional outcome as well, influenced by the proximity of pErk to its numerous adaptor proteins.

Discovery of direct RET agonists

Given the complex and unusual receptor biology of the RET/GFRa axis, the ability to activate RET directly would represent a way to get around these obstacles. In Chapter 3 our initial screens made the striking discovery that small molecules could in fact bind and lead to RET activation without GFRa1 expression. Phosphorylation levels of RET as well as that of Akt and Erk were comparable in cells expressing RET/GFRa1 or RET alone, strongly suggesting that the co-receptor was unnecessary for generating trophic signals. As we will discuss more in depth later, the molecular identity of the lead compound 8 remains to be seen, however the data are

firm in their conclusions. The SPR findings for example cannot be used to determine binding constants since the precise concentration in these experiments in not known. In conjunction with the biochemical assays, the data do support a direct interaction with the RET ectodomain. GFRa1-independence was also true regarding the quinone/quinoline series identified in Chapter 4, from the initial finding that a very simple chlorinated naphthoquinone could act as a RET activator as well. Modifying the side-chains on this molecular scaffold liberated the subsequent derivatives from GFRa1-dependence. We can only speculate at this point how this may be possible. As has been proposed by the dynamic equilibrium model of RET signaling, there is likely to be a certain amount of dimeric RET associated with GFRa1 on the membrane at any given moment. A molecule with limited surface area could therefore interact with this large complex to cause the relevant structural changes required for signaling. It is plausible that the GFRa1-dependent parent compound interacts at an allosteric site, and relies on GFRa1 to facilitate the rest of the conformational change needed for activation. Introducing the bulkier side chains may still allow for binding the same site, but this time establishing new contact points with RET residues, and ultimately stabilizing an active conformation on its own. This is a fascinating aspect of receptor biology that unfortunately is very tedious to explore. Crystallographic studies, for example, would be ideal in understanding this concept further. The very recent rise of the Cryo-EM technique has yielded extremely high resolution conformations of RET in complex with its ligands and co-receptors, and this is expected to provide new insights into how drug targeting of specific protein-protein interfaces might impact receptor signaling and its outcomes.

Probing the roles of the GFRa1 co-receptor

With the discovery of new classes of molecules that activate RET irrespective of its co-receptor, we now possessed the means to address new biological questions. Studies examining the signaling and functional outcomes GFRa1 exerts on RET are scarce, largely because of the lack of tools at our disposal. In Chapter 3, our findings from the *in vitro* survival assays indicated that GFRa1 was negatively regulating RET activation induced by lead Compound 8. Substantially higher compound concentrations were needed to yield a trophic effect in MG87 RET/GFRa1 than in MG87 RET cells. However, the short-term signaling characteristics of

Compound 8 were not remarkably different between the two cell types. The disconnect between pAkt/pErk signaling and the survival outcome was therefore also mediated by the presence of GFRa1, and suggests a complex and dynamic regulatory system at work. It is important to consider that a direct association between downstream signaling and functional outcome is not always the case, and these findings highlight the importance of that relationship as a means to understand how receptors and their ligands interact with each other.

Further evidence for GFRa1 as being an active participant in RET signaling nuances came from our studies using XIB4035. While this compound has a bit of a murky past, initially and incorrectly categorized as a GFRa1 agonist, it has recently been rechristened as a positive modulator of GFRa1. Bearing no intrinsic activity on its own, it seems to enhance GDNF signaling and prolong the presence of phosphorylated RET. Activated RET has a short residence time on the membrane, as it is targeted for ubiquitination and degraded rapidly. The exact mechanism of XIB4035 remains unproven, but it can be envisioned as facilitating and stabilizing some interaction within the RET/GFRa1 complex. We found that pre-treatment with XIB4035 substantially reduced signals by Compound 8. Since we verified Compound 8 as a direct RET agonist, this allowed us to conclude that GFRa1 interactions could indeed influence RET signaling at the level of pAkt and pErk, and this was clearly a negative regulation. However, the picture broadens in light of the findings from chapter 4. Combining the quinone/quinoline derivatives with XIB4035 generated a pErk signaling bias which resulted from two distinct regulatory outcomes; either through the reduction of pAkt while sparing pErk, or the increasing of pErk while sparing pAkt. These are the first reported instances of RET ligands that differentially interact with GFRa1, and implicate the GFRa1 co-receptor as being able to modulate RET signaling in a variety of ways depending on the ligand. Overall, these findings expand upon the already intriguing receptor biology of the RET/GFRa1 signaling axis, and open new avenues for the development of more effective therapeutics.

Studies with RET agonists and their implications for therapy

What are these new avenues exactly? To begin, as we previously discussed, the failure of GDNF in the retinal explant paradigm showcases an obvious advantage of the small molecule targeting of RET. In all fairness, the experiments do not address specifically *how* GDNF failed,

though we can at least assume that kinetic factors are a minor possibility. This is because of the fact that the retinal cultures permit a fairly stable environment, with a consistent volume maintained throughout the culturing period, quite unlike an *in vivo* situation. It is possible that GDNF reaching the retina may be unable to activate RET due to its entrapment by a component of the extracellular matrix, as this is a known feature of many trophic factors. However, if we are to consider that GDNF is sufficiently bioavailable, then its failure is most likely due to a GFRa1 –related event. Since RET/GFRa1 interactions are challenging to probe in complex systems like the retina (or any tissue), our findings advocate for direct RET targeting as a simpler therapeutic route which circumvents the need for understanding the influence of GFRa1.

That being said, our results also suggest that as our understanding of RET/GFRa1 dynamics in disease deepens, we may harness this knowledge to enhance therapeutic efficacy. As mentioned before, this field is in its infancy, and the current literature trends give no clear indication of how soon it will develop to be of any real relevance. When that time comes however, our findings in Chapter 4 with the quinoline/quinone pair studies may become particularly useful. As we demonstrated that direct RET agonists can be dynamically modulated by GFRa1, we open the possibility of generating biased signals through pAkt and pErk. The value of biased signaling in a therapeutic context is that one can tailor more specific signaling outcomes. This could lead to a maintaining of the neuroprotective effect, while at the same time mitigating an unwanted side-effect.

Antagonism or agonism as neurodegenerative therapies?

As this work has addressed therapeutic strategies geared toward restoring the balance from either side, it is worthy to compare their strengths and weaknesses. The blockade of inflammatory and neurotoxic messengers like TNFa through p75 or TrkC.T1 requires continuous intervention; as the antagonist is cleared, the underlying pathological mechanisms remain. From a clinical standpoint, chronic dosing regimens can be difficult to navigate from patient to patient, and there may be compensatory mechanisms which develop in the disease over time. Indeed, as we have seen, even in heterozygous mice where TrkC.T1 is genetically downregulated, this only results in a transient rescue of photoreceptor loss in the RP model [9].

On the other hand, activating trophic, or anti-apoptotic signaling cascades may induce changes which improve the disease phenotype in the long term. Akt activation for example, regulates the transcription of Bcl-2 family proteins responsible for determining cell fate [156]. Acute signaling processes can therefore translate into lasting impacts within the cell, sustaining their lifespan. However, this approach is not without fault either. Aberrant signals can cause unwanted side-effects. For example, the use of NGF in pain models showed improvements under some conditions, but resulted in hyperalgesia in others [157]. GDNF administration has been linked to tissue hypertrophy [90], and RET over-activation is an underlying cause of some aggressive cancers [158]. In some ways, less is more as far as agonism through neurotrophic receptors is concerned.

This leaves one important detail, one which warrants further exploration. It is likely that given the complex nature of degenerative diseases, multiple targets may need to be engaged to achieve the best efficacy. The future of small molecule therapy should hopefully give way to a combinatorial approach, one that perhaps employs both antagonists and angonists together. P75 blockade in addition to RET activation has not been attempted. This is an exciting prospect, and at the moment leaves much room for speculation.

A brief critique on chemical library screening

Our discovery that compound 8 was incorrectly curated and that the true molecular identity of the active fraction remains unknown raises some important considerations. Errors in compound labelling and even their storage conditions are likely to be more prevalent than we might expect, and this can be a hard truth to face for the drug developer. Many large libraries do not have quality control measures in place, and some will state that they are not responsible for any mistakes on their part. On some level this is understandable, given the sheer number of compounds a library may contain. The onus does fall on the researcher ultimately, but we may be misled by a false sense of security. There are numerous publications citing intriguing and useful biological activity from database screening efforts, without any structural verification or resynthesis attempts. The end result is somewhat of a “one step forward, two steps backward” situation that can complicate the drug development process. Furthermore, as chemical library curators tend to withhold or do not know information such as the origin, storage time/conditions,

and synthesis of their compounds, this creates more setbacks in the event that a structural discrepancy is found. There are faults on both sides to be considered, thus a more open line of data sharing and communication amongst researchers and library suppliers is advocated and should strengthen the drug development community as a whole.

Conclusion

The work presented in this thesis brings clarity to the trophic-imbalance hypothesis of neurodegeneration through the use of small molecules. Anti-neurotoxic strategies involving the blockade of p75 and TrkC.T1 were explored in a model of retinitis pigmentosa, and displayed efficacy through the reduction of toxic mediators like TNFa. As well, pro-survival strategies were also undertaken by targeting the RET tyrosine kinase receptor, and in doing so, a series of newly discovered RET agonists emerged. These signal without depending on the GFRa1 co-receptor, unlike GDNF. As such, they provide additional means to validate RET as a disease target, and to study the receptor biology of RET/GFRa1 interactions.

Drug development is a perilous endeavor, and as the very poor pre-clinical success rates would suggest, the odds are never in one's favor. Success hinges on a solid foundation, and in this case that foundation is the target. Thorough target identification and validation are extremely important, and the work as a whole serves to contribute to these concepts in the quest to cure the incurable.

Appendix I

Supporting Information for Chapter 3

	MG87 RET/GFRa1		MG87 RET	
Compound	**5 μM**	**20 μM**	**5 μM**	**20 μM**
116	**102.3124**	**134.8646**	**99.44444**	**117.8862**
206	**162.1520**	**122.5338**	**121.6667**	**102.0325**
210	**268.2869**	**265.0870**	**133.3333**	**121.1382**
302	**121.7084**	**180.3675**	**102.7778**	**105.2846**
226	**262.9070**	**227.1760**	**182.7778**	**163.4146**
224	**131.9018**	**247.6306**	**99.44444**	**111.7886**
65	**162.0104**	**230.2708**	**130.5556**	**174.3902**
47	**136.6210**	**166.2476**	**140.0000**	**180.4878**
29	**258.9429**	**330.0290**	**185.0000**	**252.0325**

Supplemental Table 1. Initial Compound Screening. In initial screens, ~200 compounds were tested in MG87 cells with and without GFRα1 expression at 5 and 20 μM. Data from a select panel are shown as the average relative increase in luminescence versus vehicle from 4 experiments. Compound 29 was selected as a candidate hit as it generated significant increases in both cell types, and subsequent analogues were then tested. In these assays, GDNF as positive control induces higher increases in luciferase activity, ranging from 60-80 fold over vehicle, consistent with previous reports (Sidorova et al, 2010).

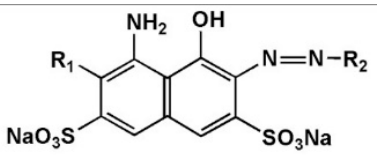

	R_1	R_2
15	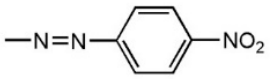	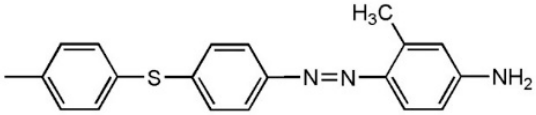
24	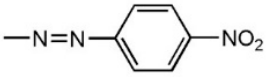	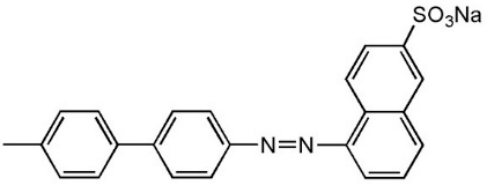
28	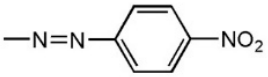	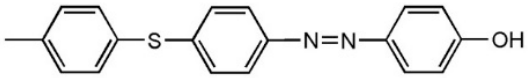
29	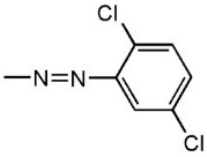	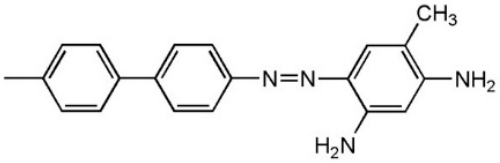
35	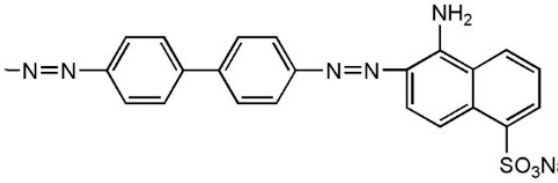	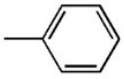
36	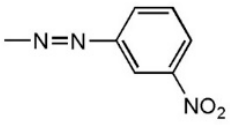	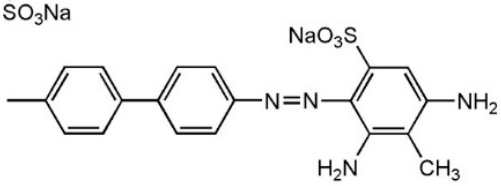
23	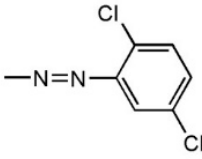	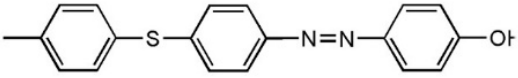

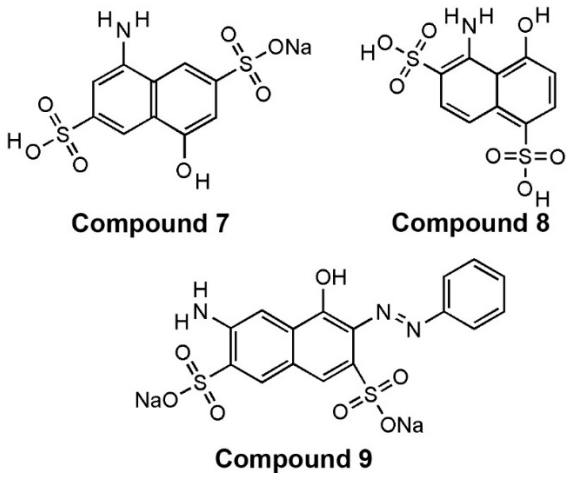

Supplemental Figure 1. Compound Structures. Overview of the structures as they are described by the NCI.

Structural Properties of NCI Database Compounds and 4-amino-5-hydroxynaphthalene-1,3-disulfonic Acid

4-amino-5-hydroxynaphthalene-1,3-disulfonic acid was obtained commercially from TCI America (Product Code: A0363) as a dark powder with reported purity of >85.0%. Both Compound 8 and this product were purified on a 250 mm x 10 mm Kromasil 100-5-C18 semi-preparative column. A solvent gradient of 5-30%B was used for 30 minutes, where solvent A was HPLC grade H_2O with 0.1% TFA, and solvent B was a 70/30 mix of Acetonitrile/H_2O with 0.1% TFA. Samples of each were lyophilized yielding an off-white powder and dissolved in D_2O for subsequent 1H-NMR at 500 MHz. ESI mass spectra were obtained in negative mode with a Bruker Maxis Impact. Compounds 15, 23, 29, and 35 were dissolved in DMSO for mass spec analysis. Sulfonic acids ionize preferentially in negative mode, and commonly yield di-charged ions by ESI (Holcapek 1999).

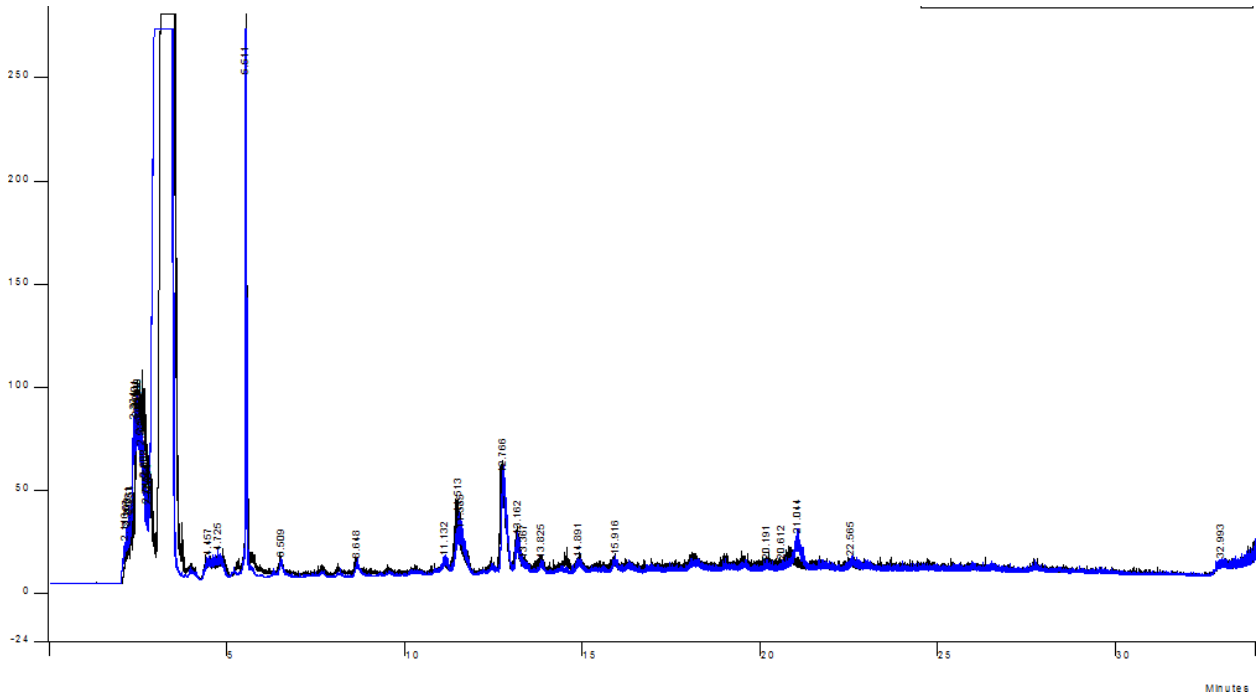

Supplemental Figure 2. HPLC chromatogram of the 5-30%B gradient showing 2 mg injections of <u>4-amino-5-hydroxynaphthalene-1,3-disulfonic Acid</u> [159] and <u>Compound 8</u> (Black). Both were relatively pure with the major fraction eluting ~3min. The close overlay of the chromatograms suggest that the impurities in the mixture are likely to be similar.

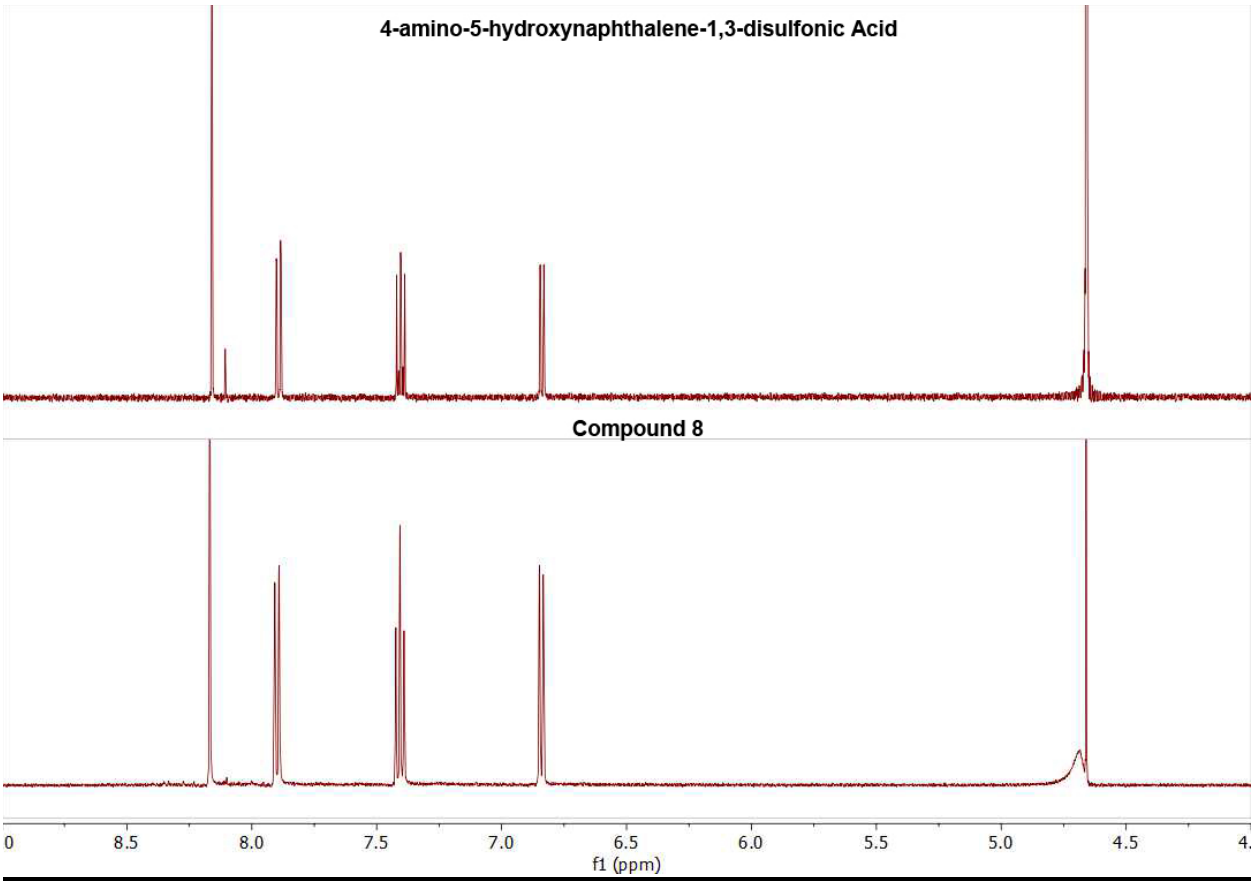

Supplemental Figure 3. H-NMR resonances and detected mass of 4-amino-5-hydroxynaphthalene-1,3-disulfonic Acid and Compound 8 show they are likely the same molecule, supporting that compound 8 is incorrectly identified in the NCI database.

Compound 8 (NSC37052)

1H-NMR (D_2O, 500 MHz): δ 8.17 (s, 1H), 7.90 (dd, J = 8.6, 0.9 Hz, 1H), 7.44 – 7.37 (t, 1H), 6.84 (dd, J = 7.8, 0.9 Hz, 1H).

MS (ESI,-) *m/z* calcd for $C_{10}H_7NO_7S_2$ $[M-2H]^{2-}$ calcd: 158.4837, found: 158.4841

4-amino-5-hydroxynaphthalene-1,3-disulfonic acid

1H-NMR (D_2O, 500 MHz): δ 8.16 (s, 1H), 7.89 (dd, J = 8.5, 1.0 Hz, 1H), 7.44 – 7.37 (t, 1H), 6.84 (dd, J = 7.8, 1.1 Hz, 1H).

MS (ESI,-) *m/z* calcd for $C_{10}H_7NO_7S_2$ $[M-2H]^{2-}$ calcd: 158.4837, found: 158.4840

Compound 15 (NSC65571)

MS (ESI,-) *m/z* calcd for $C_{35}H_{25}N_9O_9S_3$ $[M-2H]^{2-}$ calcd: 405.5474, found: 405.5460

Compound 23 (NSC75661)

MS (ESI,-) *m/z* calcd for $C_{34}H_{21}Cl_2N_7O_8S_3$ $[M-2H]^{2-}$ calcd: 410.5001, found: 410.5009

Compound 29 (NSC79730)

MS (ESI,-) *m/z* calcd for $C_{35}H_{25}Cl_2N_9O_7S_2$ $[M-2H]^{2-}$ calcd: 408.5353, found: 408.5356

Compound 35 (NSC79745)

MS (ESI,-) *m/z* calcd for $C_{38}H_{25}N_8NaO_{10}S_3$ $[M-2H]^{2-}$ calcd: 436.0382, found: 436.0397

Appendix II

Supporting Information for Chapter 4

Abbreviations:

DBNQ - 2,3-dibromonaphthalene-1,4-dione

DCNQ - 2,3-dichloronaphthalene-1,4-dione (dichlone)

TEA – trimethylamine

MeOH – methanol

Et_2O – diethyl ether

DO – dioxane

EA – ethyl acetate

DCM – dichloromethane

DMF – dimethyl formamide

SP-HPLC – semi-preparative high pressure liquid chromatography

NCS – N-chlorosuccinimide

Chl - chloroform

Synthesis of novel naphthoquinone derivatives

Methyl 4-(((3-chloro-1,4-dioxo-1,4-dihydronaphthalen-2-yl)amino)methyl) benzoate (Q101)

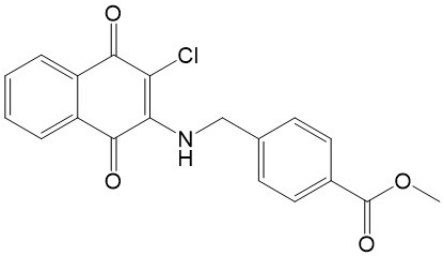

113 mg (0.5 mmol) of DCNQ, 101 mg (0.5 mmol) of methyl 4-(aminomethyl)-benzoate hydrochloride and 70 ul (0.5 mmol) of TEA were dissolved in 10 ml of MeOH and stirred for 18 h at RT. After precipitation with small amount of Et_2O, the red-orange solid was filtered and washed with cold Et_2O, yielding 47% of Q101.

^{1}H NMR ($CDCl_3$, 400 MHz) □8.21 (d, 2H), 8.18 (d, 2H), 8.07 (dd, 2H), 7.68 (d, 2H), 5.15 (d, 2H), 3.96 (s, 3H).

MS (ESI,+) *m/z* calcd for $C_{19}H_{15}ClNO_4$ $[M+H]^+$ calcd 356.06, found 356.3.

Methyl 2-(4-((3-chloro-1,4-dioxo-1,4-dihydronaphthalen-2-yl)amino)phenyl) acetate (Q105)

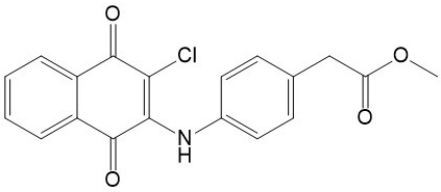

113 mg (0.5 mmol) of DCNQ, 83 mg (0.5 mmol) of methyl 2-(4-aminophenyl)acetate and 70 ul (0.5 mmol) of TEA were dissolved in 12 ml of MeOH and stirred 3 h at RT. After concentration of the solvent were isolated dark red needles with m.p.163-4^{o} C.

^{1}H NMR ($CDCl_3$, 400 MHz) □8.24 (d, 1H), 8.22 (d, 1H), 7.82 (m, 3H), 7.30 (d, 2H), 7.07 (d, 2H), 3.75 (s, 3H), 3.68 (s, 2H).

MS (ESI,+) *m/z* calcd for $C_{19}H_{15}ClNO_4$ $[M+H]^+$ 356.06, found 356.3.

2-Chloro-3-((2-(1-methylpyrrolidin-2-yl)ethyl)amino)naphthalene-1,4-dione (Q112)

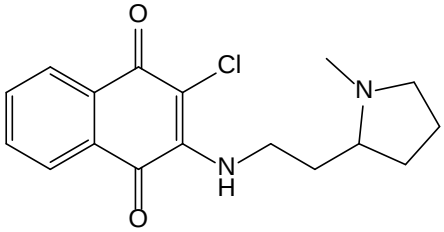

57 mg (0.25 mmol) of DCNQ, 37.3 ul (0.25 mmol) of 2-(1-methyl-pyrrolidin-2-yl)ethan-1-amine and 35 ul (0.25 mmol) of TEA in 5 ml dry MeOH were stirred at RT for 3 hours and the solvent was concentrated *in vacuo*. The product yielded 33 mg (41%) as orange crystals. Chemical Formula: $C_{17}H_{19}ClN_2O_2$. Exact Mass: 318.11. MS (ESI,+) *m/z* calcd for $C_{17}H_{20}ClN_2O_2$ $[M+H]^+$ 319.11, found 319.1205

Methyl 2-(4-((3-bromo-1,4-dioxo-1,4-dihydronaphthalen-2-yl)amino)phenyl) acetate (Q141)

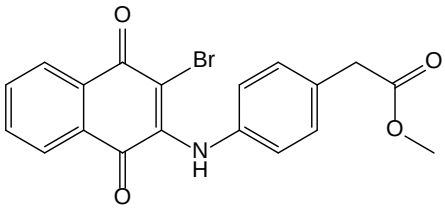

15.8 mg (0.05 mmol) of DBNQ and 8.3 mg (0.05 mmol) of methyl 2-(4-aminophenyl) acetate were dissolved in 1 ml 50% ethanol in water. The solution was stirred and heated at 60^{o} C for 2 hrs. The dark red crystals were filtered and washed with small amount of cold ethanol. Yield 13 mg (64%).

^{1}H NMR ($CDCl_3$, 400 MHz) □8.24 (d, 1H), 8.22 (d, 1H), 7.78 (m, 3H), 7.32 (d, 1H), 7.09 (d, 2H), 3.75 (s, 3H), 3.68 (s, 2H).

MS (ESI,+) *m/z* calcd for $C_{19}H_{15}BrNO_4$ $[M+H]^+$ 400.01, found 400.1

2-Chloro-3-((4-isothiocyanatophenyl)amino)naphthalene-1,4-dione (Q143)

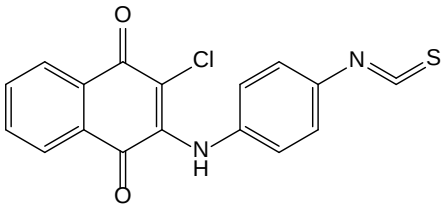

To a solution of 2-((4-aminophenyl)amino)-3-chloronaphthalene-1,4-dione (Ryan Inc) (23.8 mg, 0.08 mmol) in 20 ml of dry DCM was added37.1 mg (0.16 mmol) of 1,1'-thiocarbonylbis(pyridin-2(1H)-one). The mixture was stirred for 2 h at RT under nitrogen and concentrated under vacuum. The solvent was evaporated and the crude product was subjected to flash chromatography with chloroform as eluent. Fractions 2-6 were pooled and concentrated to afford 16 mg (88%) of Q143 as a dark red solid.

1H NMR (300 MHz, DMSO-d6) δ 9.46 (s, 1H), 8.11 – 8.02 (m, 2H), 7.96 – 7.78 (m, 2H), 7.46 – 7.35 (m, 2H), 7.23 – 7.08 (m, 2H).

MS (ESI,+) *m/z* calcd for $C_{17}H_{10}ClN_2O_2S$ $[M+H]^+$ 341.01, found 341.1.

7-Chloro-6-((4-(hydroxymethyl)phenyl)amino)quinoline-5,8-dione (Q525-1)

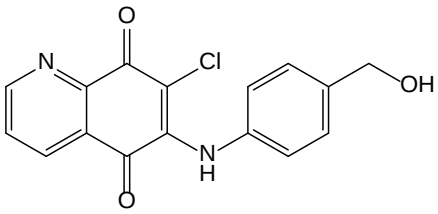

22.7 mg (0.1 mmol) of 6,7-dichloroquinoline-5,8-dione, 15.1 mg(0.1 mmol) of p-aminobenzyl alcohol were dissolved in 2 ml 50% ethanol and stirred at RT for 2 h until completion of the reaction (TLC). The solvent was concentrated and the two diastereomers were separated on semi-preparative HPLC. The H-NMR spectra of both compounds were run and analysed. The 6-substituted (7-Cl) isomer (structure shown above), was isolated in larger amount.

1H NMR (600 MHz, Methanol-d4) δ 8.84 (d, J = 4.7 Hz, 1H), 8.40 (dd, J = 7.9, 1.6 Hz, 1H), 7.69 (dd, J = 7.8, 4.8 Hz, 1H), 7.28 – 7.22 (m, 2H), 7.08 – 7.03 (m, 2H), 4.52 (s, 2H).

MS (+ESI) *m/z* calcd for $C_{16}H_{12}ClN_2O_3$ $[M+H]^+$ 315.05, found 315.07.

6-((4-(Hydroxymethyl)phenyl)amino)quinoxaline-5,8-dione (Q1041)

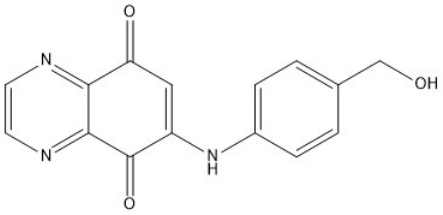

3 mg (0.019 mmol) of quinoxaline-5,8-dione, 2.54 mg (0.02 mmol) of p-aminobenzyl alcohol and 7.68 mg (0.02 mmol) of $CeCl_3.7H_2O$ are dissolved in 0.5 ml of absolute ethanol and stirred at RT overnight. After addition of 1 ml of water the mixture was extracted 3x with chloroform, the organic layer was dried with MgSO4, filtered and evaporated. The SP-HPLC purification afforded two peaks, which were subjected to MS. The rose peak with RT=11’ belonged to the expected product was lyophilized.

1H NMR (400 MHz, DMSO-d6) δ 9.49 (s, 1H), 9.02 (dd, J = 14.2, 2.3 Hz, 2H), 7.41 (d, J = 8.5 Hz, 2H), 7.36 (d, J = 8.5 Hz, 2H), 6.22 (s, 1H), 5.23 (s, 1H), 4.52 (d, J = 4.2 Hz, 2H).

MS (MALDI-TOF) *m/z* calcd for $C_{15}H_{12}N_3O_3$ $[M+H]^+$ 282.08, found 282.087.

2-Chloro-3-((4-(hydroxymethyl)phenyl)amino)naphthalene-1,4-dione (Q1047)

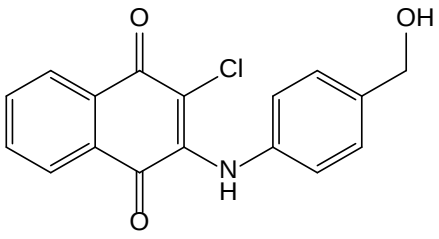

45.2 mg (0.2 mmol) of 2-chloronaphthalene-1,4-dione and 25 mg (0.2mmol) of (4-aminophenyl)methanol were dissolved in 3 ml of dry methanol and stirred overnight at room temperature. The mixture was left for 10 min at 4^{o} C, the unreacted products were filtered and after the evaporation of the solvent, the residue was dissolved in a minimal amount of 1.5% DMF in chloroform and subjected on a flash chromatography. Fractions 11-19 were collected.

R_f=0.2 (chloroform/methanol=98/2), R_f=0.78 (ethyl acetate).

1H NMR (400 MHz, DMSO-d6) δ 9.30 (s, 1NH), 8.04 (d, 2H), 7.84 (dtd, J = 7.5, 1.4 Hz, 2H), 7.26 (d, J = 8.2 Hz, 2H), 7.09 (d, J = 8.2 Hz, 2H), 5.17 (s, 1OH), 4.48 (s, 2H).

MS: (TOF, positive) *m/z* calcd for $C_{17}H_{13}ClNO_3$ $[M+H]^+$ 314.05, found 314.0589

6-Chloro-7-((4-(hydroxymethyl)phenyl)amino)quinoxaline-5,8-dione (Q1048)

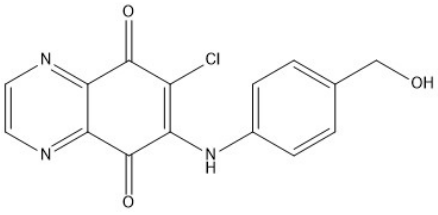

A solution of 2-chloro-3-((4-(hydroxymethyl)phenyl)amino)naphthalene-1,4-dione (Q1047) (1.9 mg, 6.76 umol) in 0.75 ml methanol was treated with NCS (0.9 mg, 6.75 umol). The mixture was stirred at RT overnight, the solvent was evaporated and the residue was purified by flash chromatography on Silica gel 60A in mini column with ethyl acetate as an eluent. Fractions 2-6 were collected, pooled and the solvent was evaporated to afford 0.5 mg of Q-1048 as a red solid.

MS (+ESI) *m/z* calcd for $C_{15}H_{11}ClN_3O_3$ $[M+H]^+$ 316.05, found 316.049.

2-Chloro-3-((4-(hydroxymethyl)phenyl)amino)naphthalene-1,4-dione (Q2003)

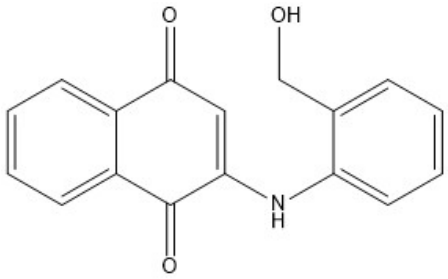

189.6 mg (1.2 mmol) of naphthalene-1,4-dione and 123 mg (1 mmol) of o-aminobenzyl alcohol are dissolved in 8 ml of methanol and stirred overnight at 45^{o} C. The solvent was evaporated and the residue was subjected to flash chromatography with chloroform, C/MeOH=99/1 and C/MeOH=98/2. Fractions 11-15 were pooled and the solvent was evaporated to afford the Q2003 as a dark red solid.

1H NMR (400 MHz, Methanol-d4) δ 8.14 (d, J = 7.6 Hz, 1H), 8.04 (d, J = 7.7 Hz, 1H), 7.81 (t, J = 7.5 Hz, 1H), 7.75 (dd, J = 8.3, 6.7 Hz, 1H), 7.49 (d, J = 7.6 Hz, 1H), 7.46 – 7.38 (m, 2H), 7.28 (t, J = 7.1 Hz, 1H), 6.03 (d, J = 1.5 Hz, 1H), 4.64 (s, 2H), 4.58 (s, 0H).

MS (+ESI) *m/z* calcd for $C_{17}H_{14}NO_3$ $[M+H]^+$ 280.09, found 280.097.

2-((2-(1-Methylpyrrolidin-2-yl)ethyl)amino)naphthalene-1,4-dione (Q2004)

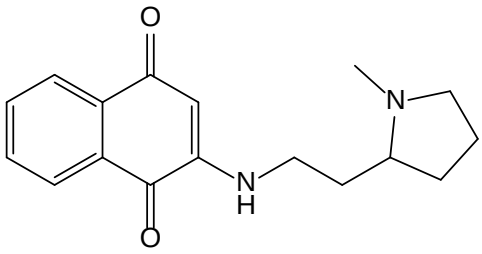

87 mg (0.55 mmol) of naphthalene-1,4-dione and 72 ul (0.5 mmol) of 2-(1-methyl-pyrrolidin-2-yl)ethan-1-amine were dissolved in 2 ml of MeOH and stirred for 2 hrs at RT. The solvent was evaporated, the crude product was dissolved in minimal amount of chloroform and purified by flash chromatography. As eluent was used chloroform with increasing concentration of MeOH up to 25%. The product was collected from fractions 12-20. After evaporating of the organic solvents, Q2004 yielded 60 mg (42%) as a dark orange solid.

1H NMR (400 MHz, Chloroform-d) δ 8.11 (dt, J = 7.8, 0.8 Hz, 1H), 8.04 (ddd, J = 7.7, 1.4, 0.5 Hz, 1H), 7.72 (td, J = 7.6, 1.4 Hz, 1H), 7.61 (td, J = 7.6, 1.3 Hz, 1H), 5.70 (s, 1H), 3.26 (ddq, J = 20.0, 13.4, 6.7 Hz, 2H), 2.40 (s, 4H), 2.01 (s, 1H), 1.77 (s, 2H), 1.58 (s, 6H).

MS (+ESI) *m/z* calcd for $C_{17}H_{21}N_2O_2$ $[M+H]^+$ 285.15, found 285.07.

References

1. Teng, K.K. and B.L. Hempstead, *Neurotrophins and their receptors: signaling trios in complex biological systems.* Cell Mol Life Sci, 2004. **61**(1): p. 35-48.
2. Chao, M.V., R. Rajagopal, and F.S. Lee, *Neurotrophin signalling in health and disease.* Clin Sci (Lond), 2006. **110**(2): p. 167-73.
3. Zaccaro, M.C., et al., *p75 Co-receptors regulate ligand-dependent and ligand-independent Trk receptor activation, in part by altering Trk docking subdomains.* J Biol Chem, 2001. **276**(33): p. 31023-9.
4. Tsoulfas, P., et al., *The rat trkC locus encodes multiple neurogenic receptors that exhibit differential response to neurotrophin-3 in PC12 cells.* Neuron, 1993. **10**: p. 975-90.
5. Esteban, P.F., et al., *A kinase-deficient TrkC receptor isoform activates Arf6-Rac1 signaling through the scaffold protein tamalin.* J Cell Biol, 2006. **173**(2): p. 291-9.
6. Menn, B., et al., *Spatiotemporal expression of noncatalytic TrkC NC2 isoform during early and late CNS neurogenesis: a comparative study with TrkC catalytic and p75NTR receptors.* Eur J Neurosci, 2000. **12**(9): p. 3211-23.
7. Palko, M.E., V. Coppola, and L. Tessarollo, *Evidence for a role of truncated trkC receptor isoforms in mouse development.* J. Neurosci., 1999. **19**: p. 775-82.
8. Bai, Y., et al., *In glaucoma the upregulated truncated TrkC.T1 receptor isoform in glia causes increased TNF-alpha production, leading to retinal ganglion cell death.* Invest Ophthalmol Vis Sci, 2010. **51**(12): p. 6639-51.
9. Galan, A., et al., *In retinitis pigmentosa TrkC.T1-dependent vectorial Erk activity upregulates glial TNF-alpha, causing selective neuronal death.* Cell Death Dis, 2017. **8**(12): p. 3222.
10. Brahimi, F., et al., *The Paradoxical Signals of Two TrkC Receptor Isoforms Supports a Rationale for Novel Therapeutic Strategies in ALS.* PLoS One, 2016. **11**(10): p. e0162307.
11. Jayaram, H., et al., *Comparison of MicroRNA Expression in Aqueous Humor of Normal and Primary Open-Angle Glaucoma Patients Using PCR Arrays: A Pilot Study.* Invest Ophthalmol Vis Sci, 2017. **58**(7): p. 2884-2890.
12. Dedoni, S., et al., *Interferon-beta Inhibits Neurotrophin 3 Signalling and Pro-Survival Activity by Upregulating the Expression of Truncated TrkC-T1 Receptor.* Mol Neurobiol, 2017. **54**(3): p. 1825-1843.
13. Ibanez, C.F. and A. Simi, *p75 neurotrophin receptor signaling in nervous system injury and degeneration: paradox and opportunity.* Trends Neurosci, 2012. **35**(7): p. 431-40.
14. Takahashi, M., J. Ritz, and G.M. Cooper, *Activation of a novel human transforming gene, ret, by DNA rearrangement.* Cell, 1985. **42**(2): p. 581-8.
15. Takahashi, M. and G.M. Cooper, *ret transforming gene encodes a fusion protein homologous to tyrosine kinases.* Mol Cell Biol, 1987. **7**(4): p. 1378-85.
16. Lin, L.F., et al., *GDNF: a glial cell line-derived neurotrophic factor for midbrain dopaminergic neurons.* Science, 1993. **260**(5111): p. 1130-2.
17. Trupp, M., et al., *Functional receptor for GDNF encoded by the c-ret proto-oncogene.* Nature, 1996. **381**(6585): p. 785-9.
18. Jing, S., et al., *GDNF-induced activation of the ret protein tyrosine kinase is mediated by GDNFR-alpha, a novel receptor for GDNF.* Cell, 1996. **85**(7): p. 1113-24.
19. Santoro, M., et al., *Activation of RET as a dominant transforming gene by germline mutations of MEN2A and MEN2B.* Science, 1995. **267**(5196): p. 381-3.

20. Sanicola, M., et al., *Glial cell line-derived neurotrophic factor-dependent RET activation can be mediated by two different cell-surface accessory proteins.* Proc Natl Acad Sci U S A, 1997. **94**(12): p. 6238-43.
21. Eketjall, S., et al., *Distinct structural elements in GDNF mediate binding to GFRalpha1 and activation of the GFRalpha1-c-Ret receptor complex.* EMBO J, 1999. **18**(21): p. 5901-10.
22. Bespalov, M.M. and M. Saarma, *GDNF family receptor complexes are emerging drug targets.* Trends Pharmacol Sci, 2007. **28**(2): p. 68-74.
23. Mischel, P.S., et al., *Nerve growth factor signals via preexisting TrkA receptor oligomers.* Biophys J, 2002. **83**(2): p. 968-76.
24. LeSauteur, L., et al., *Small molecule nerve growth factor analogs image receptors in vivo.* Nat Biotechnol, 1996. **14**(9): p. 1120-2.
25. Salvatore, M.F., et al., *Point source concentration of GDNF may explain failure of phase II clinical trial.* Exp Neurol, 2006. **202**(2): p. 497-505.
26. Bespalov, M.M., et al., *Heparan sulfate proteoglycan syndecan-3 is a novel receptor for GDNF, neurturin, and artemin.* J Cell Biol, 2011. **192**(1): p. 153-69.
27. Sandmark, J., et al., *Structure and biophysical characterization of the human full-length neurturin-GFRa2 complex: A role for heparan sulfate in signaling.* J Biol Chem, 2018. **293**(15): p. 5492-5508.
28. Smith, R.C., et al., *Increased brain bio-distribution and chemical stability and decreased immunogenicity of an engineered variant of GDNF.* Exp Neurol, 2015. **267**: p. 165-76.
29. Zhang, J. and E.J. Huang, *Dynamic expression of neurotrophic factor receptors in postnatal spinal motoneurons and in mouse model of ALS.* J Neurobiol, 2006. **66**(8): p. 882-95.
30. Jomary, C., et al., *Expression of neurturin, glial cell line-derived neurotrophic factor, and their receptor components in light-induced retinal degeneration.* Invest Ophthalmol Vis Sci, 2004. **45**(4): p. 1240-6.
31. Josephy-Hernandez, S., et al., *Neurotrophin receptor agonists and antagonists as therapeutic agents: An evolving paradigm.* Neurobiol Dis, 2017. **97**(Pt B): p. 139-155.
32. Hartong, D.T., E.L. Berson, and T.P. Dryja, *Retinitis pigmentosa.* Lancet, 2006. **368**(9549): p. 1795-809.
33. Daiger, S.P., S.J. Bowne, and L.S. Sullivan, *Perspective on genes and mutations causing retinitis pigmentosa.* Arch Ophthalmol, 2007. **125**(2): p. 151-8.
34. Ferrari, S., et al., *Retinitis pigmentosa: genes and disease mechanisms.* Curr Genomics, 2011. **12**(4): p. 238-49.
35. van Soest, S., et al., *Retinitis pigmentosa: defined from a molecular point of view.* Surv Ophthalmol, 1999. **43**(4): p. 321-34.
36. Zeng, H.Y., et al., *Identification of sequential events and factors associated with microglial activation, migration, and cytotoxicity in retinal degeneration in rd mice.* Invest Ophthalmol Vis Sci, 2005. **46**(8): p. 2992-9.
37. Martinez-Fernandez de la Camara, C., et al., *Adalimumab Reduces Photoreceptor Cell Death in A Mouse Model of Retinal Degeneration.* Sci Rep, 2015. **5**: p. 11764.
38. Bringmann, A., et al., *Muller cells in the healthy and diseased retina.* Prog Retin Eye Res, 2006. **25**(4): p. 397-424.
39. Mandell, J.W. and S.R. VandenBerg, *ERK/MAP kinase is chronically activated in human reactive astrocytes.* Neuroreport, 1999. **10**(17): p. 3567-72.
40. Subramaniam, S. and K. Unsicker, *ERK and cell death: ERK1/2 in neuronal death.* FEBS J, 2010. **277**(1): p. 22-9.

41. Galan, A., et al., *Neuronal injury external to the retina rapidly activates retinal glia, followed by elevation of markers for cell cycle re-entry and death in retinal ganglion cells.* PLoS One, 2014. **9**(7): p. e101349.
42. Bai, Y., et al., *Chronic and acute models of retinal neurodegeneration TrkA activity are neuroprotective whereas p75NTR activity is neurotoxic through a paracrine mechanism.* J Biol Chem, 2010. **285**(50): p. 39392-400.
43. Barcelona, P.F., et al., *p75NTR and Its Ligand ProNGF Activate Paracrine Mechanisms Etiological to the Vascular, Inflammatory, and Neurodegenerative Pathologies of Diabetic Retinopathy.* J Neurosci, 2016. **36**(34): p. 8826-41.
44. Galan, A., et al., *Subconjunctival Delivery of p75NTR Antagonists Reduces the Inflammatory, Vascular, and Neurodegenerative Pathologies of Diabetic Retinopathy.* Invest Ophthalmol Vis Sci, 2017. **58**(7): p. 2852-2862.
45. Platon-Corchado, M., et al., *p75NTR antagonists attenuate photoreceptor cell loss in murine models of retinitis pigmentosa.* Cell Death Dis, 2017. **8**(7): p. e2922.
46. Patapoutian, A. and L.F. Reichardt, *Trk receptors: mediators of neurotrophin action.* Curr Opin Neurobiol, 2001. **11**(3): p. 272-80.
47. Saragovi, H.U. and M.C. Zaccaro, *Small molecule peptidomimetic ligands of neurotrophin receptors, identifying binding sites, activation sites and regulatory sites.* Curr Pharm Des, 2002. **8**(24): p. 2201-16.
48. Ivanisevic, L., et al., *TrkA receptor "hot spots" for binding of NT-3 as a heterologous ligand.* J Biol Chem, 2007. **282**(23): p. 16754-63.
49. Guo, X.J., et al., *Dysregulation of neurotrophic and inflammatory systems accompanied by decreased CREB signaling in ischemic rat retina.* Exp Eye Res, 2014. **125**: p. 156-63.
50. Bazan, N.G., *Neurotrophins induce neuroprotective signaling in the retinal pigment epithelial cell by activating the synthesis of the anti-inflammatory and anti-apoptotic neuroprotectin D1.* Adv Exp Med Biol, 2008. **613**: p. 39-44.
51. Cui, Q., et al., *Expression of trkA, trkB, and trkC in injured and regenerating retinal ganglion cells of adult rats.* Invest Ophthalmol Vis Sci, 2002. **43**(6): p. 1954-64.
52. Bovolenta, P., et al., *Neurotrophin-3 antibodies disrupt the normal development of the chick retina.* J Neurosci, 1996. **16**(14): p. 4402-10.
53. Tessarollo, L., *Pleiotropic functions of neurotrophins in development.* Cytokine Growth Factor Rev, 1998. **9**(2): p. 125-37.
54. Huang, E.J. and L.F. Reichardt, *Neurotrophins: roles in neuronal development and function.* Annu Rev Neurosci, 2001. **24**: p. 677-736.
55. Sarthy, V.P., et al., *Establishment and characterization of a retinal Muller cell line.* Invest Ophthalmol Vis Sci, 1998. **39**(1): p. 212-6.
56. Jian, Y., R.J. Zawadzki, and M.V. Sarunic, *Adaptive optics optical coherence tomography for in vivo mouse retinal imaging.* J Biomed Opt, 2013. **18**(5): p. 56007.
57. Li, J., et al., *Performance and scalability of Fourier domain optical coherence tomography acceleration using graphics processing units.* Appl Opt, 2011. **50**(13): p. 1832-8.
58. Maisonpierre, P.C., et al., *Neurotrophin-3: a neurotrophic factor related to NGF and BDNF.* Science, 1990. **247**(4949 Pt 1): p. 1446-51.
59. Curtis, K.M., L.A. Gomez, and P.C. Schiller, *Rac1b regulates NT3-stimulated Mek-Erk signaling, directing marrow-isolated adult multilineage inducible (MIAMI) cells toward an early neuronal phenotype.* Mol Cell Neurosci, 2012. **49**(2): p. 138-48.

60. Rodgers, E.E. and A.B. Theibert, *Functions of PI 3-kinase in development of the nervous system.* Int J Dev Neurosci, 2002. **20**(3-5): p. 187-97.
61. Jeon, S., et al., *NGF-induced moesin phosphorylation is mediated by the PI3K, Rac1 and Akt and required for neurite formation in PC12 cells.* Neurochem Int, 2010. **56**(6-7): p. 810-8.
62. Cueva Vargas, J.L., et al., *Soluble Tumor Necrosis Factor Alpha Promotes Retinal Ganglion Cell Death in Glaucoma via Calcium-Permeable AMPA Receptor Activation.* J Neurosci, 2015. **35**(35): p. 12088-102.
63. Lebrun-Julien, F., et al., *ProNGF induces TNFalpha-dependent death of retinal ganglion cells through a p75NTR non-cell-autonomous signaling pathway.* Proc Natl Acad Sci U S A, 2010. **107**(8): p. 3817-22.
64. Chen, D., et al., *Bivalent peptidomimetic ligands of TrkC are biased agonists and selectively induce neuritogenesis or potentiate neurotrophin-3 trophic signals.* ACS Chem Biol, 2009. **4**(9): p. 769-81.
65. Brahimi, F., et al., *A peptidomimetic of NT-3 acts as a TrkC antagonist.* Peptides, 2009. **30**(10): p. 1833-9.
66. Lyu, P.C., et al., *Position-Dependent Stabilizing Effects in α-Helices: N-Terminal Capping in Synthetic Model Peptides.* JACS, 1992. **114**: p. 6560-2.
67. Zhao, T.T., C.Y. Tian, and Z.Q. Yin, *Activation of Muller cells occurs during retinal degeneration in RCS rats.* Adv Exp Med Biol, 2010. **664**: p. 575-83.
68. Metrailler, S., et al., *ERK1/2 pathway is activated in degenerated Rpe65-deficient mice.* Exp Eye Res, 2013. **116**: p. 86-95.
69. Groeger, G., et al., *Reactive oxygen species regulate prosurvival ERK1/2 signaling and bFGF expression in gliosis within the retina.* Invest Ophthalmol Vis Sci, 2012. **53**(10): p. 6645-54.
70. Yang, J.Y., et al., *ERK promotes tumorigenesis by inhibiting FOXO3a via MDM2-mediated degradation.* Nat Cell Biol, 2008. **10**(2): p. 138-48.
71. Fischer, A.J., et al., *Mitogen-activated protein kinase-signaling regulates the ability of Muller glia to proliferate and protect retinal neurons against excitotoxicity.* Glia, 2009. **57**(14): p. 1538-52.
72. Fischer, A.J., M.A. Scott, and W. Tuten, *Mitogen-activated protein kinase-signaling stimulates Muller glia to proliferate in acutely damaged chicken retina.* Glia, 2009. **57**(2): p. 166-81.
73. Nakazawa, T., et al., *Attenuated glial reactions and photoreceptor degeneration after retinal detachment in mice deficient in glial fibrillary acidic protein and vimentin.* Invest Ophthalmol Vis Sci, 2007. **48**(6): p. 2760-8.
74. Nakazawa, T., et al., *Tumor necrosis factor-alpha mediates photoreceptor death in a rodent model of retinal detachment.* Invest Ophthalmol Vis Sci, 2011. **52**(3): p. 1384-91.
75. Jones, B.W., et al., *Retinal remodeling in human retinitis pigmentosa.* Exp Eye Res, 2016.
76. Al-Gayyar, M.M. and N.M. Elsherbiny, *Contribution of TNF-alpha to the development of retinal neurodegenerative disorders.* Eur Cytokine Netw, 2013. **24**(1): p. 27-36.
77. Liu, Y., et al., *Correlation of cytokine levels and microglial cell infiltration during retinal degeneration in RCS rats.* PLoS One, 2013. **8**(12): p. e82061.
78. Garcia-Junco-Clemente, P. and P. Golshani, *PTEN: A master regulator of neuronal structure, function, and plasticity.* Commun Integr Biol, 2014. **7**(1): p. e28358.
79. C, O.N., *PI3-kinase/Akt/mTOR signaling: impaired on/off switches in aging, cognitive decline and Alzheimer's disease.* Exp Gerontol, 2013. **48**(7): p. 647-53.
80. Nutt, J.G., et al., *Randomized, double-blind trial of glial cell line-derived neurotrophic factor (GDNF) in PD.* Neurology, 2003. **60**(1): p. 69-73.
81. Runeberg-Roos, P. and M. Saarma, *Neurotrophic factor receptor RET: structure, cell biology, and inherited diseases.* Ann Med, 2007. **39**(8): p. 572-80.

82. Ibanez, C.F., *Structure and physiology of the RET receptor tyrosine kinase.* Cold Spring Harb Perspect Biol, 2013. **5**(2).
83. Airaksinen, M.S. and M. Saarma, *The GDNF family: signalling, biological functions and therapeutic value.* Nat Rev Neurosci, 2002. **3**(5): p. 383-94.
84. Boucher, T.J., et al., *Potent analgesic effects of GDNF in neuropathic pain states.* Science, 2000. **290**(5489): p. 124-7.
85. McGee Sanftner, L.H., et al., *Glial cell line derived neurotrophic factor delays photoreceptor degeneration in a transgenic rat model of retinitis pigmentosa.* Mol Ther, 2001. **4**(6): p. 622-9.
86. Gregory-Evans, K., et al., *Ex vivo gene therapy using intravitreal injection of GDNF-secreting mouse embryonic stem cells in a rat model of retinal degeneration.* Mol Vis, 2009. **15**: p. 962-73.
87. Ohnaka, M., et al., *Long-term expression of glial cell line-derived neurotrophic factor slows, but does not stop retinal degeneration in a model of retinitis pigmentosa.* J Neurochem, 2012. **122**(5): p. 1047-53.
88. Whone, A., et al., *Randomized trial of intermittent intraputamenal glial cell line-derived neurotrophic factor in Parkinson's disease.* Brain, 2019. **142**(3): p. 512-525.
89. Gash, D.M., et al., *Trophic factor distribution predicts functional recovery in parkinsonian monkeys.* Ann Neurol, 2005. **58**(2): p. 224-33.
90. Touchard, E., et al., *Non-viral gene therapy for GDNF production in RCS rat: the crucial role of the plasmid dose.* Gene Ther, 2012. **19**(9): p. 886-98.
91. Sariola, H. and M. Saarma, *Novel functions and signalling pathways for GDNF.* J Cell Sci, 2003. **116**(Pt 19): p. 3855-62.
92. Hamilton, J.F., et al., *Heparin coinfusion during convection-enhanced delivery (CED) increases the distribution of the glial-derived neurotrophic factor (GDNF) ligand family in rat striatum and enhances the pharmacological activity of neurturin.* Exp Neurol, 2001. **168**(1): p. 155-61.
93. Ivanisevic, L., K. Banerjee, and H.U. Saragovi, *Differential cross-regulation of TrkA and TrkC tyrosine kinase receptors with p75.* Oncogene, 2003. **22**(36): p. 5677-85.
94. Brantley, M.A., Jr., et al., *Neurturin-mediated ret activation is required for retinal function.* J Neurosci, 2008. **28**(16): p. 4123-35.
95. Sidorova, Y.A., et al., *Persephin signaling through GFRalpha1: the potential for the treatment of Parkinson's disease.* Mol Cell Neurosci, 2010. **44**(3): p. 223-32.
96. Leppanen, V.M., et al., *The structure of GFRalpha1 domain 3 reveals new insights into GDNF binding and RET activation.* EMBO J, 2004. **23**(7): p. 1452-62.
97. Kim, S., et al., *PubChem Substance and Compound databases.* Nucleic Acids Res, 2016. **44**(D1): p. D1202-13.
98. Li, T., et al., *Transgenic mice carrying the dominant rhodopsin mutation P347S: evidence for defective vectorial transport of rhodopsin to the outer segments.* Proc Natl Acad Sci U S A, 1996. **93**(24): p. 14176-81.
99. Bonafina, A., et al., *GDNF/GFRalpha1 Complex Abrogates Self-Renewing Activity of Cortical Neural Precursors Inducing Their Differentiation.* Stem Cell Reports, 2018. **10**(3): p. 1000-1015.
100. Catapano, L.A., et al., *Specific neurotrophic factors support the survival of cortical projection neurons at distinct stages of development.* J Neurosci, 2001. **21**(22): p. 8863-72.
101. Mologni, L., et al., *Inhibition of RET tyrosine kinase by SU5416.* J Mol Endocrinol, 2006. **37**(2): p. 199-212.
102. Pierchala, B.A., J. Milbrandt, and E.M. Johnson, Jr., *Glial cell line-derived neurotrophic factor-dependent recruitment of Ret into lipid rafts enhances signaling by partitioning Ret from proteasome-dependent degradation.* J Neurosci, 2006. **26**(10): p. 2777-87.

103. Hedstrom, K.L., et al., *Treating small fiber neuropathy by topical application of a small molecule modulator of ligand-induced GFRalpha/RET receptor signaling.* Proc Natl Acad Sci U S A, 2014. **111**(6): p. 2325-30.
104. Del Rio, P., et al., *GDNF-induced osteopontin from Muller glial cells promotes photoreceptor survival in the Pde6brd1 mouse model of retinal degeneration.* Glia, 2011. **59**(5): p. 821-32.
105. Hauck, S.M., et al., *GDNF family ligands trigger indirect neuroprotective signaling in retinal glial cells.* Mol Cell Biol, 2006. **26**(7): p. 2746-57.
106. Bespalov, M.M., et al., *Novel agonist of GDNF family ligand receptor RET for the treatment of experimental neuropathy.* bioRxiv, 2016.
107. Saarma, M., et al., *Methods of facilitating neural cell survival using gdnf family ligand (gfl) mimetics or ret signaling pathway activators*. 2011, Google Patents.
108. Sidorova, Y.A., et al., *A Novel Small Molecule GDNF Receptor RET Agonist, BT13, Promotes Neurite Growth from Sensory Neurons in Vitro and Attenuates Experimental Neuropathy in the Rat.* Front Pharmacol, 2017. **8**: p. 365.
109. Ivanova, L., et al., *Small-Molecule Ligands as Potential GDNF Family Receptor Agonists.* ACS Omega, 2018. **3**(1): p. 1022-1030.
110. Tokugawa, K., et al., *XIB4035, a novel nonpeptidyl small molecule agonist for GFRalpha-1.* Neurochem Int, 2003. **42**(1): p. 81-6.
111. Ivanova, L., et al., *Molecular Dynamics Simulations of the Interactions between Glial Cell Line-Derived Neurotrophic Factor Family Receptor GFRalpha1 and Small-Molecule Ligands.* ACS Omega, 2018. **3**(9): p. 11407-11414.
112. Treanor, J.J., et al., *Characterization of a multicomponent receptor for GDNF.* Nature, 1996. **382**(6586): p. 80-3.
113. Maliartchouk, S., et al., *A designed peptidomimetic agonistic ligand of TrkA nerve growth factor receptors.* Mol Pharmacol, 2000. **57**(2): p. 385-91.
114. Maliartchouk, S., et al., *Genuine monovalent ligands of TrkA nerve growth factor receptors reveal a novel pharmacological mechanism of action.* J Biol Chem, 2000. **275**(14): p. 9946-56.
115. Lindgren, N., et al., *Activation of the extracellular signal-regulated kinases 1 and 2 by glial cell line-derived neurotrophic factor and its relation to neuroprotection in a mouse model of Parkinson's disease.* J Neurosci Res, 2008. **86**(9): p. 2039-49.
116. Trupp, M., et al., *Multiple GPI-anchored receptors control GDNF-dependent and independent activation of the c-Ret receptor tyrosine kinase.* Mol Cell Neurosci, 1998. **11**(1-2): p. 47-63.
117. Zaccaro, M.C., et al., *Selective small molecule peptidomimetic ligands of TrkC and TrkA receptors afford discrete or complete neurotrophic activities.* Chem Biol, 2005. **12**(9): p. 1015-28.
118. Massa, S.M., et al., *Small molecule BDNF mimetics activate TrkB signaling and prevent neuronal degeneration in rodents.* The Journal of Clinical Investigation, 2010. **120**(5): p. 1774-1785.
119. Guillemard, V., et al., *An agonistic mAb directed to the TrkC receptor juxtamembrane region defines a trophic hot spot and interactions with p75 coreceptors.* Dev Neurobiol, 2010. **70**(3): p. 150-64.
120. Landers, R.A., et al., *Increased retinal synthesis of heparan sulfate proteoglycan and HNK-1 glycoproteins following photoreceptor degeneration.* J Neurochem, 1994. **63**(2): p. 737-50.
121. Guadagni, V., et al., *Pharmacological approaches to retinitis pigmentosa: A laboratory perspective.* Prog Retin Eye Res, 2015. **48**: p. 62-81.
122. Wahlin, K.J., et al., *Neurotrophic factors cause activation of intracellular signaling pathways in Muller cells and other cells of the inner retina, but not photoreceptors.* Invest Ophthalmol Vis Sci, 2000. **41**(3): p. 927-36.

123. Allocca, M., et al., *Constitutive and AP20187-induced Ret activation in photoreceptors does not protect from light-induced damage.* Invest Ophthalmol Vis Sci, 2007. **48**(11): p. 5199-206.
124. Koeberle, P.D. and M. Bahr, *The upregulation of GLAST-1 is an indirect antiapoptotic mechanism of GDNF and neurturin in the adult CNS.* Cell Death Differ, 2008. **15**(3): p. 471-83.
125. Inglese, J., C.E. Shamu, and R.K. Guy, *Reporting data from high-throughput screening of small-molecule libraries.* Nat Chem Biol, 2007. **3**(8): p. 438-41.
126. Allen, J.E., et al., *Dual inactivation of Akt and ERK by TIC10 signals Foxo3a nuclear translocation, TRAIL gene induction, and potent antitumor effects.* Sci Transl Med, 2013. **5**(171): p. 171ra17.
127. Jacob, N.T., et al., *Pharmacophore reassignment for induction of the immunosurveillance cytokine TRAIL.* Angew Chem Int Ed Engl, 2014. **53**(26): p. 6628-31.
128. Widhalm, J.R. and D. Rhodes, *Biosynthesis and molecular actions of specialized 1,4-naphthoquinone natural products produced by horticultural plants.* Hortic Res, 2016. **3**: p. 16046.
129. Bolton, J.L. and T. Dunlap, *Formation and Biological Targets of Quinones: Cytotoxic versus Cytoprotective Effects.* Chem Res Toxicol, 2017. **30**(1): p. 13-37.
130. Klotz, L.O., X. Hou, and C. Jacob, *1,4-naphthoquinones: from oxidative damage to cellular and inter-cellular signaling.* Molecules, 2014. **19**(9): p. 14902-18.
131. Perron, M.D., et al., *Allosteric noncompetitive small molecule selective inhibitors of CD45 tyrosine phosphatase suppress T-cell receptor signals and inflammation in vivo.* Mol Pharmacol, 2014. **85**(4): p. 553-63.
132. Wang, L., et al., *Protective effect of shikonin in experimental ischemic stroke: attenuated TLR4, p-p38MAPK, NF-kappaB, TNF-alpha and MMP-9 expression, up-regulated claudin-5 expression, ameliorated BBB permeability.* Neurochem Res, 2014. **39**(1): p. 97-106.
133. Yuan, J.H., et al., *Neuroprotection by plumbagin involves BDNF-TrkB-PI3K/Akt and ERK1/2/JNK pathways in isoflurane-induced neonatal rats.* J Pharm Pharmacol, 2017. **69**(7): p. 896-906.
134. Frasson, M., et al., *Glial cell line-derived neurotrophic factor induces histologic and functional protection of rod photoreceptors in the rd/rd mouse.* Invest Ophthalmol Vis Sci, 1999. **40**(11): p. 2724-34.
135. Garcia-Caballero, C., et al., *Photoreceptor preservation induced by intravitreal controlled delivery of GDNF and GDNF/melatonin in rhodopsin knockout mice.* Mol Vis, 2018. **24**: p. 733-745.
136. Baranov, P., et al., *A Novel Neuroprotective Small Molecule for Glial Cell Derived Neurotrophic Factor Induction and Photoreceptor Rescue.* J Ocul Pharmacol Ther, 2017. **33**(5): p. 412-422.
137. Platon-Corchado, M., et al., *p75(NTR) antagonists attenuate photoreceptor cell loss in murine models of retinitis pigmentosa.* Cell Death Dis, 2017. **8**(7): p. e2922.
138. Afzal, O., et al., *A review on anticancer potential of bioactive heterocycle quinoline.* Eur J Med Chem, 2015. **97**: p. 871-910.
139. Graham Robinett, R., et al., *The discovery of substituted 4-(3-hydroxyanilino)-quinolines as potent RET kinase inhibitors.* Bioorg Med Chem Lett, 2007. **17**(21): p. 5886-93.
140. Schmidt, F., et al., *Chemicals possessing a neurotrophin-like activity on dopaminergic neurons in primary culture.* PLoS One, 2009. **4**(7): p. e6215.
141. Whalen, E.J., S. Rajagopal, and R.J. Lefkowitz, *Therapeutic potential of beta-arrestin- and G protein-biased agonists.* Trends Mol Med, 2011. **17**(3): p. 126-39.
142. Rajagopal, S., et al., *Biased agonism as a mechanism for differential signaling by chemokine receptors.* J Biol Chem, 2013. **288**(49): p. 35039-48.
143. Zhao, P., M. Metcalf, and N.W. Bunnett, *Biased signaling of protease-activated receptors.* Front Endocrinol (Lausanne), 2014. **5**: p. 67.

144. Yang, J., et al., *PSPN/GFRalpha4 has a significantly weaker capacity than GDNF/GFRalpha1 to recruit RET to rafts, but promotes neuronal survival and neurite outgrowth.* FEBS Lett, 2004. **569**(1-3): p. 267-71.
145. Vilar, M., et al., *Ligand-independent signaling by disulfide-crosslinked dimers of the p75 neurotrophin receptor.* J Cell Sci, 2009. **122**(Pt 18): p. 3351-7.
146. Paratcha, G., et al., *Released GFRalpha1 potentiates downstream signaling, neuronal survival, and differentiation via a novel mechanism of recruitment of c-Ret to lipid rafts.* Neuron, 2001. **29**(1): p. 171-84.
147. Mikaels-Edman, A., C. Baudet, and P. Ernfors, *Soluble and bound forms of GFRalpha1 elicit different GDNF-independent neurite growth responses in primary sensory neurons.* Dev Dyn, 2003. **227**(1): p. 27-34.
148. Fleming, M.S., et al., *Cis and trans RET signaling control the survival and central projection growth of rapidly adapting mechanoreceptors.* Elife, 2015. **4**: p. e06828.
149. Mullican, S.E., et al., *GFRAL is the receptor for GDF15 and the ligand promotes weight loss in mice and nonhuman primates.* Nat Med, 2017. **23**(10): p. 1150-1157.
150. Marin, I. and J. Kipnis, *Learning and memory ... and the immune system.* Learn Mem, 2013. **20**(10): p. 601-6.
151. Roh, M., et al., *Etanercept, a widely used inhibitor of tumor necrosis factor-alpha (TNF-alpha), prevents retinal ganglion cell loss in a rat model of glaucoma.* PLoS One, 2012. **7**(7): p. e40065.
152. Taban, M., et al., *Etanercept (enbrel)-associated inflammatory eye disease: case report and review of the literature.* Ocul Immunol Inflamm, 2006. **14**(3): p. 145-50.
153. Barcelona, P.F. and H.U. Saragovi, *A Pro-Nerve Growth Factor (proNGF) and NGF Binding Protein, alpha2-Macroglobulin, Differentially Regulates p75 and TrkA Receptors and Is Relevant to Neurodegeneration Ex Vivo and In Vivo.* Mol Cell Biol, 2015. **35**(19): p. 3396-408.
154. Zanellato, A., et al., *Developing rat retinal ganglion cells express the functional NGF receptor p140trkA.* Dev. Biol., 1993. **159**: p. 105-13.
155. Wu, F., et al., *Onecut1 is essential for horizontal cell genesis and retinal integrity.* J Neurosci, 2013. **33**(32): p. 13053-65, 13065a.
156. Orike, N., et al., *Role of PI 3-kinase, Akt and Bcl-2-related proteins in sustaining the survival of neurotrophic factor-independent adult sympathetic neurons.* J Cell Biol, 2001. **154**(5): p. 995-1005.
157. Watson, J.J., S.J. Allen, and D. Dawbarn, *Targeting nerve growth factor in pain: what is the therapeutic potential?* BioDrugs, 2008. **22**(6): p. 349-59.
158. Siqueira, D.R., et al., *Role of RET genetic variants in MEN2-associated pheochromocytoma.* Eur J Endocrinol, 2014. **170**(6): p. 821-8.
159. Weber, P., et al., *Mice deficient for tenascin-R display alterations of the extracellular matrix and decreased axonal conduction velocities in the CNS.* J Neurosci, 1999. **19**(11): p. 4245-62.